CHALMERS
UNIVERSITY OF TECHNOLOGY

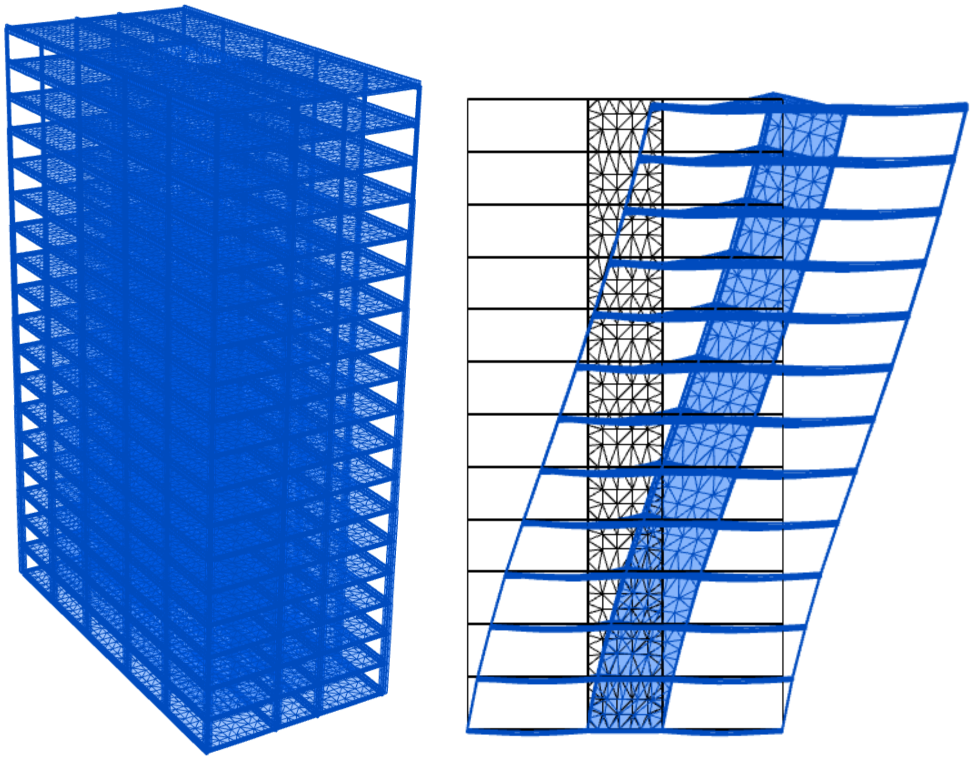

# Stability of timber structures under wind-induced forces

## A parametric study of stabilizing systems in timber structures

Master's thesis in Structural Engineering


OLIVER WENNERHOLM
WILLIAM THULIN

DEPARTMENT OF ARCHITECTURE AND CIVIL ENGINEERING

CHALMERS UNIVERSITY OF TECHNOLOGY
Gothenburg, Sweden 2023
www.chalmers.se

Master's thesis ACEX30 2023

# Stability of timber structures under wind-induced forces

A parametric study of stabilizing systems in timber structures

OLIVER WENNERHOLM
WILLIAM THULIN

Department of Architecture and Civil Engineering
*Division of Structural Engineering*
Research group for Lightweight Structures
Chalmers University of Technology
Gothenburg, Sweden 2023

Stability of timber structures under wind-induced forces
A parametric study of stabilizing systems in timber structures
OLIVER WENNERHOLM
WILLIAM THULIN



Supervisor: Gustav Söderlund & Alexander Vallanger, PE Teknik & Arkitektur
Examiner: Robert Jockwer, Chalmers University of Technology

Master's Thesis ACEX30 2023
Department of Architecture and Civil Engineering
Division of Structural Engineering
Research group for Lightweight Structures
Chalmers University of Technology
SE-412 96 Gothenburg
Telephone +46 31 772 1000

Cover: Visualization of structure in 3D modelled with grasshopper and the deflections of the structure in 2D.

Typeset in LaTeX
Gothenburg, Sweden 2023

Stability of timber structures under wind-induced forces
A parametric study of stabilizing systems in timber structures
OLIVER WENNERHOLM
WILLIAM THULIN
Department of Architecture and Civil Engineering
Chalmers University of Technology

# Abstract

The use of timber as a construction material has gained popularity in recent years and is continuously growing due to increased interest in climate neutrality. This is mostly the result of staying in line with the Paris Agreement, but also due to the new legislation from Boverket in 2021 demanding a climate declaration on all newly built structures. However, challenges arise when constructing timber structures due to their limited stiffness and mass compared to concrete buildings of similar geometry. This thesis examines various structural systems commonly employed in timber construction to assess their performance under wind loading, specifically in terms of lateral deformation and wind-induced acceleration. Finite element analysis (FEA) is conducted using a parametric model implemented in Grasshopper with Karamba3d. The objective of this research is to provide engineers with guidance for the preliminary design of the stabilizing system in timber structures.

The model was verified with FEM-design. The verified finite element model was used to assess the behavior of timber structures, with particular focus on cross-laminated timber walls, which are currently not supported in Karamba3D. The comparison between the model and FEM-design showed small differences, mostly below 5% and never exceeding 10%.

The analysis evaluated wind-induced acceleration according to EKS12 against the comfort demands specified in ISO10137 and ISO6897, while transversal deflection results were compared to the general engineering practice of h/500. The findings demonstrate that both stiffness and mass significantly influence the building's ability to meet these demands. Mass was found to be particularly important for acceleration, whereas stiffness played a crucial role in deflection control.

Among the pure timber concepts examined, with a footprint of 41x21 meters and office building requirements, the design featuring a 320mm timber core with two 990x625mm timber trusses on each side achieved the highest structural height of 35 meters. Additionally, by incorporating a concrete floor slab, it has the potential to reach heights of 63 meters or more.

Keywords: Structural dynamics, Stabilizing system, Timber structures, Wind-induced acceleration, Global deflection, Parametric analysis, Karamba3D, Grasshopper.

# Acknowledgements

First of all, we would like to thank PE Teknik & Arkitektur for letting us collaborate with them writing a thesis which is of great interest of ours. We would like to express a special gratitude to our supervisors Gustav Söderlund and Alexander Vallanger for their great interest and expertise in the area of the thesis as well as to Cecilia Hallgren in tireless commitment of passing on her competence in parametric design.

We would also like to thank Robert Jockwer for being our supervisor and examiner at Chalmers University of Technology.

Oliver Wennerholm & William Thulin

Gothenburg, June 2023

# Acronyms

| | |
|---|---|
| **C** | Concrete |
| **CLT** | Cross-laminated Timber |
| **CT** | Construction timber |
| **DT** | Double Truss |
| **EC** | Eurocode |
| **EoM** | Equation of Motion |
| **EWP** | Engineered wood product |
| **FEA** | Finite Element Analysis |
| **Glulam** | Glue-laminated timber |
| **MDOF** | Multi Degree-of-freedom |
| **MRF** | Moment-Resisting Frames |
| **SDOF** | Single Degree-of-freedom |
| **SLS** | Service-limit State |
| **ST** | Single Truss |
| **STS** | Self-Tapping Screws |
| **ULS** | Ultimate-limit State |

# Nomenclature

### Greek upper case symbols

| | |
|---|---|
| $\mathbf{\Omega^2}$ | Diagonal matrix of eigenvalues |
| $\mathbf{\Omega}$ | Diagonal matrix of eigenfrequencies |
| $\mathbf{\Phi}$ | Modal matrix |
| $\sum F$ | Sum of all forces |

### Greek lower case symbols

| | |
|---|---|
| $\boldsymbol{\phi}$ | Natural mode, or mode shape, vector |
| $\delta_a$ | Logaritmic decrement with regards to aerodynamic damping |
| $\delta_s$ | Logaritmic decrement with regards to mechanical damping |
| $\kappa$ | Shear correction factor of CLT panels |
| $\mu_i$ | Form factor |
| $\nu$ | Poisson's ratio |
| $\omega$ | Eigenfrequency |
| $\omega^2$ | Eigenvalue |
| $\phi_1$ | Fundamental flexural mode |
| $\phi_b$ | Size factor with respect to width |
| $\phi_h$ | Size factor with respect to height |
| $\phi_{ij}$ | Natural mode or mode shape |

$\rho$ Air density ]

$\sigma_{\ddot{x}}(z)$ Standard deviation of the acceleration

$\upsilon$ Up-crossing frequency

$\upsilon_b$ reference wind with a return period of 50 years

$\upsilon_{T_a}$ Reference wind after $T_a$ years

$\xi$ Exponent of mode shape

$\zeta$ Damping ratio

**Latin upper case symbols**

$\boldsymbol{K}$ Stiffness matrix

$\boldsymbol{K}_m$ Modal stiffness matrix

$\boldsymbol{M}$ Mass matrix

$\boldsymbol{M}_m$ Modal mass matrix

$\boldsymbol{V}$ Viscous damping matrix

$\boldsymbol{V}_m$ Modal viscous damping matrix

$A$ Cross-sectional Area, Amplitude or peak acceleration

$A_{ref}$ Reference area

$B^2$ Background response factor

$C_e$ Exposure factor

$C_t$ Thermal factor

$E$ Modulus of elasticity

$E_0$ Modulus of elasticity of timber, parallel to the fibre

$E_{90}$ Modulus of elasticity of timber, perpendicular to the fibre

$F$ Non-dimensional frequency

$G_k$ Characteristic dead load

$G_{mean}$ Modulus of longitudinal shear of timber

$G_R$ Modulus of rolling shear of timber

$G_{xz}$ Out-of-plane shear of CLT panels, in the xz-plane

$G_{yz}$ Out-of-plane shear of CLT panels, in the yz-plane

$I_v$ Turbulence intensity

$I_{0,net}$ Net value of moment of inertia parallel to grain of CLT panels

$I_{90,net}$ Net value of moment of inertia perpendicular to grain of CLT panels

$K_{shear}$ Reduction factor for shear rigidity of CLT panels

$K_{twist}$ Reduction factor to reduce twisting rigidity of CLT panels

$L$ Length

$N$ Number of degrees-of-freedom

$R^2$ Resonance response factor

$T$ Period

**Latin lower case symbols**

$\ddot{\boldsymbol{u}}$ Acceleration vector

$\ddot{\boldsymbol{u}}_m$ Modal acceleration vector

$\dot{\boldsymbol{u}}$ Velocity vector

$\dot{\boldsymbol{u}}_m$ Modal velocity vector

$\boldsymbol{f}$ Force vector

$\boldsymbol{u}$ Displacement vector

$\boldsymbol{u}_m$ Modal displacement

$c_0$ Orthography factor

| | |
|---|---|
| $c_f$ | Force coefficient |
| $c_s c_d$ | Strutural factor |
| $c_{pe}$ | External pressure coefficient |
| $f_0$ | Frequency |
| $f_{c,0}$ | Compressive strength of timber, parallel to the fibre |
| $f_{c,90}$ | Compressive strength of timber, perpendicular to the fibre |
| $f_r$ | Rolling shear strength of timber |
| $f_{t,0}$ | Tensile strength of timber, parallel to the fibre |
| $f_{t,90}$ | Tensile strength of timber, perpendicular to the fibre |
| $f_v$ | Longitudinal shear strength of timber |
| $k_l$ | Turbulence factor |
| $m$ | Mass or Number of mode shapes |
| $m_e$ | Equivalent mass per unit length |
| $n_{1,x}$ | The lowest eigenfreqency in direction of wind |
| $q_k$ | Characteristic imposed load |
| $q_m(h)$ | Mean velocity pressure at height h |
| $q_p$ | Peak velocity pressure |
| $s$ | Snow load |
| $s_k$ | Snow load on the ground |
| $t$ | Time |
| $v_m$ | Mean wind velocity |
| $w_e$ | Wind pressure action on the building exterior |
| $y_C$ | Non-dimensional wind energy spectrum |

| | |
|---|---|
| $z_0$ | Roughness length |
| $z_e$ | Height above ground |
| $\ddot{u}(t)$ | Time-varying Acceleration |
| $\dot{u}(t)$ | Time-varying Velocity |
| $f(t)$ | Time-varying Force |
| $f$ | Eigenfrequency |
| $k$ | Spring Stiffness |
| $u(t)$ | Time-varying Displacement |
| $v$ | Viscous Damping |

# Contents

# List of Figures

# List of Tables

# 1
# Introduction

## 1.1 Background

Building structures in timber are becoming more popular due to the environmental benefits compared to other building materials. In Sweden, timber is widely used when constructing smaller residential structures, such as private villas, but it is not as common for larger structures such as offices and bigger multi-storey residential buildings from a historical perspective.

In cities, a key factor for making the built environment more sustainable is densification since it increases resource efficiency, reduces energy consumption and improves urban livability (Adolfsson Jörby, 2016). With a denser city comes higher structures, and with higher structures comes stability issues.

With an increase in building height, structures stabilizing system is of high importance, especially in a light weight structure such as timber structures. The stabilizing system is often governing for these kinds of structures, but it is seldom that the engineer can decide the structural system alone without interaction and collaboration with other stakeholders in the project. It also has to be adapted to the rest of the building along with the other aspects. Different stabilizing systems have different advantages and disadvantages, and which one to use highly depends on the structural height and geometry of the building.

The stabilizing system is most often decided upon in an early stage of the project, where time and resources are scarce. Since the structural system is so decisive and crucial for the rest of the building design it is important for the structural engineers to be confident with their decision early on. If a non-suitable structural system is chosen the performance, cost and sustainability of the project may be at risk. For larger timber structures it can be hard to determine which structural system to use for a certain height since previous experience from these systems often is very limited. As a result of uncertainty, timber structures are often disregarded and excluded during the early design process.

Based on this, it would be highly useful to have a better understanding of advantages, disadvantages and limitations for different structural systems in timber buildings and by that increase the confidence of the engineer in their decision making in order to find the best possible solution already in the early design process.

Previous studies show great focus on superstructures with a height of 200 meters (Gyllensten & Modig, 2020). The highest timber buildings as of today reach around 90 meters and in this span, there is a big lack of knowledge.

## 1.2 Aim

The aim of this research is to evaluate the performance of different stabilizing systems in timber structures under wind-induced loads. By studying lateral deformation and wind-induced acceleration, we aim to address challenges related to timber's limited stiffness and mass compared to concrete. The goal is to provide guidance to structural engineers during the early design process, promoting the wider use of timber in larger building construction. The findings will assist engineers in making informed decisions about stabilizing systems, advancing timber construction's sustainability and climate neutrality.

## 1.3 Methods

- Perform a literature study on commonly used stabilizing systems of timber structures. The literature study also investigates reasonable geometries on structural elements and find a building geometry that is commonly used based on length, width and floor height.
- Find a number of promising systems that can be further evaluated in a parametric study, based on the literature study.
- Perform a load-bearing calculation to achieve reasonable building properties.
- Create a base model based on calculated building properties.
- Perform a parametric study on different stabilizing systems for a timber structure with varying heights. The study is performed using parametric design software Rhino, including Grasshopper with the FE-analysis plugin Karamba3D.
- From the parametric study, evaluate systems against a set of criteria while their height will be increased.

## 1.4 Limitations

- The foundation has a high impact on global stiffness and may effect the results highly. The foundation is considered rigid.
- The study is limited to a generalized occupancy.
- The building has fixed load-bearing element placement and dimensions.
- When analysing the accelerations of the structure, only the first transversal mode shape in the weak direction is considered.
- Core is considered post-tensioned so that no cracking in the concrete walls will occur and there will be no tension in the timber joints.
- Utilization of stabilizing elements is not included.
- The maximum analysed height is 63 meter.

# 2
# Theory

The theory provides a comprehensive review of relevant literature. It involves the mechanical properties of timber, timber as a construction material and connections between timber elements. It also covers the stability of buildings and explores key phenomena that are crucial for ensuring structural stability. The fundamentals of structural dynamics and highlights its impact on buildings is described. Moreover, various stabilizing systems utilized in timber construction are examined, accompanied by an exploration of some of the tallest existing timber structures worldwide. Additionally, the theory section introduces parametric analysis software, which plays a major role in the subsequent analysis.

## 2.1 Timber as construction material

Timber has been used as a building material for thousands of years, with evidence of timber structures dating back to ancient civilizations such as Egypt, Greece, and Rome(Timber, 2018). In northern Europe, timber has been a traditional building material for centuries, with examples of timber structures dating back to the Viking Age.

During the Middle Ages, timber was a popular building material for many different types of structures, including churches, castles, and houses.

In the 19th century, as industrialization took hold in many parts of the world, timber began to be replaced by other building materials such as brick, stone, and concrete. However, timber remained an important building material in rural areas and in regions where other building materials were not readily available (Gromicko, n.d.).

In the 20th century, there was a renewed interest in timber as a construction material, particularly in Europe and North America. This was due in part to the development of new wood products, such as Glue-laminated timber (Glulam) and Cross-laminated Timber (CLT), which allowed for larger and more complex timber structures to be built. Today, timber is a popular building material for a wide variety of structures, from houses and apartments to commercial buildings and bridges. Wood has many benefits as a building material, Such as low weight, flexibility, environmentally friendly, fire safety etc (Swedish Wood, 2023c).

In the construction business, timber can be used in many different forms for many different purposes. Because timber is a natural material, its properties can vary from one tree to another, making it difficult to control these variations. In order to use this material as a construction material it is necessary to get an estimate of the properties (Swedish wood, 2022). This is done through grading which sorts the timber into different strenght classes. Another very important aspect that differ timber from other construction materials is its orthotropic behaviour. Timber is built up from fiber cells and these cells have a principal direction. These cells have different behaviour depending on the direction in relation to the principal direction. In a larger scale, this means that timber has different properties depending on the direction in relation to the fibers. When used in construction, Timber is generally divided into two subcategories based on how they are produced and how refined the product is: Construction timber (CT) and Engineered wood product (EWP).

### 2.1.1 Construction Timber

CT is the most common type of timber and it is widely used due to its flexibility. CT is made by sawing planks from the logs of the tree. Depending on the size of the log, the number of planks and size of them may vary. This means that the dimensions for CT is limited to what can be extracted from the logs. When sawn in into planks, they can later on be graded and sorted into different strenght classes (Swedish Wood, 2023c). Another factor influencing the structural properties of sawn timber is the existance and density of initial imperfections of the wood. the most common imperfection is knots, which gives the timber a local point of weakness. These imperfections are also considered in the grading.

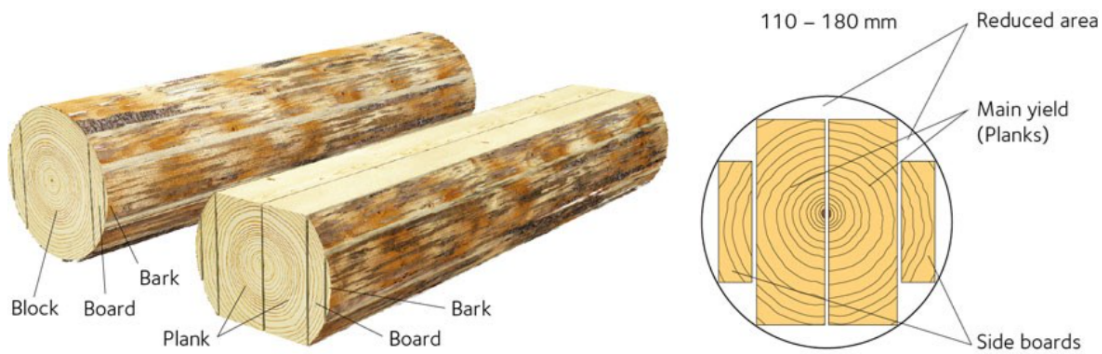


**Figure 2.1:** Illustrative picture of production of construction timber (Swedish Wood, 2023a)

### 2.1.2 Engineered wood products

As described in 2.1.1, the dimensions of timber products are limited to the size of what can be extracted from the logs. This creates a problem when there is a need for products with a larger cross-section or a cross-section with a different design than rectangular. This problem arises when wanting to build large structures with long spans or with high loads. Luckily, EWP products has solved this problem. Swedish Wood (2023c, p.47) defines EWP as: "EWPs are made of wood in the form of sawn timber boards, veneers, particles or fibres held together with, in most cases, some type of adhesive.". Using EWP, There is theoretically no limit to how big or what shape the product can have. Common examples of EWP products are Large beams or floor slabs. Another strong advantage of using EWP is that the orthotropic behaviour as well as the existence of imperfections can be taken into consideration in a good way, making use of the material in the best possible way. EWP products are divided into subcategories based on their way of production, design and purpose and the most common ones are CLT, and Glulam.

#### 2.1.2.1 Gluelam

Glulam is short for "Glue laminated timber" and is an EWP. Glulam is made from lamellas of wood that has been glued together (Swedish Wood, 2023b). These lamellas is normally 45mm thick, but the dimensions may vary based on the purpose and shape of the final purpose. Typical for Glulam is that all lamellas are glued with the same direction of fibers as each other, giving the final product the same type of orthotropic behaviour as normal construction timber, see Figure 2.2. What makes this product better than than CT, apart from larger sizes, is that the strength of the timber can be used in a more efficient way. Since the largest stresses occur in the outer fibers of the product, the outer lamellas can have a higher strength than the inner ones. In this way, the utilization of the material can be optimized.

**Figure 2.2:** Glulam beam. Source (Parlato, 2023)

#### 2.1.2.2 Cross-laminated timber

Another common EWP product is CLT. In contrast to Glulam, described in 2.1.2.1, lamellae are not glued together with fibers in the same direction. Instead, individual lamellae are glued together in finger joint creating longer boards. These boards are then glued together side by side into layers. When the glue in the individual layers have hardened, they can be glued together into CLT panels by placing the layers in a 90°angle to each other. A CLT needs to be comprised of at least 3 layers but can also be much thicker and have a variation of layer thicknesses and orientations, Figure 2.3 illustrates a CLT panel with 5 layers (Gustafsson et al., 2019).

**Figure 2.3:** CLT panel with 5 layers. Source (Mass timber services, 2023)

### 2.1.3 Mechanical properties of timber

Timber have different capacity in tension compared to compression, much like concrete. Furthermore, the capacity of timber is also dependent on the direction of the material, which is a phenomena of orthotropic materials. Tension and compression capacity of timber is much higher parallel to the fibres of the wood compared to the perpendicular direction. The fibres of the wood is oriented along the length of the tree. Due to this, the strength of timber is divided into direction of the fibres and also whether it is loaded in tension or compression. Where $f_{c,0}$ is the strength in compression parallel to the fibres, $f_{c,90}$ compression perpendicular, $f_{t,0}$ tension parallel and $f_{t,90}$ tension perpendicular.

The shear of timber is divided into three different directions depending on the shear loading. The directions is shown in Figure 2.4 where the directions L stands for longitudinal, T for tangential and R for radial.

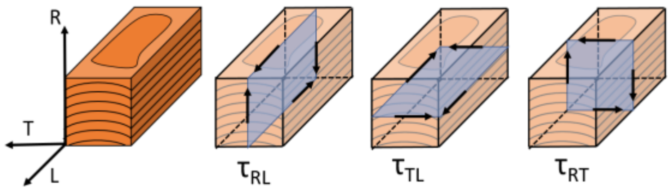


**Figure 2.4:** Shear directions for timber. Source: (Johansson & Johansson, 2021)

For engineering purposes the two shears in longitudinal direction $\tau_{RL}$ and $\tau_{TL}$ is assumed to be equal, the longitudinal shear strength is denoted as $f_{v,090}$ or just $f_v$. The third shear direction, $\tau_{RT}$, is called rolling shear which is mainly relevant for Glulam beams and CLT. The strength for rolling shear is about half of the other directions, and is denoted as $f_{v,9090}$ or $f_r$ (Johansson & Johansson, 2021). Directions 0 and 90 is referred to depending on directions of the fibres, whether it is in the parallel direction or not. Where 0 is the L direction and 90 is the R and T direction seen in Figure 2.4.

The stiffness of timber materials are assumed to be equal in tension and compression according to Johansson and Johansson (2021), dividing it into $E_0$ and $E_{90}$ only, for the parallel and perpendicular direction respectively. The shear stiffness is divided into $G_{mean}$ and $G_R$, described in Table 2.1.

**Table 2.1:** Timber material stiffnesses depending on fibre direction (Gustafsson et al., 2019)

| | |
|---|---|
| The modulus of elasticity parallel to the grain | $E_{0,mean}$ |
| The modulus of elasticity perpendicular to the grain | $E_{90,mean}$ |
| The modulus of longitudinal shear | $G_{mean,090}$ or $G_{mean}$ |
| The modulus of rolling shear | $G_{mean,9090}$ or $G_R$ |

#### 2.1.3.1 Mechanical properties of CLT

Unlike other timber products such as CT or Glulam, with all of their fibres oriented in the same direction, the stiffness of a CLT is not only dependent on the direction of the element but also the orientation and thicknesses of the layers, making it multi-layered orthotropic. The CLT handbook (Gustafsson et al., 2019) refers to $x$, $y$ and $z$ as directions of CLT panels, see Figure 2.5.

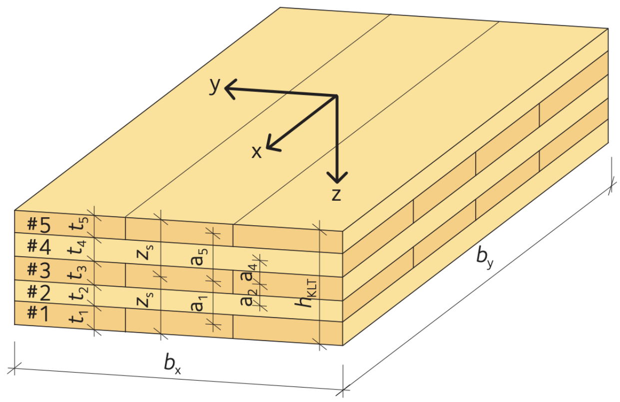


**Figure 2.5:** Direction of a 5-layered CLT panel. Source (Gustafsson et al., 2019)

When calculating the stiffness of a CLT panel, the modulus of elasticity perpendicular to the grain, $E_{90,mean}$ in Table 2.1, is often assumed to be zero. This is because these layers will not contribute if they are not connected to each other, and therefore is dependent on the glue between them. Figure 2.5 represent a 5-layered CLT panel where layer 1, 3 and 5 has their fibres oriented in the x-direction and layer 2 and 4 in the $y$ direction. This means that layers 2 and 4 will not contribute to the stiffness in the $x$ direction, but they do in the $y$ direction. This also means that layer 1, 3 and 5 only contributes to the stiffness in the $x$ direction, which then has more layers that contributes, making it the more stiff direction and can be referred to as the main direction of the CLT panel (Gustafsson et al., 2019).

The out-of-plane shear stiffnesses of the CLT panels, $G_{xz}$ and $G_{yz}$, is also dependent on the fibre orientation of the layers. Where the out-of-plane shear stiffness in the $xz$ plane of layer 1, 3 and 5 is $G_{mean}$ and layer 2 and 4 is $G_R$, and the opposite in the $yz$ plane. There is a correction factor, $\kappa$, depending on support conditions, material properties and the direction of the plane of the CLT panel (Gustafsson et al., 2019).

The shear stiffness in the $xy$ plane of the CLT panel is $G_{mean}$ for all of the layers, but has reduction factors depending on whether the panel is loaded out-of-plane or in-plane. Where $K_{twist}$ is a reduction factor for twisting stiffness used in calculating the shear stiffness in the $xy$ plane when loaded out-of-plane and $K_{shear}$ is a reduction factor for shear rigidity used in calculating the shear stiffness in the $xy$ plane when loaded in-plane (Stora Enso, 2015).

The CLT handbook also presents a stiffness matrix which can be established for orthotropic shell components based on Timoshenko beam theory. This stiffness matrix describes bending, torsional and shear stiffness properties of CLT panels used as slabs or loaded out-of-plane. The stiffness matrix also describes the axial stiffness properties, relevant when loading the panel in-plane, as a wall for example. The stiffness matrix is structured as a $9x9$ matrix seen in Figure 2.6.

$$\begin{bmatrix} D_{11} & D_{12} & 0 & 0 & 0 & 0 & 0 & 0 \\ D_{21} & D_{22} & 0 & 0 & 0 & 0 & 0 & 0 \\ 0 & 0 & D_{33} & 0 & 0 & 0 & 0 & 0 \\ 0 & 0 & 0 & D_{44} & 0 & 0 & 0 & 0 \\ 0 & 0 & 0 & 0 & D_{55} & 0 & 0 & 0 \\ 0 & 0 & 0 & 0 & 0 & D_{66} & D_{67} & 0 \\ 0 & 0 & 0 & 0 & 0 & D_{76} & D_{77} & 0 \\ 0 & 0 & 0 & 0 & 0 & 0 & 0 & D_{88} \end{bmatrix}$$

**Figure 2.6:** Stiffness matrix of an orthotropic shell component (Gustafsson et al., 2019)

Where:

- The $3x3$ matrix consisting of $D_{11}$ to $D_{33}$ describes the bending and torsional properties, or Flexural stiffness.
- The $2x2$ matrix consisting of $D_{44}$ to $D_{55}$ describes the out-of-plane shear stiffness.
- The $3x3$ matrix consisting of $D_{66}$ to $D_{88}$ describes the axial stiffness.

The stiffnesses of the CLT panels is depending on material properties, cross-section properties and factors. Some of the stiffness values involves poisson's ratio, $\nu$, which is usually assumed to be equal to zero. Resulting in $D_{12}$, $D_{21}$, $D_{67}$ and $D_{76}$ being equal to zero and the remaining stiffnesses is calculated as in Equation 2.1 according to Stora Enso (2015), which uses the same stiffness matrix as the CLT handbook.

$$\begin{aligned} D_{11} &= E_{0,mean} \cdot I_{0,net} \\ D_{22} &= E_{0,mean} \cdot I_{90,net} \\ D_{33} &= K_{twist} \cdot G_{0,mean} \cdot \frac{b \cdot d^3}{12} \\ D_{44} &= \kappa_x \cdot \sum G_{i,x} \cdot t_i \\ D_{55} &= \kappa_y \cdot \sum G_{i,y} \cdot t_i \\ D_{66} &= \sum h_{0,net} \cdot E_{0,mean} \\ D_{77} &= \sum h_{90,net} \cdot E_{0,mean} \\ D_{88} &= G_{0,mean} \cdot d \cdot K_{shear} \end{aligned} \tag{2.1}$$

The CLT handbook (Gustafsson et al., 2019) and Stora Enso (2015) modifies the cross-section properties such as area, moment of inertia and torsional resistance to achieve the correct stiffness matrix for CLT panels. The properties is modified because the material properties varies in the same cross-section due to the varying layer orientation, thickness and quality of timber.

### 2.1.4 Timber Connections

Joints in timber construction can be done in a variety of ways. in the following three sections describes the most commonly used connection in Gluelam and CLT and how their stiffness can be obtained.

#### 2.1.4.1 Connections between Glulam elements

Connections are of high importance when designing timber structures since the connector is often weaker than the connecting members. There are a wide range of possible ways to connect one member to another and connectors. Regular carpentry joints normally consists of screws or nails, but when talking about larger structures and especially when building with Glulam, larger and stronger joints are of importance. Two of the most common connection types of this sort is either glued in rods or slotted plates.

Glued in rods are common with both Glulam and LVL to transfer axial loads since they are considered rigid in this direction. They are also beneficial in terms of fire safety since the steel is protected from fire from the surrounding timber (Hedås & Skoglund, 2022). Slotted steel plates are another common connection type. These plates helps to connect a Glulam beam to another beam or to a steel structure. The plate can either be placed on the outside of the beam or be slotted and thereby fitted within the beam itself. By using slotted-in plates, one can benefit from more than two places of connections and increase the overall strength of the connection (Swedish wood, 2016). Timber and steel is connected trough dowels made from either steel or timber that is fitted through pre-drilled holes. This type of connection is commonly used in trusses in order to transfer axial- and shear forces (Hedås & Skoglund, 2022).

#### 2.1.4.2 Connections between CLT elements

Just as for Glulam connections, CLT connections can be done in a variety of ways and the choise of connection dependents on what type of force it is subjected to. Some of them are presented in the report by Mohammad et al. (2013). The most common ones in Wall-to-wall connections are either by the use of splines, Self-Tapping Screws (STS) or metal brackets.

#### 2.1.4.3 Stiffness of timber connections.

Flexibility and variability in these types of connection is infinite since number of plates, size of dowels and number of dowels can be varied in a wide range of different combination. As a results it is difficult to state a strength or stiffness as a whole. To find a value in design one simply has to calculate it for each specific case. When analysing the overall building behaviour in a parametric model where alterations is a major part of the process, the type of connection is not of interest. What is interesting is the level of rigidity it provides to the structure as a whole. For a beam connection a suitable way would be to relate a connection stiffness to the beam stiffness, which is done by Hedås and Skoglund (2022).

In preliminary tests their slotted plates receives a stiffness of 60% of the beam axial stiffness and states that this is a reasonable value.

Similarly, extensive test on the stiffness of Joints in CLT walls have been performed by Hossain et al. (2019) depending on joint type, the shear stiffness ranged between 500 and 7500 $kN/m/m$.

## 2.2 Wind action

Wind is a phenomenon that occurs as an effect of the thermodynamic effects of air. The reduced density of hot air in relation to cold air makes the hot air to rise. The vertical movement of the hot air induces a reduced pressure in its origin making the surrounding air move towards it. The moving air will, when encountering an object, push the object in the direction of the wind. This can be seen as a pressure or force acting on the object. The wind seldom has a constant flowing action, but rather acts with a varying pressure. This is referred to as wind gusts. For a building, the fluctuating wind force both makes the building deflect, but also puts in vibration (A. Alawan and J. Larsson, 2019). Wind speed, and therefore wind-pressure, tends to increase with height and gusts tends to decrease. The effects of the wind is normally divided in two categories based on their direction of action: Along-wind and Cross-wind, illustrated in Figure 2.7. Feng (2018) states that the wind speed highly effects which of the two categories is most dominant, where along-wind is dominant at low wind speeds and cross-winds are more dominant at higher wind speeds.

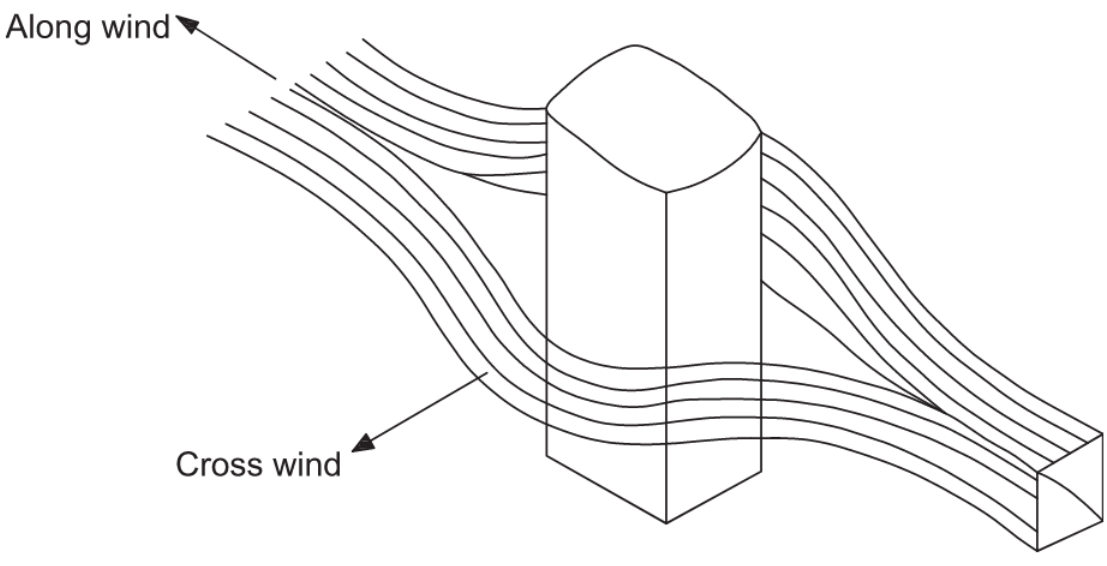


**Figure 2.7:** Illustration of along-wind and crosswind on a tall building (Feng, 2018)

## 2.3 Basics of structural dynamics

Not only must the stabilizing system be stable enough to resist the global displacement of the structure due to the wind pressure, but also its dynamic effects comes in play; frequency and lateral acceleration of the building.

### 2.3.1 Single Degree-of-freedom

A Single Degree-of-freedom (SDOF) system is a system that can only move or rotate in one direction, illustrated as a mass-spring system in Figure 2.8:

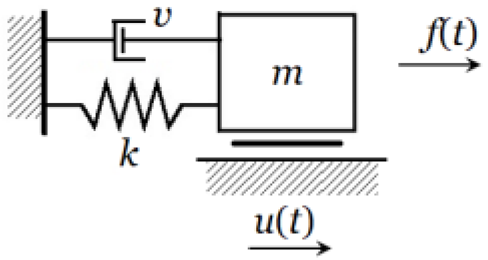


**Figure 2.8:** SDOF system with mass, spring and damping (Abrahamsson, 2019)

The equation for calculating such a system is based on Newton's second law, which says that "the acceleration of an object depends on the mass of the object and the amount of force applied". The equation for this law could be formulated as Equation 2.2:

$$\sum F = m\ddot{u}(t) \tag{2.2}$$

Where $\ddot{u}(t)$ is the acceleration and $m$ is the mass. The sum of all forces, $\sum F$, includes an external force ($f(t)$), this external force will result in a displacement ($u(t)$) and a velocity ($\dot{u}(t)$) of the system. For a structural dynamic system, the displacement and velocity is relevant because they will cause two internal forces due to the resistance of the system. These resistances is dependent on the stiffness ($k$) and damping ($v$) of the system, where the stiffness is resisting the displacement and the damping is resisting the velocity, seen in Equation 2.3:

$$\sum F = f(t) - ku(t) - v\dot{u}(t) \tag{2.3}$$

The governing equation for a SDOF dynamic system, also called Equation of Motion (EoM) can be formed:

$$ku(t) + v\dot{u}(t) + m\ddot{u}(t) = f(t) \tag{2.4}$$

The $(t)$ in the end of a variable means that it is time-dependent.

### 2.3.2 Eigenfrequency of an undamped SDOF system

Eigenfrequency is the frequency in which a system will vibrate without any external force, during so called free vibration, which is a phenomenon in mechanics where a system oscillates about an equilibrium point. This phenomenon is shown in Figure 2.9.

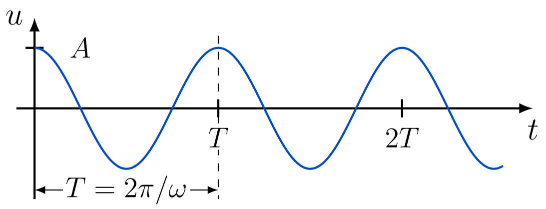


**Figure 2.9:** Harmonic oscillator without damping as a cosine wave. Displacement versus time, showing Period ($T$) and amplitude ($A$).

To set a system in free vibration, an initial force or displacement is needed. Figure 2.9 shows an undamped motion of a system that has been initially displaced with an amplitude of $A$, which causes it to vibrate freely. After the initial displacement, if no additional external forces is applied, such a system can be assumed to oscillate like a cosine function. The equation for this could be formulated as:

$$ku(t) + m\ddot{u}(t) = 0 \tag{2.5}$$

Where the displacement of the system can be calculated as:

$$u(t) = Acos(\omega t) \tag{2.6}$$

Where the eigenfrequency of a structural dynamic system is dependent on the stiffness and the mass. Increasing stiffness results in a higher eigenfrequency while increasing mass results in a lower eigenfrequency, see Equation 2.7 for the eigenfrequency of a SDOF system.

Eigenfrequency in unit [rad/s]:

$$\omega = \sqrt{\frac{k}{m}} \tag{2.7}$$

Eigenfrequency in unit [Hz] can be obtained by:

$$f = \frac{\omega}{2\pi} \tag{2.8}$$

### 2.3.3 Acceleration of an undamped SDOF system

The acceleration is the first derivative of the velocity or the second derivative of the displacement with respect to time and therefore becomes:

$$\ddot{u}(t) = \frac{d^2u}{dt^2} = \frac{d\dot{u}}{dt} = -A\omega^2 cos(\omega t) \tag{2.9}$$

Included in the equation for acceleration is the so called eigenvalue, $\omega^2$, which is the eigenfrequency squared and is used in systems with more than a SDOF.

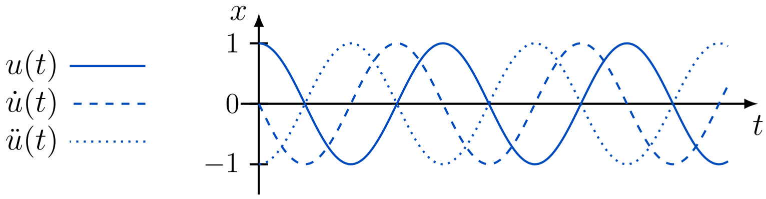


**Figure 2.10:** Harmonic oscillator without damping as a cosine wave. Displacement $u(t)$, velocity $\dot{u}(t)$ and acceleration $\ddot{u}(t)$.

Where the velocity of the system, which is relevant in a damped system, is:

$$\dot{u}(t) = \frac{du}{dt} = -A\omega sin(\omega t) \tag{2.10}$$

### 2.3.4 Damping

The damping does not affect the eigenfrequency of the system, which is only dependent on the stiffness and mass. However, as Figure 2.11 presents, it reduces the amplitude of the displacement and therefore also the acceleration.

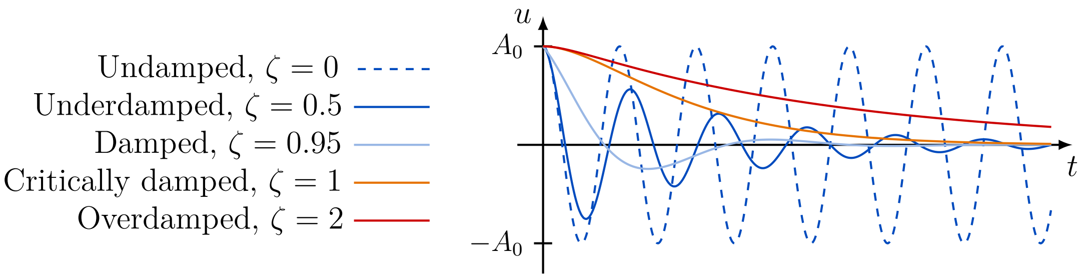


**Figure 2.11:** Harmonic oscillator with varying damping. Where the amplitude $A_0$ of displacement with a damped system decreases with time depending on the damping ratio, $\zeta$.

## 2.4 Stability of buildings

In 1961, Fazlur R. Khan developed a theory called "premium for height". This theory is based on the fact that an increase in building height will increase the lateral loads. These loads will thereby create an additional need for structural system. This results in an exponential increase in structural material consumption, illustrated in figure 2.12. It is because of this the need for an efficient lateral system comes into play in order to both make the building buildable, but also affordable. (Ali & Al-Kodmany, 2022)

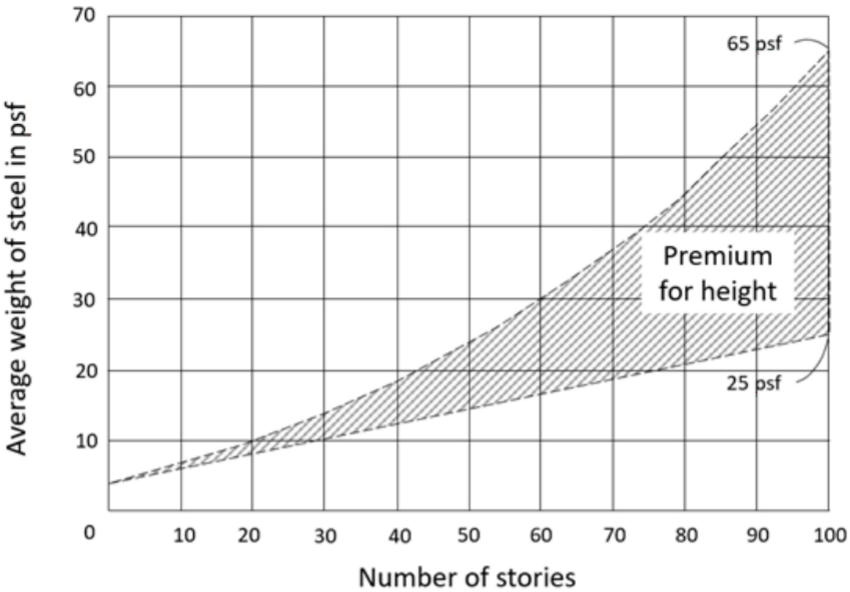


**Figure 2.12:** "premium for height" concept by Fazlur R.Khan. Source:(Ali & Al-Kodmany, 2022)

In general, the stability of a buildings can be divided into two blocks: *Statics* and *Dynamics*. When talking about statics, verifications has to be made so that the structure can transfer lateral loads down to the foundation without collapsing. There is also a limit on the allowable size of lateral deflections that should not be exceeded. To limit these, the global stiffness of the structure is of relevance, which mainly depends on material stiffness, geometric placement and boundary conditions. When talking about dynamics, verifications has to be made so that the wind-induced accelerations and vibrations stay below the threshold stated in the comfort demands. Important parameters affecting this is again the global stiffness, but here also the mass and dampening of the structure has a significant impact.

### 2.4.1 Stability of buildings in statics

A structure will deform in a combination of two deformation types based on the relation between their flexural- and shear stiffness, see Figure 2.13. Flexural deformation, also known as bending deformation, occurs when a structural element is subjected to bending moments, causing it to bend or deform. This type of deformation is common in beams, columns or shear walls which have a low flexural stiffness compared to their shear stiffness. The bending moment causes the material on one side of the member to compress, while the material on the other side stretch, leading to deformation.

Shear deformation, on the other hand, occurs when the forces acting on a structure cause it to deform or slide along a plane parallel to its surface. This type of deformation in moment resisting frames which have a low shear stiffness compared to its flexural stiffness.

Since both shear- and flexural stiffness both are related to the geometry as well as material properties, big differences in deformation behaviour can be seen when changing the material but keeping the same type of structural system. For timber construction this means that there may be advantages to gain that may not be forseen from experience in construction with concrete or steel.

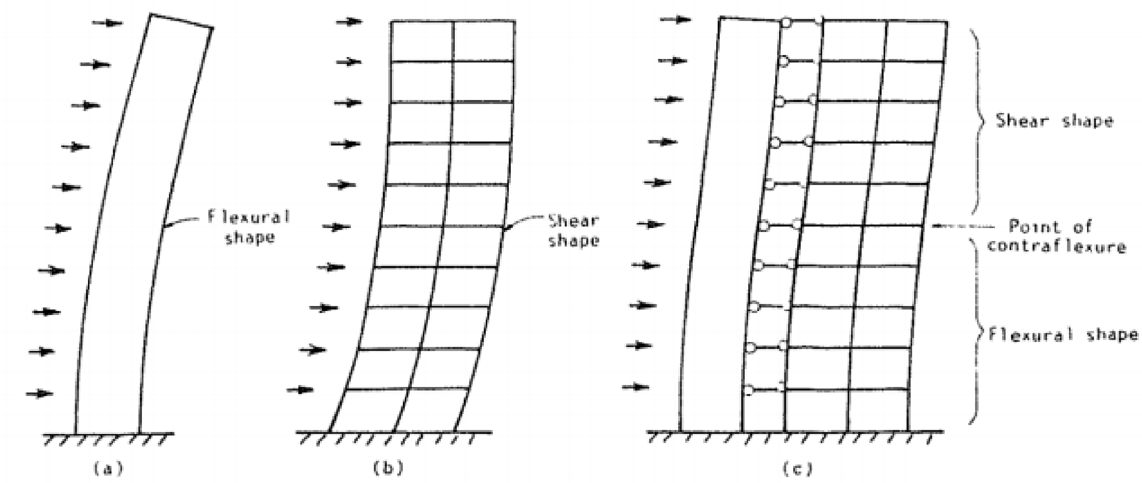


**Figure 2.13:** Illustration of deformation shapes of a tall building due to lateral load (Stafford Smith & Coull, 1991). a) Bending deformation, b) Shear deformaion and c) combined deformation

### 2.4.2 Dynamics applied on buildings

When analysing the dynamics effects on buildings, a SDOF system mentioned in 2.3 is not sufficient for calculations since a SDOF system only has one degree-of-freedom. A system with more than one degree-of-freedom is called a Multi Degree-of-freedom (MDOF) system, illustrated in Figure 2.14.

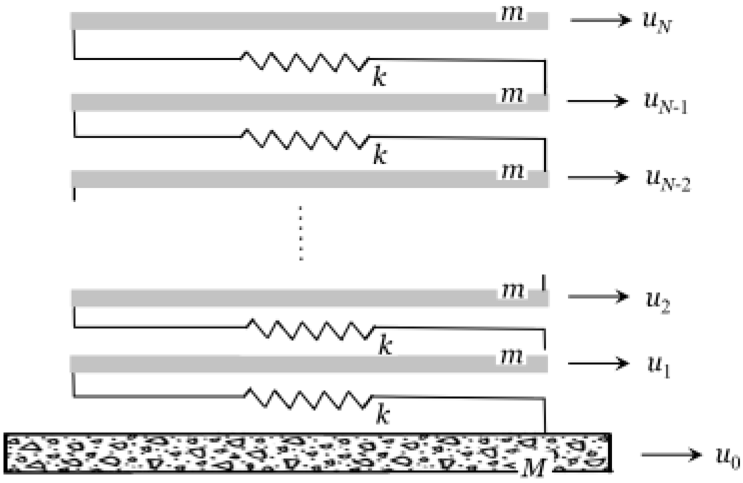


**Figure 2.14:** Multi-degree-of-freedom of a simplified multi-storey building system (Abrahamsson, 2019)

The system illustrated in Figure 2.14 represents a building where the mass of each floor, $m$ is lumped at all the floor levels, and the stiffness of all the elements between all the floors is summed up and presented as $k$. The system has $N$ degrees-of-freedom which corresponds to the horizontal displacement in one direction of each floor.

The EoM, Equation 2.4, for a MDOF system includes a matrix each for the stiffness, mass and damping, and a vector each for the displacement, velocity, acceleration and force. Equation 2.11 shows the EoM for a MDOF without damping, as in the system shown in Figure 2.14:

$\boldsymbol{Ku} + \boldsymbol{M\ddot{u}} = \boldsymbol{f}$, or in matrix form:

$$\begin{bmatrix} k & -k & \cdots & 0 & 0 \\ -k & 2k & \cdots & 0 & 0 \\ \vdots & \vdots & \ddots & \vdots & \vdots \\ 0 & 0 & \cdots & 2k & -k \\ 0 & 0 & \cdots & -k & k \end{bmatrix} \begin{bmatrix} u_0 \\ u_1 \\ \vdots \\ u_{N-1} \\ u_N \end{bmatrix} + \begin{bmatrix} M & 0 & \cdots & 0 & 0 \\ 0 & m & \cdots & 0 & 0 \\ \vdots & \vdots & \ddots & \vdots & \vdots \\ 0 & 0 & \cdots & m & 0 \\ 0 & 0 & \cdots & 0 & m \end{bmatrix} \begin{bmatrix} \ddot{u}_0 \\ \ddot{u}_1 \\ \vdots \\ \ddot{u}_{N-1} \\ \ddot{u}_N \end{bmatrix} = \begin{bmatrix} f_0 \\ f_1 \\ \vdots \\ f_{N-1} \\ f_N \end{bmatrix} \tag{2.11}$$

Where the stiffness and mass matrix is a $N \times N$-matrix and the displacement, velocity and force vector is $N \times 1$. A damping matrix, $\boldsymbol{V}$, would be structured similar to the stiffness matrix and velocity vector, $\dot{\boldsymbol{u}}$, simular to the other vectors.

#### 2.4.2.1 Modal method

Modal method is an approximate method commonly used in Finite Element Analysis (FEA) to reduce the runtime of dynamics analysis. The modal method uses superposition to approximate displacements of the structure in different mode shapes.

In a book by Gawronski (January 2004) the theory behind modal method is explained by considering a structure without damping under free vibration, like Equation 2.11 without any external force, resulting in:

$$\boldsymbol{K}\boldsymbol{u} + \boldsymbol{M}\ddot{\boldsymbol{u}} = \boldsymbol{0} \tag{2.12}$$

The solution of this is $\boldsymbol{u} = \boldsymbol{\phi} e^{i\omega t}$, where the second derivative of the solution becomes $\ddot{\boldsymbol{u}} = -\omega^2 \boldsymbol{\phi} e^{i\omega t}$. With the solutions, Equation 2.12 can be rewritten as:

$$(\boldsymbol{K} - \omega^2 \boldsymbol{M})\boldsymbol{\phi} e^{i\omega t} = \boldsymbol{0} \tag{2.13}$$

The natural mode, or mode shape, $\boldsymbol{\phi}$, is a vector with the size of $N \times 1$, one value for each degree-of-freedom in the system.

A total number of mode shapes $m$ that does not exceed the number of degrees-of-freedom; $N \leq m$, is possible. With multiple mode shapes, a so called modal matrix, $\boldsymbol{\Phi}$, can be formed. It involves all the mode shape vectors and has the size of $N \times m$, see Equation 2.14:

$$\boldsymbol{\Phi} = \begin{bmatrix} \boldsymbol{\phi}_1 & \boldsymbol{\phi}_2 & \cdots & \boldsymbol{\phi}_m \end{bmatrix} = \begin{bmatrix} \phi_{11} & \phi_{21} & \cdots & \phi_{m1} \\ \phi_{12} & \phi_{22} & \cdots & \phi_{m2} \\ \vdots & \vdots & \ddots & \vdots \\ \phi_{1N} & \phi_{2N} & \cdots & \phi_{mN} \end{bmatrix} \tag{2.14}$$

The mode shapes, $\phi_{ij}$, in Figure 2.15 is structured according to Equation 2.14. Where $\phi_{ij}$ refers to the $j$-th displacement of the $i$-th mode.

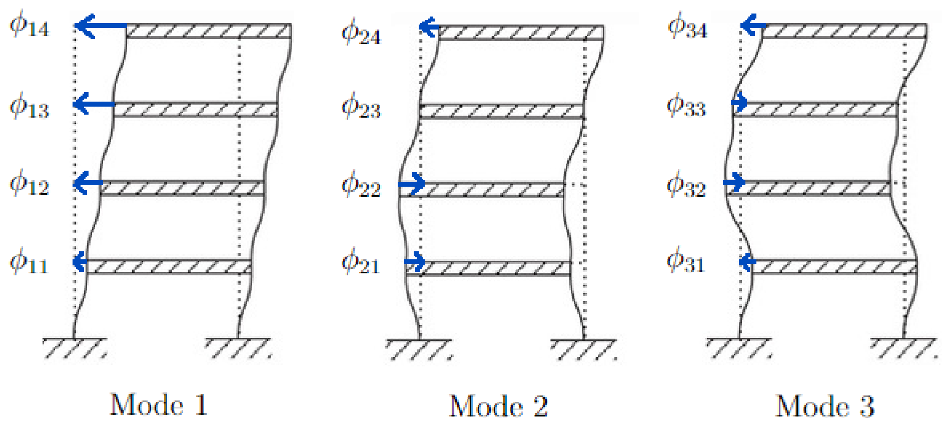


**Figure 2.15:** The three first transversal modes in the same direction

Modal models of structures are expressed in modal coordinates, therefore the displacement is replaced by a so called modal displacement, $\boldsymbol{u}_m$, that satisfies the following: $\boldsymbol{u} = \boldsymbol{\Phi}\boldsymbol{u}_m$. The same goes for the acceleration, resulting in $\ddot{\boldsymbol{u}} = \boldsymbol{\Phi}\ddot{\boldsymbol{u}}_m$. With these new variables and additionally left-multiplying with $\boldsymbol{\Phi}^T$, the EoM of a MDOF system, as in Equation 2.11, can be rewritten as:

$$\boldsymbol{\Phi}^T\boldsymbol{K}\boldsymbol{\Phi}\boldsymbol{u}_m + \boldsymbol{\Phi}^T\boldsymbol{M}\boldsymbol{\Phi}\ddot{\boldsymbol{u}}_m = \boldsymbol{\Phi}^T\boldsymbol{f} \tag{2.15}$$

The modal matrix and its transpose, $\boldsymbol{\Phi}$ and $\boldsymbol{\Phi}^T$, from Equation 2.15 diagonalizes the mass and stiffness matrices, $\boldsymbol{M}$ and $\boldsymbol{K}$, in Equation 2.11. This results in the so called modal mass matrix, $\boldsymbol{\Phi}^T\boldsymbol{M}\boldsymbol{\Phi} = \boldsymbol{M}_m$ and modal stiffness matrix, $\boldsymbol{\Phi}^T\boldsymbol{K}\boldsymbol{\Phi} = \boldsymbol{K}_m$. Where the modal mass and stiffness matrices has the size of $m \times m$, with values in the diagonal only and the rest being zeros. Where the $i$-th diagonal value of the matrices corresponds to the $i$-th mode shape, $\boldsymbol{\phi}_i$.

Regarding the eigenfrequency, a nontrivial solution for the homogeneous equations included in Equation 2.13 exists only if the determinant of $\boldsymbol{K} - \omega^2\boldsymbol{M} = \boldsymbol{0}$ equals zero; $det(\boldsymbol{K} - \omega^2\boldsymbol{M}) = \boldsymbol{0}$. This is satisfied for a set of $m$ values of eigenfrequency $\omega$, denoted as $\omega_1$, $\omega_2$, $\ldots$, $\omega_m$. Where $\omega_i$ is the $i$-th eigenfrequency, which corresponds to the $i$-th mode shape, $\boldsymbol{\phi}_i$. For a notational convenience, a diagonal matrix of eigenfrequencies, $\boldsymbol{\Omega}$, can be formed from as:

$$\boldsymbol{\Omega} = \begin{bmatrix} \omega_1 & 0 & \cdots & 0 \\ 0 & \omega_2 & \cdots & 0 \\ \vdots & \vdots & \ddots & \vdots \\ 0 & 0 & \cdots & \omega_m \end{bmatrix} \tag{2.16}$$

Resulting in a matrix of eigenvalues, $\boldsymbol{\Omega}^2$, with $\omega_1^2$, $\omega_2^2$, $\ldots$, $\omega_m^2$ diagonally. This is associated with the modal mass and stiffness matrices as follows:

$$\boldsymbol{\Omega}^2 = \boldsymbol{M}_m^{-1}\boldsymbol{K}_m \tag{2.17}$$

Gawronski (January 2004) continues to explain hos the modal damping matrix, $\boldsymbol{V}_m$, and other parameters of structural dynamics comes into the equation. With these marices, an approximation of the displacements of a complex structure can be calculated for several mode shapes.

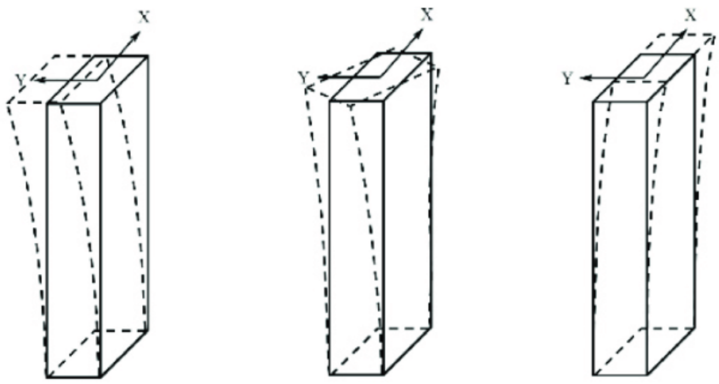


**Figure 2.16:** The first mode shapes of a building with the first transversal mode in y-direction, first rotational mode and first transversal mode in x-direction in that order from left to right (Wang et al., 2018).

the types of mode shapes in Figure 2.16 can occur in different orders depending on the structure, where the first mode shape occurs at the lowest frequency mode of vibration and as the frequency of vibration increases, the second mode shape can be reached and so on. The different types of modes involves more than one mode shape, as an example the transversal mode in x-direction could have mode shapes similar to the ones illustrated in Figure 2.15. The lowest frequency mode of vibration of a structure is commonly referred to as the fundamental mode shape, it is not unusual that this mode is the first transversal/flexural mode in the y-direction (weak direction) from Figure 2.16.

#### 2.4.2.2 Wind induced acceleration

For the structure to start oscillating, a displacement or force is needed. An Earthquake or the wind is typical forces acting on buildings, but since earthquakes is not taken into consideration in Sweden, the main force causing a structure to oscillate here is the wind. With that said, as described in 2.2, the wind acts as a force on the object and unless this object is extremely streamlined or the wind velocity is too low, the force will fluctuate. Moreover, the wind is often not a laminar flow but a turbulent one. This also causes the force acting on the building to fluctuate (Strömmen, 2010). Fluctuating forces results in a fluctuating building response, putting it into movement. This movement is problematic both from a structural perspective and in the perspective of human comfort.

From the structural point of view, movements may cause damage in terms of fatigue but also due to the risk of ending up in resonance-frequency, seen in the famous collapse of the Tacoma bridge in 1940 (Tacoma Narrows Bridge history, 2023). From a human perspective accelerations of the structure cause discomfort. The tolerance levels to this movement is subjective and vary in a large range that spans from $0.05m/s^2$ where some people can perceive motion up to $0.7m/s^2$ where walking is no longer possible (Stafford Smith & Coull, 1991). These wind induced accelerations causing human discomfort is accounted for by following the demands in ISO10137 (2008) and ISO6897 (1984).

## 2.5 Stabilizing systems

There are many ways a lateral system can be designed provide stability. The most common systems, where most of them were invented by Fazlur R. Khan in the 60's, are: *Braced frames, Moment resisting frames, Shear wall systems, Shear wall-Frame Interaction systems, Core-outrigger systems, Tubular systems and Advanced Tubular systems* (Ali & Al-Kodmany, 2022). What differs them is how they create stiffness in the building and a major difference among these systems is their deformation behaviour.

### 2.5.1 Braced frames

Braced frames are maybe the simplest and most intuitive form of lateral stability. By adding at least one diagonal element within a frame, Lateral loads can be resisted through axial stiffness of the diagonal bracing. Braces can then handle lateral loads through both tension and compression of the member(s). The bracing can have many different designs, but the most common ones is "diagonal brace" or "X-brace", illustrated in figure 2.17. In relation to section 2.4.1, the primary deformation shape of this system is shear deformation.

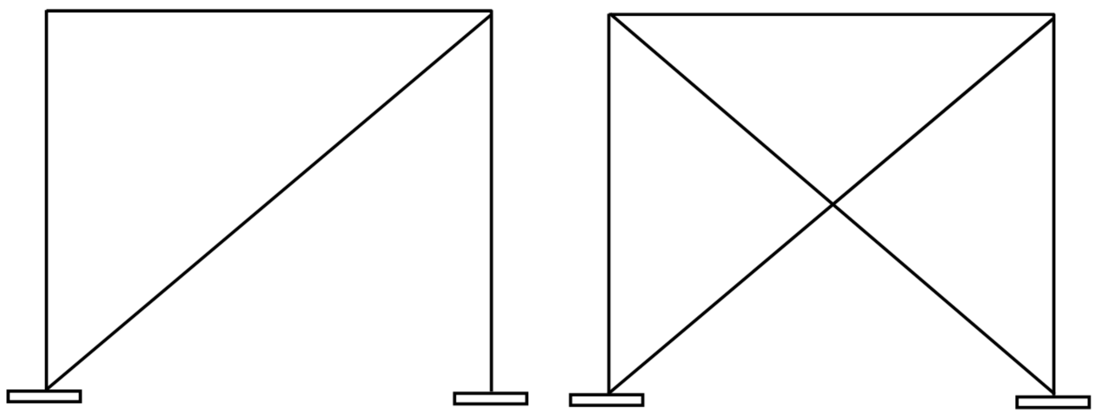

**Figure 2.17:** Illustration of diagonal- and x-bracing respectively.

### 2.5.2 Shear Walls and Cores

Shear walls are structural elements that resist lateral loads in buildings. They are typically made of reinforced concrete but can also be made from CLT and are designed to transfer these loads from the roof and upper floors to the foundation. They work by transferring the lateral loads to the foundation through a combination of bending and shear forces. The second moment of area of a shear wall is normally large and a small number of walls often provide enough stiffness to resist lateral loads (Karoly A. Zalka, 2013). In single-story buildings, shear walls are typically located at the perimeter of the building. In office buildings, shear walls are typically located at the center of the building forming a core of the building. Shear walls will deform according to flexural deformation described in Figure 2.13 since their shear stiffness can be considered infinately large in comparison to the flexural stiffness.

Shear walls are often considered as 2-D element where the stiffness in its weak direction is neglected. Cores however, can be seen as a combination of two or more shear walls which form a 3-D element. Apart from giving the structure lateral stiffness in two direction, cores also provide torsional stiffness (Karoly A. Zalka, 2013).

### 2.5.3 Shear Wall-Frame interaction system

If both shear walls and Moment-Resisting Frames (MRF) is used, the two systems will not work independently of each other, but rather as a one unit with a deformation shape based on the combined effect of both flexural and shear deformation. This is illustrated in c) in 2.13. Which shape that will be dominating can be complex to predict, but it will be related to the relative stiffness of the different systems along the height of the structure (Ali & Al-Kodmany, 2022). Shear shape has largest increase in deformation in the bottom, and flexural shape has the largest deformation in the top. The result of the combined system is then that the shear deformations in the bottom is resisted by the flexural mode. The same happens in the top of the building: since flexural deformations here are large and not as large in shear deformations, the flexural deformations will be resisted by the shear mode.

### 2.5.4 Tubular- and advanced tubular systems systems

The behaviour of tubular system can be compared to a cantilevered hollow core section. By having the Lateral load resisting elements as far away from the centroid as possible, the sturcture receives maximum second moment of area making it very stiff. Since buildings needs windows, the tubular system cannot be a solid hollow core section. This results in a number of different subcategories for tubular systems.

*Framed Tubes* can be seen as a solid hollow core section with "punched holes" that makes room for windows. even though the design makes the impression of a solid, this would be to hard to manufacture. The system is rather a beam-column system with closely spaced columns and deep beams(Ali & Al-Kodmany, 2022).

*Braced Tubes* can, in contrast to *framed tubes*, have large spaces between perimiter columns since they are stiffened up by large diagonals. The large diagonals that can span several floors will make the tube act more like a wall in the sence that bending moment is drastically reduced.

*Tube in Tube* is when an outer tube, such as the *framed tube* or *Braced Tube* is further stiffened by a central tube.

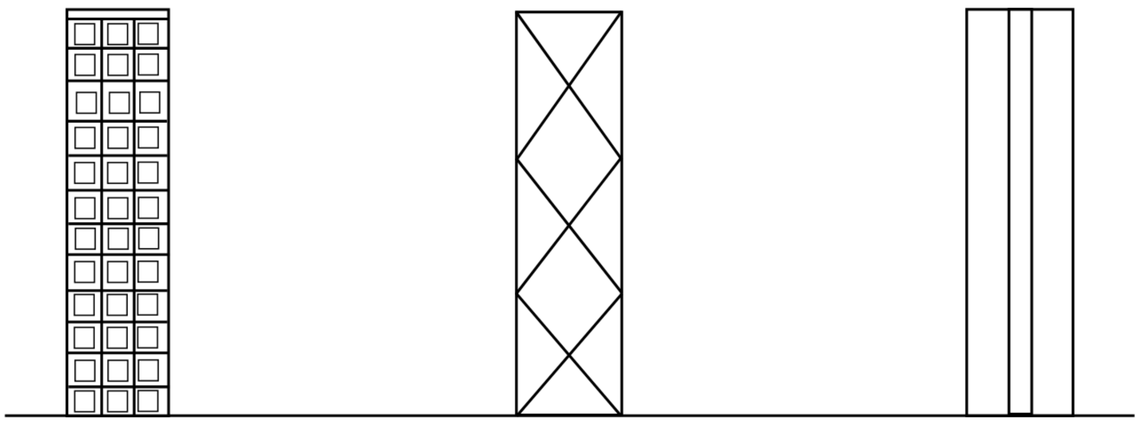

**Figure 2.18:** Framed tube, Braced tube and Tube in Tube from left to right. (Sketched by W.Thulin)

## 2.6 Case study of existing tall timber structures

A key issue when working with timber is the horizontal stability, and the choice of stabilising system plays an important role in the structure as a whole (Swedish Wood, 2018). For lower timber structures, it is generally sufficient to use diaphragm action in the walls to stabilize the building. This type of action comes from the use of wood- or plaster boards, that also serves another purpose in the building. When building higher it is common to use rigid joints, braced frame and diaphragm action. However, both rigid joints and braced frames are problematic when working with timber since it is hard to make rigid connections(Ali & Al-Kodmany, 2022). Another key issue is the lightness of timber structures. This created dynamical issues since mass in one of the most important parameters to reduce accelerations. A case study of existing timber structures is made where these key issues is brought up and how they solved them.

### 2.6.1 Mjøstornet

Mjøstornet in Norway is a 18-storey timber structure that was completed in mars 2019. The tower is 81 meters high and was, when finished, the world record holder for the worlds highest timber structure (Abrahamsen, 2018). The structural system is a combined system where the vertical loads are carried by Glulam columns, Glulam beams and CLT-walls. The lateral stability is handled by a large Glulam truss system in the facade. In relation to section 2.5, this is of the type *braced frame*. Even though CLT-walls could be used in lateral stability, Abrahamsen (2018) states that they do not contribute. The truss system is sufficient to handle the loads, but other Service-limit State (SLS) demands related to acceleration made it inevitable to increase the building mass on the upper floors. As explained in section 2.4.2, increased mass in the upper part will increase the modal mass significantly and thereby reduce accelerations. This was made by using concrete slabs, instead of Moelven's "TRÄ-8" wooden slab system that is used in the rest of the building.

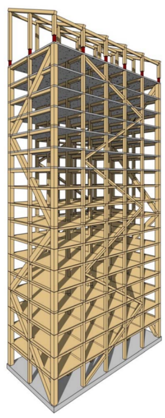

**Figure 2.19:** Structural system in Mjöstornet, Norway. (Abrahamsen (2018)

### 2.6.2 Ascent MKE Building

The Ascent is was finished in 2022 and is yet today the highest timber structure in the world, surpassing Mjöstornet in Norway. The 25-storey building is 86meters tall and is located in Milwaukee, Wisconsin. The Timber structure stands on top of a five-story garage complex, and is based on a beam-column system with Glulam elements. Between the beams spans CLT slabs. The lateral stability is provided by two concrete cores(Tomasetti, 2023). Because of the concrete cores, the dynamic effects is not an issue since they provide sufficient mass and stiffness to the structure.

### 2.6.3 Sara kulturhus

Sara kulturhus is a 74 meter high timber construction in Skellefteå, Sweden. It was constructed through a collaboration between White architects, Martinssons and TK Botnia. The final 20th floor was finalized in 2021. The structure is mainly constructed with CLT-walls and Gluelam beams. As for the lateral systems, Several CLT-cores in the building center takes most of the lateral loads(White arkitekter, n.d.). To account for the dynamic effects, concrete slabs was used on specific floors to increase mass and reduce accelerations.

### 2.6.4 Treet Bergen

Treet in Bergen, Norway, Is a 14 storey building with a height of 49m(Abrahamsen, 2015). Treet and Mjöstornet both share the same contractor, Moelven, as well as structural engineering team, SWECO Norge. Therefore many similarities can be seen among the two buildings. The structural system in Treet consists of a Glulam beams and columns and a CLT Core. To account for lateral stability, a large gluelam truss is positioned in the building perimeter. The CLT-walls do not contribute to the lateral stability. Treet is a module based building. 3 four-storey modules are stacked on top of each other, with a "power-storey" in between, see Figure **??**. The power-storey has an increased strenght and also a concrete slab. the storey has several functions: Firstly, it acts as a base for the imposed module. Secondly, it connects the truss system by incorporating it in the concrete slab. Lastly, the concrete increases the building mass to improve dynamical behaviour.

## 2.7 Parametric analysis in Rhino 7

To perform the analysis and evaluate results for this type of analysis, a powerful software is needed. The software has to be able to handle complex 3D structures with a high level of precision and accuracy. Since many different concepts are to be evaluated, the software also needs to allow for rapid customization of the model with on-time evaluation of changes. It is therefore of great benefit if both design and analysis can be performed within the same software. Rhino7 is a 3D-modelling software widely used in architecture, but also in engineering and industrial design. It provides the user to create, edit and analyse a 3d models with a userfriendly user interface.

### 2.7.1 Grasshopper

Grasshopper is a tool that works inside Rhino. It is a visual programming language which allows the user to create and manipulate parametric design through a graphical interface. This makes it easy to alter the design in an easy manner through iterations. Grasshopper also helps the user to create geometric forms that would be cumbersome to create manually.

### 2.7.2 Karamba 3D

Karamba3D is a plugin to grasshopper that allows the user to perform structural analysis within grasshopper. Karamba3D is a tool that is able to perform a Finite Element Analysis (FEA) for both statical and dynamical analysis. The results can be directly visualised in Rhino which facilitates understanding and makes the design alterations easy to compare and evaluate.

# 3
# Base model

The base model includes all that was kept similar in all concepts, laying the base for what later was developed into different concepts with stabilizing systems. The base model involves the layout of the building, vertical loads used in design, element placement as well as element dimensions with others.

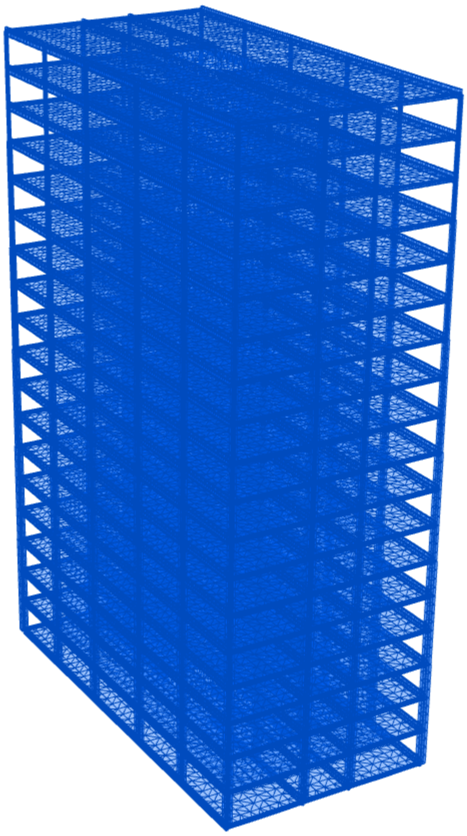

**Figure 3.1:** Illustration of the base model, modelled in Rhino with Grasshopper plug-in

The structure was designed as an office building situated in Göteborg, Sweden. The building has a footprint of $41x21m^2$, these measures was based on the size of the core and placement of the load-bearing elements.

## 3.1 Vertical Loads

Vertical loads involves all the loads in the structure caused by gravity. All vertical loads acting on the structure has been calculated in accordance to regulations stated by Eurocode (EC) a long with the national annex for Sweden.

Imposed load of $q_k = 2,5kN/m^2$ for office buildings was applied on all floors except the roof according to Section C Table C-1, Boverket (2022). The roof is loaded with a snow load. The snow load is calculated as:

$$s = \mu_i \cdot C_e \cdot C_t \cdot s_k \tag{3.1}$$

where $s_k = 1.5kN/m^2$ according to Figure C-2, Boverket (2022). With factors $\mu_i$, $C_e$ and $C_t$ set to one so that $s = s_k$.

Listed in Table 3.1 is elements of the building that is not load-bearing but only adds extra weight to the structure as dead loads:

**Table 3.1:** Self-weights of non-bearing building parts

| Building part: | Dead load ($G_k$): |
|---|---|
| Non-bearing walls and flooring | $0.65kN/m^2$ |
| Roofing | $0.15kN/m^2$ |
| Facade | $1.375kN/m$ |
| Staircase | $6.25kN/m^2$ |
| One Elevator | $49kN$ |

Load from the internal non-bearing walls is presented as area load, meaning they are spread out on the slab as an average load per square meter. The facade is made of glass, where the weight of the cross-section was chosen as $40kg/m^2$ (Pilkington Floatglas AB, 2015). The self-weight of the staircase is calculated by the volume of the stairs and resting planes per floor and the density of concrete as $2400kg/m^3$. The elevators has a capacity of $1200kg$, and the elevators each has a self-weight of $3800kg$ including counter-weight.

Vertical load calculations used for dimensioning is presented in Appendix A.1.

## 3.2 Load-bearing elements

The base of the model in regards to elements is designed for the vertical load only, the dimensions and materials of elements included in the analysed stabilizing systems will be adjusted. The floor height of the building was chosen to 3.5 meter. The choice of building size was based on the size of the core. The aim for the building measures where to achieve reasonable span lengths and also to match commonly used measures of already built timber structures, such measures is presented in a report written by Abrahamsen (2020).

### 3.2.1 Load-bearing element placements

Placement of the load-bearing elements was chosen to fit the office environment with possibilities to have large open spaces but also reasonable spans for the slabs and the beams.

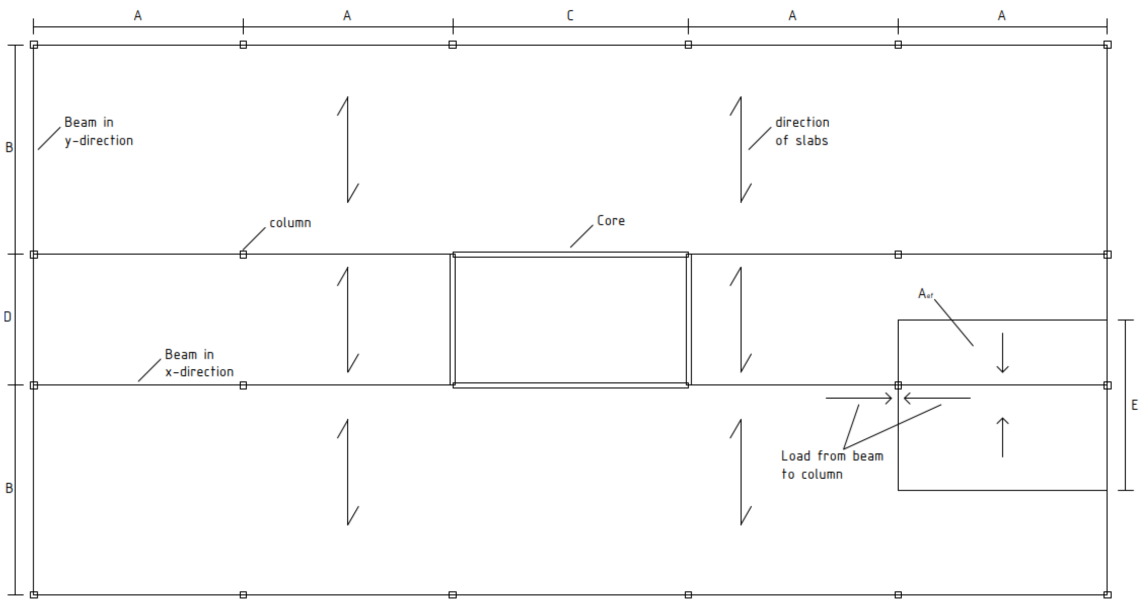


**Figure 3.2:** Placement of elements in the structure with reference measures.

The core was placed in the middle of the building, because in the cases of using the core as part of the stabilizing system, an eccentricity from the force resultant of the wind load, located in the middle of the facade, will cause rotation. Figure 3.2 shows the positions of all the elements in the building with references for the span measures.

The dimensions of the core was based on fitting a staircase and two elevators. The outer dashed lines in Figure 3.3 represents the dimensions of the core, at the center line of the walls in the core.

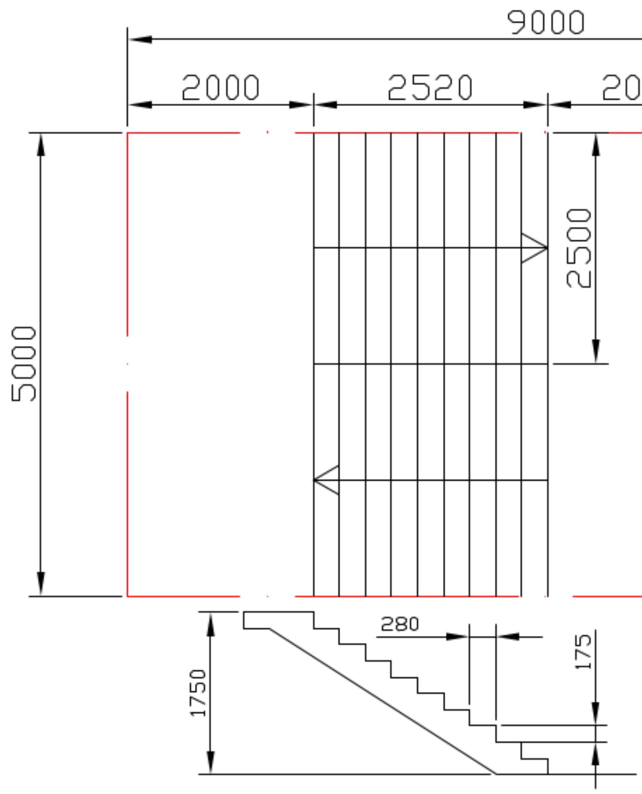


**Figure 3.3:** Core dimensions shown in [mm].

According to Forssellstrappan (2016) the stairs should have at least a width of 1.5m for two-way traffic and the length and height of the stairs was determined by the risers and treads measures. The risers should be between 170mm-180mm and the treads should be at least 250mm. Apart from that it was recommended to follow a formula; 2×riser+tread=600mm-630mm.

A stair width of 2.5m was chosen so that there was room for the gap between them and also to account for the core wall thickness. The risers and treads were chosen as 175mm and 280mm to achieve a total height gain of 3.5m in a reasonable length (2.52m) and to fulfill the formula; $2 \times 175 + 280 = 630$mm. Required space for the elevators was about 2100mm×1400mm, which is fitted into the core as well.

In total the core needed to be around at least 9m×5m, C×D in Figure 3.2.

### 3.2.2 Load-bearing element properties and dimensions

The load-bearing elements in the building, such as slabs, beams, core walls and columns were dimensioned for the vertical loads. The dimensions and material properties were used as minimum values for the structural members, these may be adjusted if they are part of the stabilizing system may be increased. Requirements and classes use in the calculations are shown in Table 3.2. The load-bearing elements was designed for the same loads as for the model, presented in section 3.1, except from the imposed load which is chosen to $q_k = 3kN/m^2$ according to CEN (2002). This was done to achieve extra capacity of the load-bearing vertical elements because they will also be affected by wind load.

Calculatis by Stora Enso (2023) is a timber design tool for engineers, with this tool the load-bearing elements was designed with regards to Ultimate-limit State (ULS), ULS Fire, SLS, Vibration. These requirements was determined by choosing Safety class, service class, fire resistance class, deflection limit, damping coefficient with others. The applied loads was divided into different load case categories.

**Table 3.2:** Requirements and Classes

| | |
|---|---|
| Safety class | SC3 (Core walls in SC1) |
| Service class | 1 |
| Fire resistance class | R90 |
| SLS instant limit | L/300 |
| SLS final limit | L/250 |
| Damping coefficient | 1% |

Table 3.2 shows used classes and such for load-bearing calcualtions. Vertical load calculations used for dimensioning is presented in Appendix A.1.

#### 3.2.2.1 Slabs

Relevant for dimensioning of the slabs was ULS, ULS Fire, SLS and vibration. Material of slabs was CLT with varying thicknesses and orientation. Length of span and support conditions was selected. The slabs was calculated per meter by dividing it into one meter wide strips. Load is applied as uniform or/and point loads along the span.

All the slabs was dimensioned for the same load on all floors of the building, imposed load and self-weight of slab. The slabs is made of CLT 300 L8s-2, see Appendix A.2 for dimensioning of slabs.

#### 3.2.2.2 Beams

The beams was dimensioned in ULS, ULS Fire, SLS and vibration. Glulam of selection and cross-section measures was chosen, length of span and support conditions was set. Load was applied as uniform or/and point loads along the span.

The beams in x-direction in Figure 3.2 is loaded by the support reaction loads from the slabs which is half of the area between beams since they are one-way simply supported. The most outer of those beams also has an extra load coming from the facade, but these will only carry load from half a span of slabs resulting in lower load. The largest area, $A_{ef}$ in Figure 3.2, of slabs resulting in the largest beam load.

The only beams in y-direction in Figure 3.2 is located on the most outer grid lines, on the short sides. These beams do not support the slabs and therefore don't carry any load from them but only from the short side facades.

GL32h were chosen as the material of all beams. The dimensions of the cross-sections:

- X-direction beams $800 \times 200mm^2$
- Y-direction beams $360 \times 200mm^2$

For dimensioning of beams, see Appendix A.3.

#### 3.2.2.3 Columns

For the columns, only ULS and ULS fire was used in the design. Support conditions were set for bending in x- and y-direction. Length, Glulam material properties and cross-section was chosen. Sides exposed to fire was also chosen for the columns. Load was applied as point load on the top of the column.

All the columns is 3.5m long and made of GL32h. The load from the roof is snow load, all other floors is affected by imposed load. The load on the columns increases for every floor above since the load stacked up and distributed to the ground, and therefore their load are dependent on the total amount of floors above them.

**Table 3.3:** Dimensions and self-weights of columns based on floors above

| Maximum floors above | Dimension | Self-Weight |
|---|---|---|
| 3 | $260 \times 260mm^2$ | $1.2kN$ |
| 6 | $360 \times 360mm^2$ | $2.3kN$ |
| 9 | $440 \times 440mm^2$ | $3.4kN$ |
| 12 | $520 \times 520mm^2$ | $4.7kN$ |
| 15 | $600 \times 600mm^2$ | $6.3kN$ |
| 18 | $640 \times 640mm^2$ | $7.2kN$ |

Dimensioning of columns in Appendix A.4.

#### 3.2.2.4 Core walls

The core walls had demands on the ULS, ULS fire and SLS. Height, length and support conditions was chosen. Voids like door openings and such was also given. Material of the core walls was CLT, where the thickness and orientation was chosen. Load was applied as uniform and point loads on top of the walls.

The core walls are supporting the slabs and stairs as uniform load over entire length. They also support the beams beside which is supported on the upper corners of the walls as point loads. The load from walls above is distributed to the wall below as uniform load along the length of the wall except at the door opening. Load from the roof acting on the walls is snow load and elevator load, which is anchored to the roof. See Appendix A.5 for dimensioning of walls, load placement and magnitudes.

The core walls are all made out of CLT L7s-2 with varying thickness except the largest one, which is CLT 320$mm$ L8s-2, see Table 3.4.

**Table 3.4:** Thickness and self-weights of core walls based on floors above

| Maximum floors above | Thickness | Weight |
|---|---|---|
| 3 | 220$mm$ | 3.85$kN/m$ |
| 6 | 220$mm$ | 3.85$kN/m$ |
| 9 | 220$mm$ | 3.85$kN/m$ |
| 12 | 280$mm$ | 4.9$kN/m$ |
| 15 | 280$mm$ | 4.9$kN/m$ |
| 18 | 320$mm$ (L8s-2) | 5.6$kN/m$ |

## 3.3 Boundary conditions, joints and mesh

Boundary conditions and joints depends on whether the element is included in the stabilizing system or not. All the elements that is not suppose to contribute to the stability such as all the columns, is pinned both in the joints in between each other and in the support, meaning they can not transfer any moment and therefore does not resist the horizontal forces. In the base model only the core walls was modelled as moment resisting, both in the joints in between them and the support in the bottom.

The mesh size and position of the nodes plays a role because the shells in Karamba3D can only connect to each other where the meshes share nodes. Any nodes in the mesh that does not share the same position will not connect and will therefore not be able to describe the joint between them.

Since the core was used as a part of the stabilizing systems, its mesh was chosen as finer than the slabs, since the slabs were only modeled for load distribution and self-weight, therefore a detailed analysis of them was not of interest.

## 3.4 Modifying material properties for CLT

With the plug-ins for grasshopper, Karamba3D and Beaver, described parameters for timber material properties of GL32h, which was used for the columns and beams was available. However, there were no prescribed material properties of any CLT panels available, which was used as the core walls and the slabs in the model. These needed to be described manually.

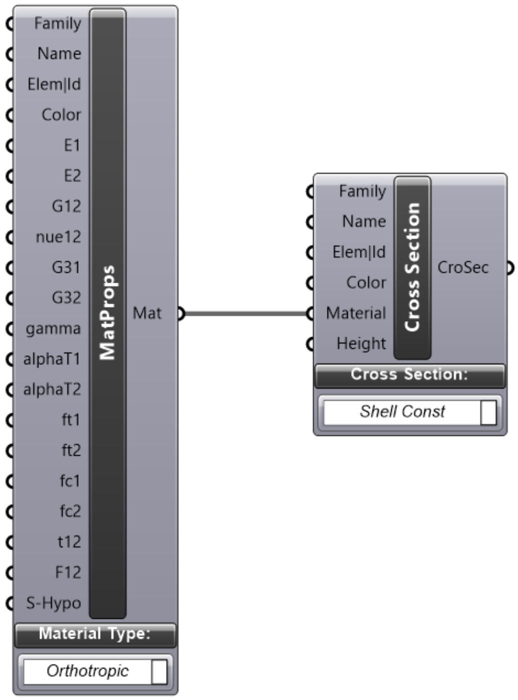


**Figure 3.4:** Available parameters for creating a cross-section of an orthotropic shell element in Karamba3D

Karamba3D does not recognize a cross-section that has varying material properties and factors that affects the stiffnesses of the material, a so called multi-layered orthotropic cross-section such as a CLT plate. The cross-section properties such as the area and moment of inersia is calculated automatically based on the height of the cross-section, as if it were a solid rectangular cross-section. From this Karamba3D create its own stiffnesses based on the given height and material properties, seen in Figure 3.4. The stiffnesses of the CLT panels can therefore not be calculated as suggested by the CLT handbook (Gustafsson et al., 2019) and Stora Enso (2015), where the cross-section properties is modified based on the Equations in 2.1.

To achieve the correct stiffnesses of the CLT panels, the stiffnesses was calculated according to Equations in 2.1 as suggested and then divided by the cross-section properties based on the height only, as if it was a constant rectangular cross-section. From this, modified material properties was achieved and when given to Karamba3D they were multiplied by the cross-section properties based on the height and the correct stiffnesses was achieved.

By modifying the material properties instead of the cross-section properties the CLT panels will not be able to get correct flexural and axial stiffnesses with the same modified value of the material properties. This is because material properties such as $E_{0,mean}$ and $G_{0,mean}$ as an example, is used for calculating both the flexural and axial stiffness but with different factors and cross-section properties, see Equations 2.1.

The CLT walls in the model was assumed to be loaded axially only when acting as a core, therefore their stiffness properties was modified according to the calculations for axial stiffness; $D_{66}$, $D_{77}$ and $D_{88}$ in Equation 2.1. Since the material properties was modified for axial loading, the flexural stiffnesses of the CLT panels in the model is incorrect, resulting in an incorrect value of the out-of-plane deflection of the slabs in the model.

**Table 3.5:** The modified material properties of CLT 220 L7s-2, CLT 280 L7s-2 and CLT 320 L8s-2 for Karamba3D, modified for axial loading

| | CLT 220 L7s-2 | CLT 280 L7s-2 | CLT 320 L8s-2 |
|---|---|---|---|
| $E1$ $[kN/cm^2]$ | 341 | 357 | 313 |
| $E2$ $[kN/cm^2]$ | 909 | 893 | 938 |
| $G12$ $[kN/cm^2]$ | 48.3 | 48.3 | 48.3 |
| $nue12$ | 0 | 0 | 0 |
| $G31$ $[kN/cm^2]$ | 34.1 | 31.6 | 29.4 |
| $G32$ $[kN/cm^2]$ | 96.9 | 90.7 | 110.2 |
| $gamma$ $[kN/m^3]$ | 4.2 | 4.2 | 4.2 |
| $alphaT1$ $[1/C°]$ | $5 \times 10^{-6}$ | $5 \times 10^{-6}$ | $5 \times 10^{-6}$ |
| $alphaT2$ $[1/C°]$ | $5 \times 10^{-6}$ | $5 \times 10^{-6}$ | $5 \times 10^{-6}$ |
| $ft1$ $[kN/cm^3]$ | 0.425 | 0.442 | 0.393 |
| $ft2$ $[kN/cm^3]$ | 1.065 | 1.047 | 1.098 |
| $fc1$ $[kN/cm^3]$ | $-0.754$ | $-0.778$ | $-0.713$ |
| $fc2$ $[kN/cm^3]$ | $-1.595$ | $-1.57$ | $-1.638$ |
| $t12$ $[kN/cm^3]$ | 0.4 | 0.4 | 0.4 |

The main bearing direction of the core walls was chosen as 2, this direction refers to the local y-axis of the CLT panels, which was modelled such that it corresponded to the global z-axis.

For calculations of modified parameters in Table 3.5, see Appendix A.6.

# 4

# Concepts of stabilizing systems

Based on the base model, several different concepts have been developed which uses different type of stabilizing systems. The concepts that has been analysed in this report is listed in Table 4.1, where explanation regarding the naming of the concepts can be found in Section 4.1. Concepts were also analysed with modifications according to Section 4.2.

**Table 4.1:** Names of analysed concepts of stabilizing systems

| Name | Stabilizing system type | Dimension |
|---|---|---|
| CLT220 | CLT core walls | $220mm$ |
| CLT280 | CLT core walls | $280mm$ |
| CLT320 | CLT core walls | $320mm$ |
| C220 | Concrete core walls | $220mm$ |
| C280 | Concrete core walls | $280mm$ |
| C320 | Concrete core walls | $320mm$ |
| ST500 | Single Truss | $500x320mm^2$ |
| ST990 | Single Truss | $990x625mm^2$ |
| DT500 | Double Truss | $500x320mm^2$ |
| DT990 | Double Truss | $990x625mm^2$ |
| ST990CLT320 | Combined | $990x625mm^2$ & $320mm$ |
| ST990C320 | Combined | $990x625mm^2$ & $320mm$ |
| DT990CLT320 | Combined | $990x625mm^2$ & $320mm$ |
| DT990C320 | Combined | $990x625mm^2$ & $320mm$ |

## 4.1 Concepts

### 4.1.1 Core Walls

In the *Core walls*-concepts, only the core contributes to the stability of the structure. Both concrete- and CLT walls have been evaluated with varying thicknesses, but the thicknesses of the walls was constant over the height for the different concepts. The naming of these concepts is the material followed by the thickness of the walls, where "C" is short for concrete, Concrete (C), "CLT" for CLT and the thickness in $mm$. As an example: CLT220 means CLT walls with 220$mm$ thickness.

### 4.1.2 Truss systems

In the *Truss*-concepts, two different truss systems have been evaluated, Single Truss (ST) and Double Truss (DT). The ST is placed in the middle span of the short side of the building, in an angle of 34°due to the floor height and span length. The DT uses two trusses placed in the outermost spans of the short side of the building, in an angle of 24°due to the floor height and span length, see fig 4.1.

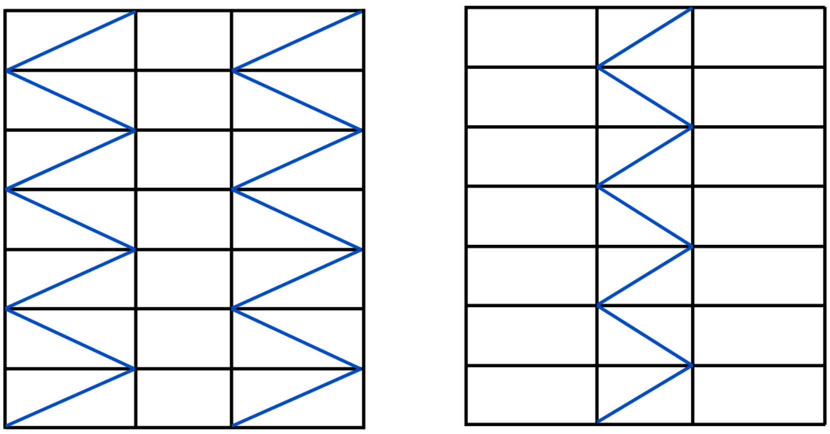

**Figure 4.1:** Illustration of truss concepts with a DT to the left and a ST in the right. Not true to scale.

### 4.1.3 Core walls and Truss systems combined

The combined system is a combination of the core systems and the truss systems. To reduce the total number of concepts, not all combination of dimensions where analyzed.

## 4.2 Modifications of Concepts

The concepts presented in Table 4.1 is also analysed with two different modifications. The first modification was done to increase the mass of the structure by choosing heavier slabs and the second modification of the structure was done to consider the global stiffness reduction from joints between timber elements. The stiffness of the joints were not considered for the regular concepts, meaning they were assumed to be infinite stiff.

### 4.2.1 Heavier slabs (-H)

The concepts where analysed with a CLT slab with a thickness of $300mm$, as in the base model. There was an interest of knowing how the mass of the structure affected the performance, therefore the CLT slabs was also replaced with a concrete slab with a thickness of $250mm$ and analyzed in all of the concepts.

This modification is marked with "-H", for "Heavy" in the end of the concept name.

### 4.2.2 Joint stiffness (-J)

The concepts where analysed with infinite joint stiffness between the elements. This modification was applied in between all the timber elements that was included in the stabilizing system of the structure to analyze how the joints affects the global stiffness. A relatively low stiffness of the joints was chosen to be able to visualize the span between infinite stiff and low stiffness.

This modification is marked with "-J", for "Joint" in the end of the concept name.

#### 4.2.2.1 Joints between CLT walls

The only joint stiffness considered is the shear stiffness of the joints between the walls next to each other. The stiffness of the joints between the walls above and under are not considered, because the core walls are assumed to be post-tensioned so that there is no displacement in the vertical direction. This also means that no cracking is allowed for the concrete and no stiffness of joints in the Concrete wall concepts is considered due to the high stiffness in joints between concrete elements.

The stiffness of the joints between the CLT panels was chosen as $1kN/mm/m$, corresponding to the shear stiffness of one lap joint with STS, tested by Hossain et al. (2019), every meter of wall (vertically). In their report they got results of stiffness between $0.8 - 1.1kN/mm$ of the lap joint with STS shown in Figure 4.2.

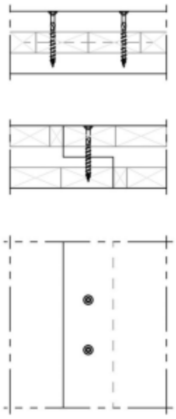

**Figure 4.2:** Lap joint with STS in shear by Hossain et al. (2019)

#### 4.2.2.2 Truss Joints

The stiffness of the joints at the ends of the trusses was chosen according to Hedås and Skoglund (2022), where they are 60% of the stiffness of the beam. The stiffness of the beam is calculated as $\frac{EA}{L}$, where $E$ is the modulus of elasticity in the fibre direction, $A$ is the cross-sectional area and $L$ the length of the truss. In Figure 4.3 an example of such a connection can be seen.

**Figure 4.3:** Connection between Glulam elements MTC solutions (2020)

# 5

# Verification of Karamba3D model

The verification of the Karamba3D model were done by implement a comparative analysis, by creating a similar model in FEM-design, which is another FEA program. Note that the content of the verification does not contribute to the primary results of the report.

## 5.1 Verification of CLT material properties

To verify that the modified CLT material properties that is presented in Table 3.5 was correct, the Karamba3D model was compared with a similar case that was modelled in FEM-Design.

In FEM-design the stiffness matrices of the CLT panels is given, this made it possible to compare it with the actual stiffness given by Stora Enso (2015) to make sure the material properties was correct. By modeling similar models both in Karamba3D and in FEM-design, where the CLT panels were confirmed to be correct, the CLT panels in Karamba3D could be verified. The stiffness matrix values given for the CLT panels used in the report is presented in Table 5.1, given by Stora Enso (2015).

**Table 5.1:** Stiffness Matrix values of CLT panels from Stora Enso (2015)

| | $D_{11}$ | $D_{22}$ | $D_{33}$ | $D_{44}$ | $D_{55}$ | $D_{66}$ | $D_{77}$ | $D_{88}$ |
|---|---|---|---|---|---|---|---|---|
| | $kNm^2/m$ | $kNm^2/m$ | $kNm^2/m$ | $kN/m$ | $kN/m$ | $kN/m$ | $kN/m$ | $kN/m$ |
| CLT 220 L7s-2 | 10115.9 | 975.0 | 398.9 | 21319 | 7509 | 2000000 | 750000 | 106260 |
| CLT 280 L7s-2 | 21133.9 | 1733.0 | 820.3 | 25418 | 8867 | 2500000 | 1000000 | 135240 |
| CLT 320 L8s-2 | 30400.0 | 3733.0 | 1224.6 | 35277 | 9408 | 3000000 | 1000000 | 154560 |

The CLT core walls was assumed to be loaded in-plane and therefore only the axial stiffnesses, $D_{66}$-$D_{88}$, needed to be correct in Karamba3D.

### 5.1.1 CLT walls

The displacements of the walls when loaded vertically was done to verify that the axial stress stiffness was correct, which is the same both in compression and tension and therefore only tested in compression, see Figure 5.1. The displacements of the walls when loaded horizontally was compared to verify that the axial shear stress was correct, see Figure 5.2. The displacement between the models is compared and presented in Table 5.2.

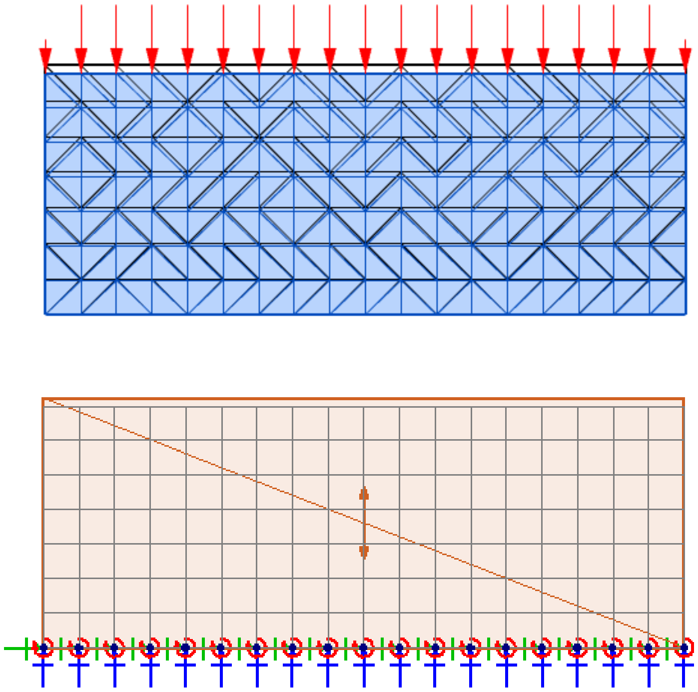

**Figure 5.1:** Axial stress stiffness of CLT wall verified by vertical loading in Karamba3d (Above) and FEM-Design (Below)

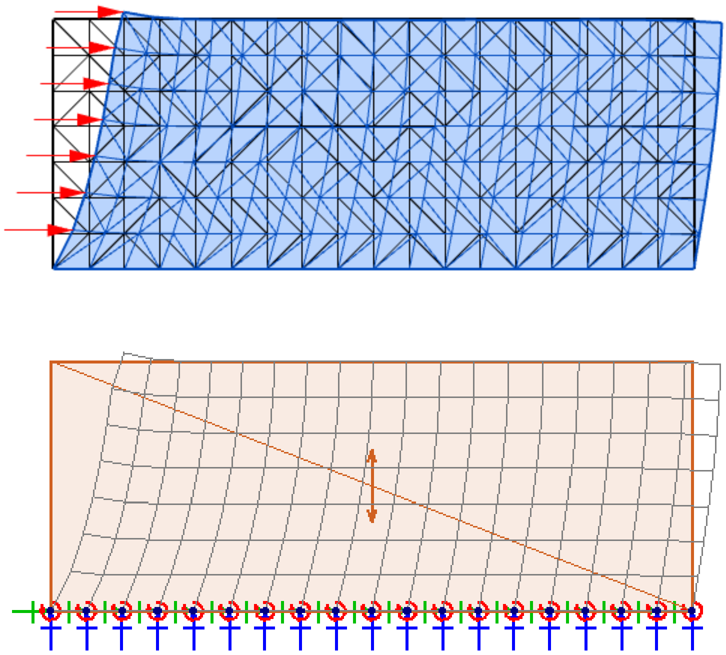

**Figure 5.2:** In-plane shear stiffness of CLT wall verified by horizontal loading in Karamba3d (Above) and FEM-Design (Below)

### 5.1.2 Core of CLT walls

Since the stiffness of the walls in Karamba3D were modified so that they only were correct for axial loading, the assumption that all of the core walls will be axially loaded was verified by measuring the displacement of the entire core loaded horizontally. The displacement is visualised in Figure 5.3 and presented in Table 5.2, where the eigenfrequencies of the cores also is compared to improve the reliability of the verification.

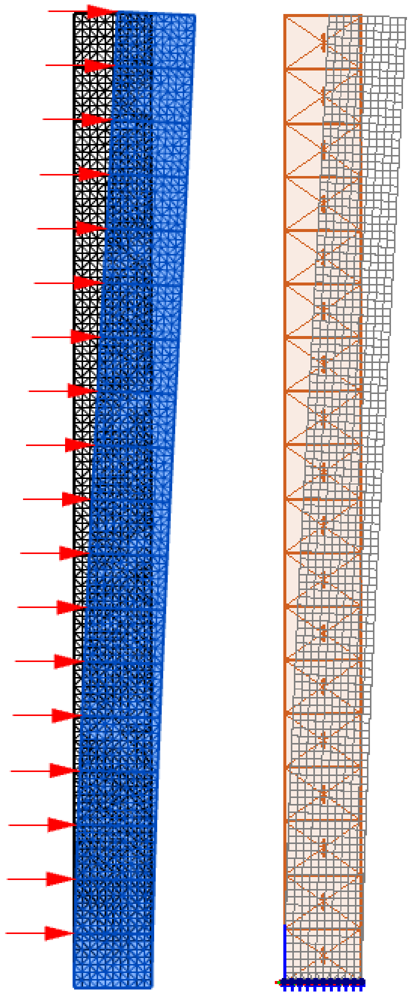

**Figure 5.3:** Axial stiffnesses of CLT walls verified by horizontally loaded core in Karamba3d (left) and FEM-Design (right)

The core includes all of the three CLT walls placed as in the base model, in Table 3.4, with:

- Floor 10-18: CLT 220 L7s-2
- Floor 4-9: CLT 280 L7s-2
- Floor 1-3: CLT 320 L8s-2

**Table 5.2:** Compared parameters of CLT 220 L7s-2, CLT 280 L7s-2 and CLT 320 L8s-2

| CLT wall | Karamba3D | FEM-Design | Difference |
|---|---|---|---|
| Axial stress stiffness | | | |
| Maximum Displacement [mm]: | | | |
| CLT 220 L7s-2 | 1.75 | 1.75 | 0% |
| CLT 280 L7s-2 | 1.40 | 1.40 | 0% |
| CLT 320 L8s-2 | 1.17 | 1.17 | 0% |
| In-plane shear stiffness | | | |
| Maximum Displacement [mm]: | | | |
| CLT 220 L7s-2 | 13.92 | 14.53 | 4.20% |
| CLT 280 L7s-2 | 10.79 | 11.23 | 3.92% |
| CLT 320 L8s-2 | 9.89 | 10.32 | 4.17% |
| Core | | | |
| Maximum Displacement [mm] | 922.80 | 957.04 | 3.58% |
| Eigenfrequency (1st mode) [Hz] | 1.359 | 1.300 | 4.54% |

## 5.2 Verification of entire structure

Not only the stiffness of CLT core walls affects the stability and the global stiffness of the building, also joint and support conditions with others. The entire building of the base model and some of the concepts and modifications were verified. An horizontal area load was applied on one side of the building to compare deflection between the models, the dynamic performance was also compared.

### 5.2.1 Base model

The building were modelled up with elements according Chapter 3. The support and joint conditions and mesh sizes that was used in the verification of the building is also presented in Chapter 3. Figure 5.4 shows the displacement of the building.

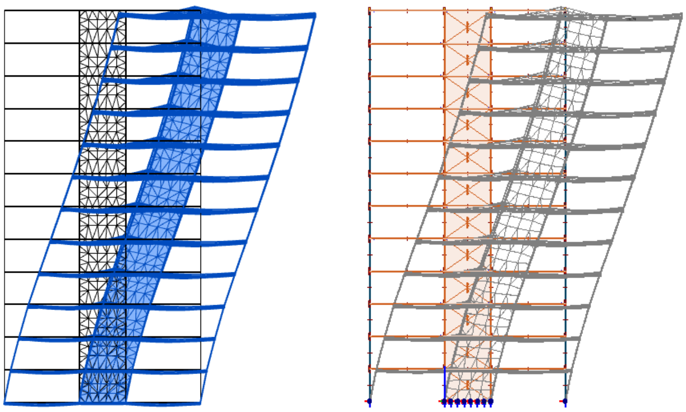

**Figure 5.4:** Upscaled horizontal displacement of base model building with varying core walls, in Karamba3d (left) and FEM-Design (right)

The results of the analysis is presented in Table 5.3. Included in the table is the eigenfrequencies of the first seven modes.

**Table 5.3:** Compared results of modelled buildings in Karamba3D and FEM-design, with varying core walls as in base model

| Parameter | Karamba3D | FEM-Design | Difference |
|---|---|---|---|
| Maximum displacement [mm] | 135.42 | 136.79 | −1.01% |
| Eigenfrequency (1st mode) [Hz] | 0.407 | 0.401 | 1.51% |
| Eigenfrequency (2nd mode) [Hz] | 0.621 | 0.613 | 1.22% |
| Eigenfrequency (3rd mode) [Hz] | 0.951 | 0.932 | 1.95% |
| Eigenfrequency (4th mode) [Hz] | 1.179 | 1.164 | 1.27% |
| Eigenfrequency (5th mode) [Hz] | 1.888 | 1.869 | 1.01% |
| Eigenfrequency (6th mode) [Hz] | 2.137 | 2.119 | 0.85% |
| Eigenfrequency (7th mode) [Hz] | 2.526 | 2.514 | 0.49% |

### 5.2.2 Concepts and modifications

Some variations of concepts and modifications presented in Chapter 4 were also verified by comparing Karamba3D results with results from FEM-design, these are shown in Table 5.4 and illustrated in Figure 5.5.

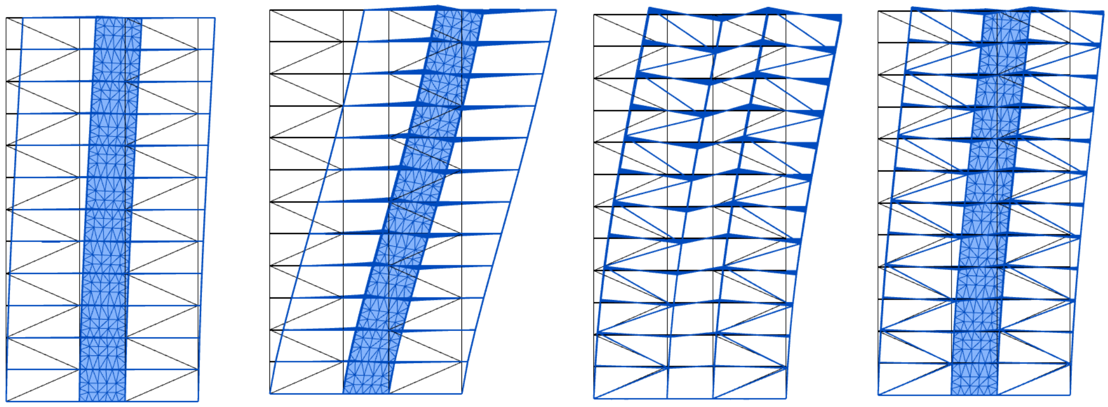

**Figure 5.5:** Upscaled illustration of horizontal displacement of C320, CLT320, DT990 and DT990CLT320 in that specific order from left to right, from Karamba3D

**Table 5.4:** Compared results of variations of concepts and modifications in Karamba3D and FEM-design

| Stabilizing System and Parameters | Karamba3D | FEM-Design | Difference |
|---|---|---|---|
| C320 | | | |
| Maximum displacement [mm] | 18.39 | 18.67 | −1.52% |
| Eigenfrequency of 1st mode [Hz] | 1.425 | 1.403 | 1.55% |
| CLT320 | | | |
| Maximum displacement [mm] | 103.34 | 104.25 | −0.88% |
| Eigenfrequency of 1st mode [Hz] | 0.467 | 0.460 | 1.50% |
| DT990 | | | |
| Maximum displacement [mm] | 60.77 | 61.64 | −1.43% |
| Eigenfrequency of 1st mode [Hz] | 0.939 | 0.992 | 1.86% |
| DT990CLT320 | | | |
| Maximum displacement [mm] | 36.92 | 37.27 | −0.95% |
| Eigenfrequency of 1st mode [Hz] | 1.043 | 1.016 | 2.61% |
| CLT320-H | | | |
| Maximum displacement [mm] | 127.49 | 128.07 | −0.45% |
| Eigenfrequency of 1st mode [Hz] | 0.203 | 0.200 | 1.45% |

# 6
# Methods

The calculations included in the analysis leading to the results of the thesis are based on EC an the swedish national annex *EKS12*. The building is assumed to be located in Göteborg. All other case specific coefficients that has been used in the calculations is presented in Appendix D.

## 6.1 Parametric model

To perform the analysis, a parametric model was built. The model was created in Grasshopper using Karamba3D as FEA program. Figure 6.1 illustrates how the model was constructed followed by description in the following subsections. The full Grasshopper-script can be found in Appendix C.

### 6.1.1 Parameters and and grid

In the first part, the initial geometry of the building was defined. number of sections, span lengths in X- and Y-direction, core size, number of floors and height of each floor is parameters which results in generation of a grid of points. The points are the ground work of the entire model.

### 6.1.2 Element creation

Based on the grid lines, lines were drawn in between points, which later defined the placement of the beams. Similarly, the floor surfaces and core surface were determined in a similar manner. Once the lines and surfaces were created, they were organized and labeled in a way that facilitated the identification and location of individual beams or surfaces.

The surfaces were transformed into meshes as part of the process. In Karamba3D, beam elements only have nodes at their endpoints. To simulate a continuous connection between the slab and beams, the beam was divided into smaller beam elements that corresponded to the size of the mesh. This ensured that the vertices aligned with the beam nodes.

Next, the lines were converted into beam elements, and the meshes were converted into shell elements. Each element was assigned an ID based on the sorting, allowing for the assignment of individual material and geometry parameters, as well as the analysis of specific elements.

### 6.1.3 Model assembly and analysis

The model was assembled by combining the beams and shells. During the assembly, support conditions, joint conditions, and loads were defined. Once the model was assembled, the analysis was performed. The displacement results were exported directly from the analysis. The eigenfrequency and modal mass corresponding to the first transversal mode, as well as the structural height, were used to calculate acceleration and later exported as results.

Subsequently, the structure's height was increased by adding another floor, and the analysis was rerun. This process was repeated until the desired number of floors, in this case, 18 floors, was reached.

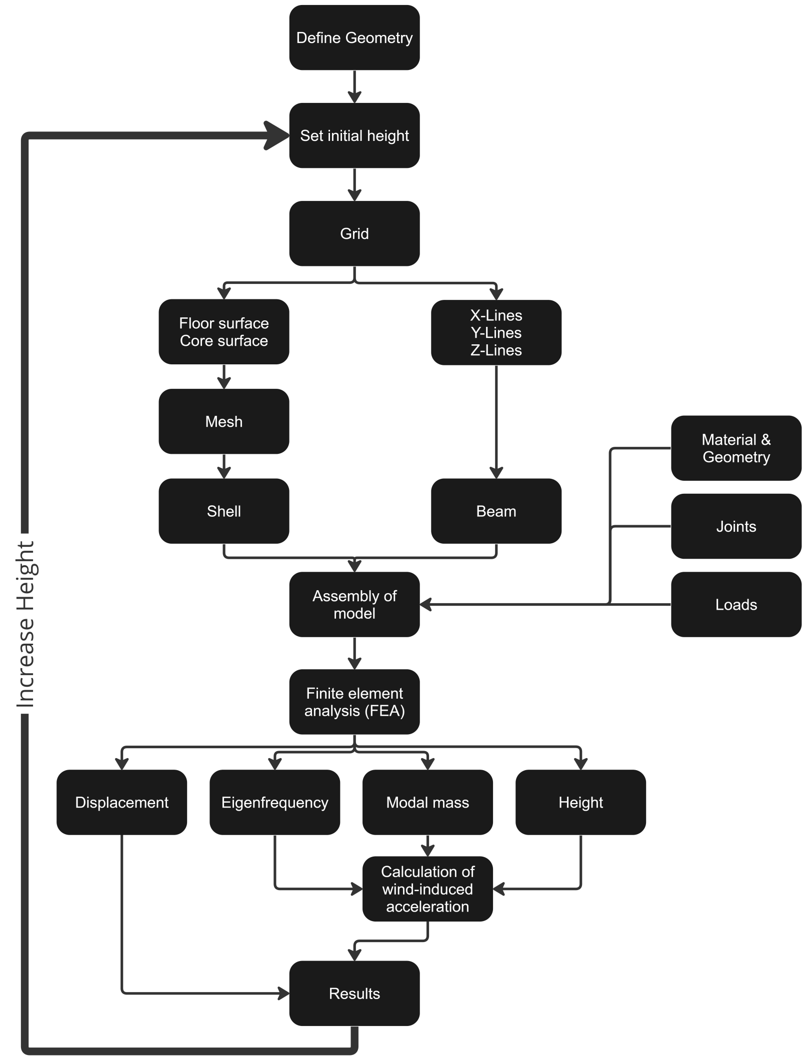


**Figure 6.1:** schematic overview of the parametric model

## 6.2 Static effects

To verify the overall stability of the building, the transversal displacement in the horizontal direction was compared to a displacement relative to the building height of $H/500$. The aim with this limit is to "arrive at a design acheiving the occupant comfort criterion, to limit p-delta effects(...)" (Ackerman et al., 2014). The transversal displacement of the structure was caused by horizontal wind-induced force.

The wind-induced force on the structure was calculated according to EC (CEN, 2005). The governing equation of the force is:

$$F_w = c_s c_d \cdot A_{ref} \cdot c_f \cdot q_p(z_e) \tag{6.1}$$

The structural factor, $c_s c_d$ was set to one meaning that dynamic effects, such as turbulence was not taken into account in the calculation of deflection.

The wind load was applied as a surface load between each storey, where the magnitude of the load was based on the the storeys height above ground. Values are calculated in a scripted python component in Grasshopper and range from approximately 0.7 to 2 $[kN/m^2]$ depending on structural height, see Figure 6.2.

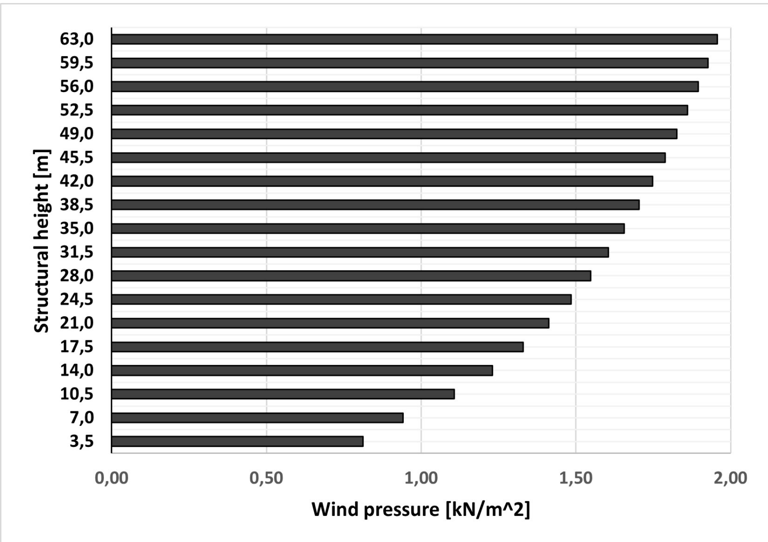


**Figure 6.2:** Wind pressure at different heights

The reference wind, $v_b$, used in calculation of the wind force, $q_p$, depend on the geographical location and spans between 21-26 [m/s] in Sweden and is 25 [m/s] in Göteborg (Boverket, 2022). This wind velocity has a return period of 50 years and is often referred to as $v_{50}$.

## 6.3 Dynamic effects

The demands related to acceleration is not stated in EC, but rather in different ISO-standards.

According ISO10137 (2008), the peak accelerations with a one year return period should not exceed the basic evaluation curve, see Figure 6.3. The curve relates the peak acceleration, $A$, to the first natural eigenfrequency of a building, $f_0$,

According to ISO6897 (1984), the root mean square of the acceleration for a wind with a five year return period shall not exceed the curve in Figure 6.4. Similarly as in ISO10137 (2008), the acceleration is related to the first natural frequency but only in the range from $0.063Hz$ to $1Hz$.

For calculations related to ISO10137 and ISO9897 other wind return periods than $\upsilon_{50}$ is of interest. To calculate the wind velocity for a different return period, the following expression can be used:

$$\upsilon_{T_a} = 0,75\upsilon_{50}\sqrt{1 - 0,2\ln\left(-\ln\left(1 - \frac{1}{T_a}\right)\right)} \tag{6.2}$$

where $T_a$is the number of years. For a wind with a return period of 1 year, the following expression is used (Lykke Christensen, 2023):

$$\upsilon_1 = 0,75\upsilon_{50} \tag{6.3}$$

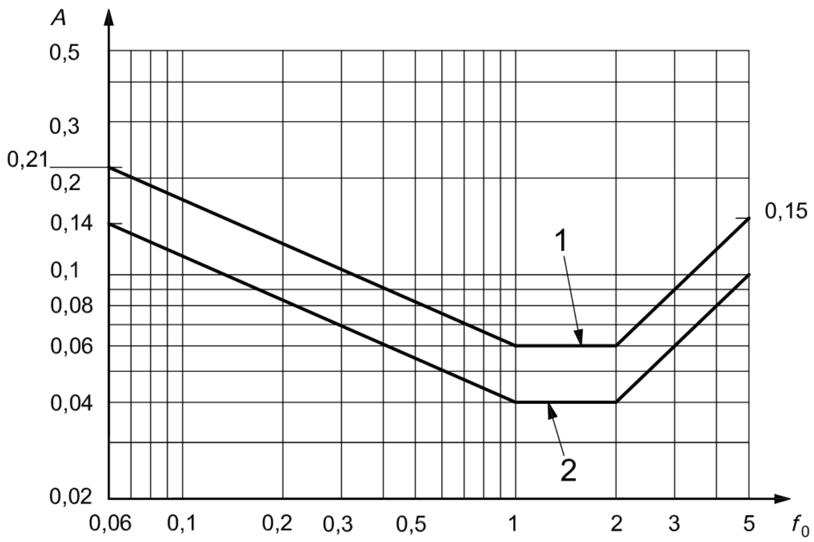


**Figure 6.3:** Evaluationcurve for accelerations for a one-year return period where curve 1 is related to offices and curve 2 for residences (ISO10137, 2008)

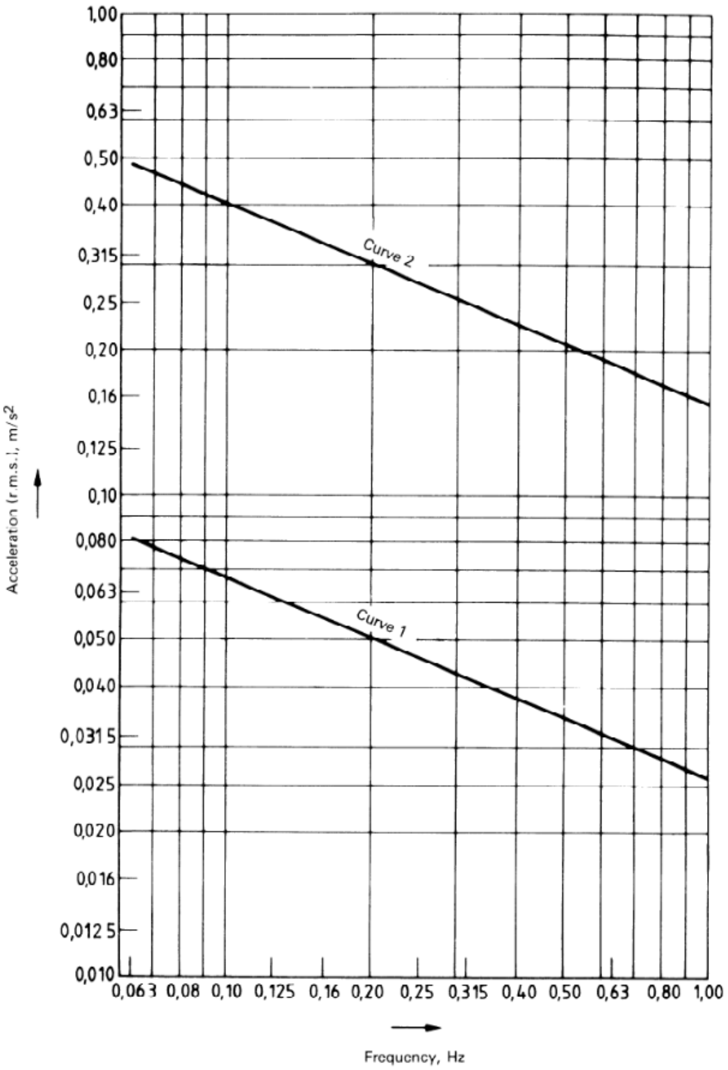


**Figure 6.4:** Evaluationcurve for accelerations for a five-year return period where curve 1 is related to recidences and curve 2 for off shore structures (ISO6897, 1984)

### 6.3.1 Peak acceleration

The peak acceleration of the building is calculated according to EKS12 (Boverket, 2022) as:

$$\ddot{X}_{max} = k_p \cdot \sigma_{\ddot{x}}(z) \tag{6.4}$$

Where the peak acceleration is achieved by applying a peak factor, $k_p$, to the standard deviation of the acceleration, $\sigma_{\ddot{x}}(z)$, which is calculated as:

$$\sigma_{\ddot{x}}(z) = \frac{3I_v(h)Rq_m(h)bc_f\phi_{1,x}(z)}{m_e} \tag{6.5}$$

Included in the calculation of the standard deviation of the acceleration is the eigenfrequency and modal mass of the fundamental flexural mode. The eigenfrequency is notated as $n_{1,x}$ in EKS12 and occurs in several equations, this was given from Karamba3D of each case analysed. The modal mass is involved through the calculation of the equivalent mass per unit length, $m_e$, which is calculated according to Equation 6.6:

$$m_e = \frac{\int_0^h m(z_e) \cdot \phi_1^2(z_e)\, dz_e}{\int_0^h \phi_1^2(z_e)\, dz_e} \tag{6.6}$$

The integral in the nominator of Equation 6.6, $\int_0^h m(z_e) \cdot \phi_1^2(z_e)\, dz_e$, represents the modal mass of the fundamental flexural mode. This integral was replaced by the modal mass was given by Karamaba3D. The fundamental flexural mode, $\phi_1(z_e)$, which is depending on the height above ground, $z_e$, is calculated as:

$$\phi_1(z_e) = (\frac{z_e}{h})^{\xi} \tag{6.7}$$

Where $\xi$ was chosen as 1,5 for slender cantilever buildings.

When the modal mass is calculated in Karamba3D, only the weight of the elements modelled is contributing. To account for additional weight, point-masses was assigned to the model. In the report the weight of following were also accounted for:

- 20% of the imposed load
- Weight of facade
- Weight of installations such as roofing, flooring and non-bearing walls

To account for these in the dynamic analysis, four point masses of 38650kg located in the corners of the core on each floor, affecting the modal mass and eigenfrequency of the structure.

### 6.3.2 Damping

The logaritmic decrement with regards to aerodynamics damping, $\delta_a$, can be calculated as:

$$\delta_a = \frac{c_f \rho v_m(z_s)}{2 n_l m_e} \tag{6.8}$$

Values for $\delta_s$ for common structure types are stated in the EC. However, no value for timber structures is stated. A. Alawan and J. Larsson (2019) suggests that it can be approximated as:

$$\delta_s = 2\pi\xi \tag{6.9}$$

Where $\xi$ is the damping factor. The value of $\xi$ differ, but is suggested to range between 1.1% and 1.9% for timber buildings with dowel-type connections (Feldmann et al., 2016).

## 6.4 Stresses of stabilizing elements

The maximum stresses of the stabilizing timber elements in the different concepts was achieved by the load cases presented in Table 6.1, which is load combinations in ULS. The load cases are based on recommendations from the Swedish national annex.

**Table 6.1:** Combination of loads

| Name | Load combination |
|---|---|
| 6.10b-Imposed | $1.2G_k + 1.5q_k + 1.5(0.3F_w + 0.7s)$ |
| 6.10b-Wind | $1.2G_k + 1.5F_w + 1.5(0.7s + 0.7q_k)$ |
| 6.10b-Wind (Vertical load favorable) | $1G_k + 1.5F_w$ |

The loads that was included in the load combinations can be found in Section 3.1 and 6.2.

# 7
# Results

The concepts presented in Chapter 4, see Table 4.1, was applied to the base model from Chapter 3. The calculation of the Acceleration and deflection was done according to the methods given in Chapter 6, where the demands and the parametric models structure is also presented, altogether leading to the final results of the thesis. Note that the maximum height analysed for all concepts was 63 meters even though graphs may indicate otherwise.The data used in the analysis of the concepts can be found in Appendix B.1.

Figure 7.1 is showing the concepts maximum structural height without exceeding the criteria, where it can be seen that all the concepts fail by acceleration-related criteria before the transversal deflection criteria.

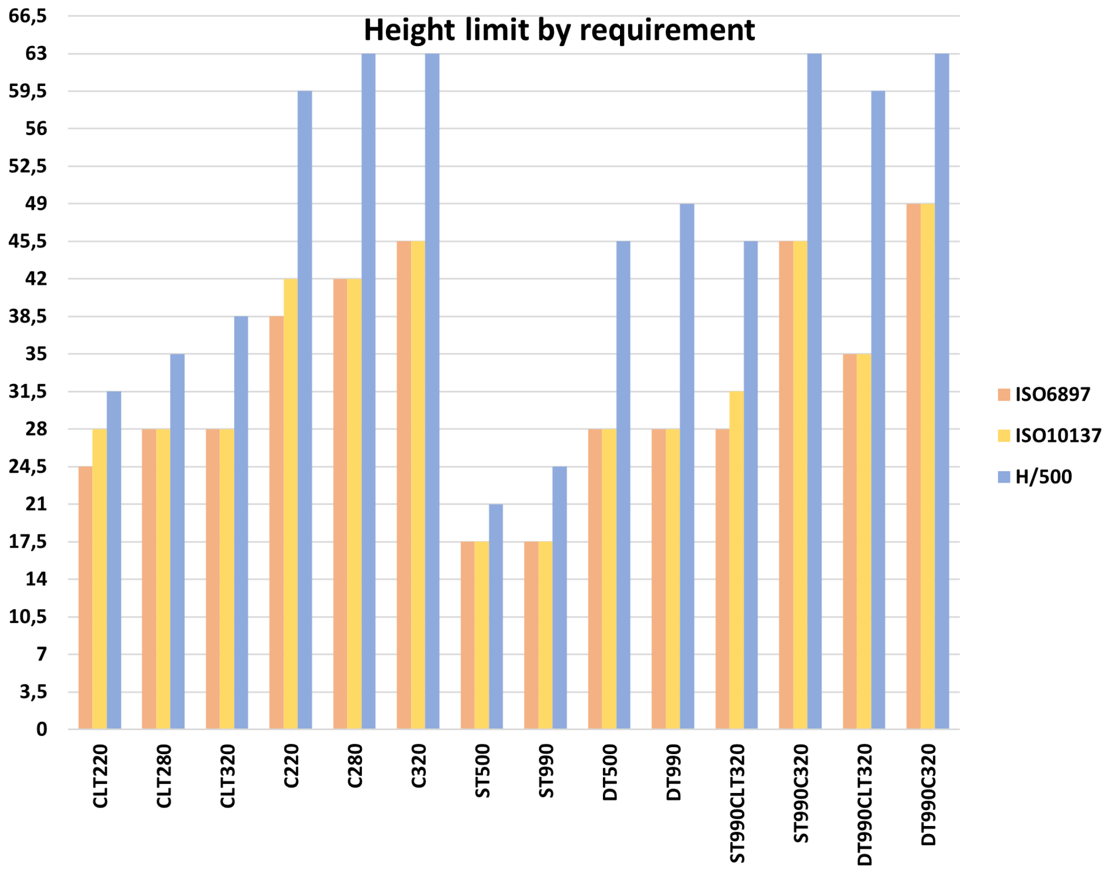


**Figure 7.1:** Height limit of concepts according to dynamic demands from ISO10137, ISO6897 and global deflection demands. Maximum analysed height is 63 meters

## 7.1 Modified concepts

Comparison between the results of the concepts with and without applied modifications is presented, where the choice of presented modification is joint stiffness (-J) for deflection and increased mass (-H) for the acceleration demands. For details about the modifications of the concepts, see 4.2.

Figure 7.2 shows height limit for concepts with a heavier slab (-H). Note that the maximum analysed height for the concepts was 63 meter meaning that some concepts might have reached further if height was increased.

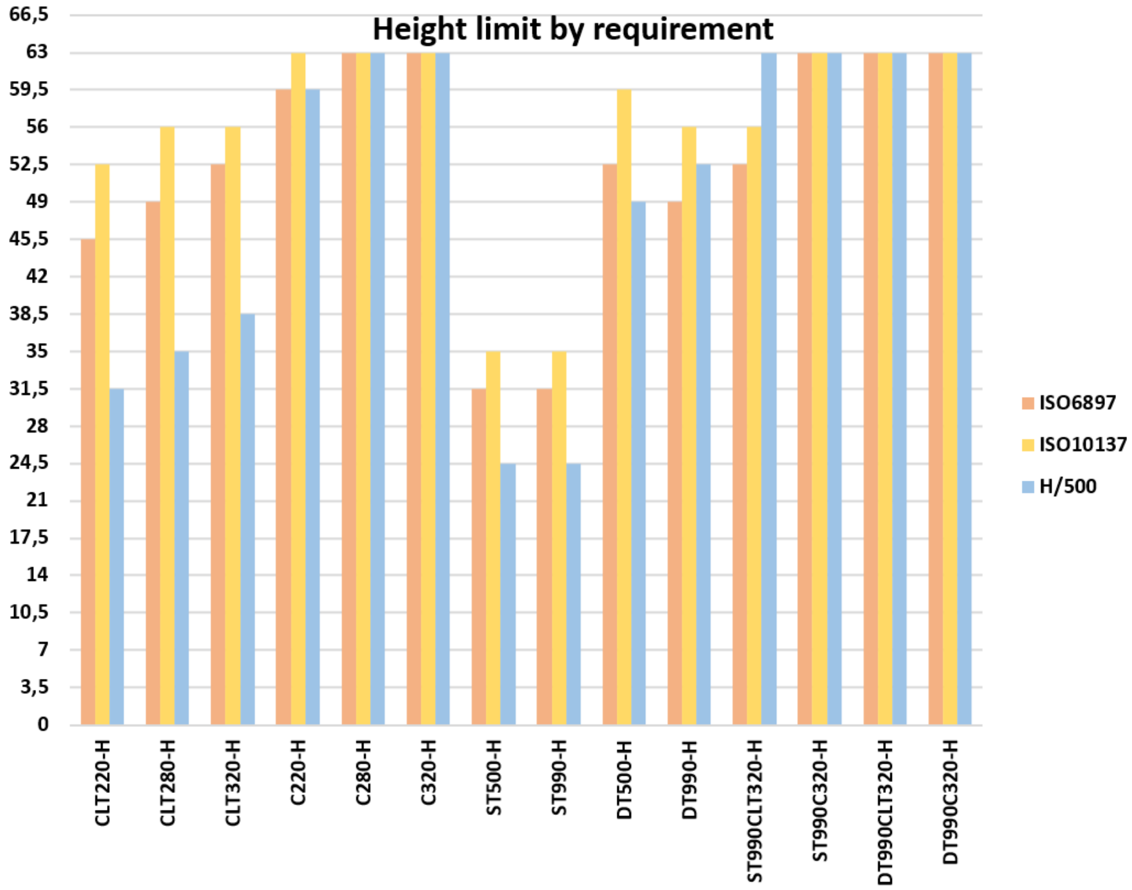


**Figure 7.2:** Height limit of concepts with modified slab according to dynamic demands from ISO10137, ISO6897 and global deflection demands. Maximum analysed height is 63 meters

### 7.1.1 Limit based on acceleration

In Figure 7.3 and 7.4 each concepts height limit is shown based on the criteria given by the two different standards ISO10137 and ISO6897. The concepts is shown with and without the modification of heavier slabs. All the concepts reach a higher structural height with the modified slab. The height increase vary but is at the lowest 14 meters.

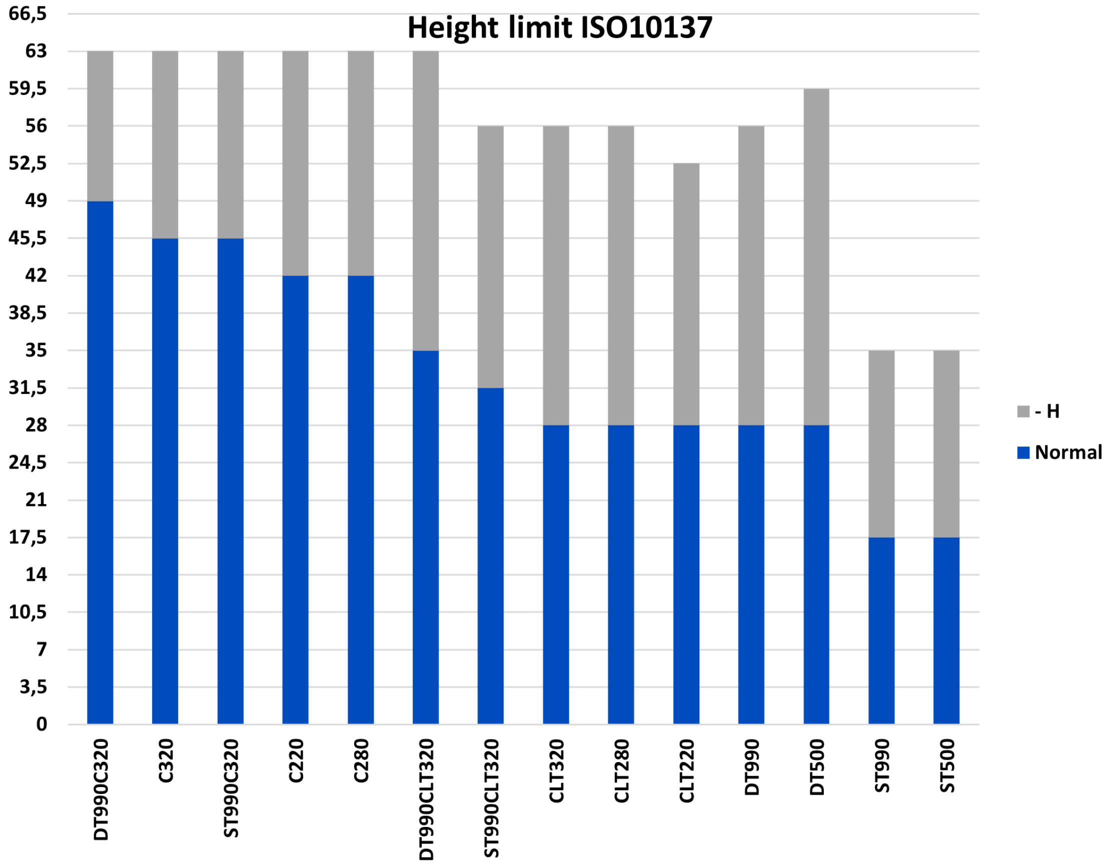


**Figure 7.3:** Height limit according to ISO10137 for concepts with their modified slabs respectively. Maximum analysed height is 63 meters.

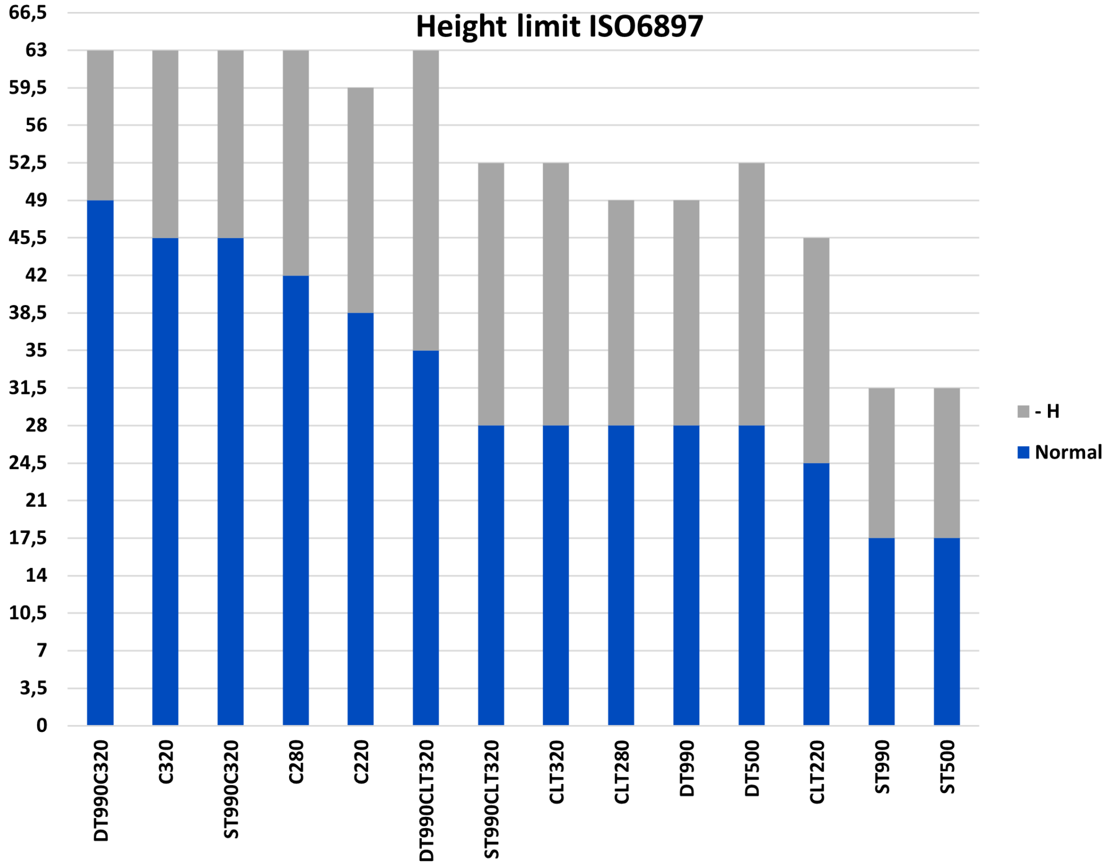


**Figure 7.4:** Height limit according to ISO6897 for concepts with their modified slabs respectively. Maximum analysed height is 63 meters.

In Figure 7.5 and 7.6 all the concepts for all their analysed heights are related to the comfort criteria stated according to ISO-standards. Modified mass reduces both frequency and acceleration. Stiffness has less impact than mass in this matter.

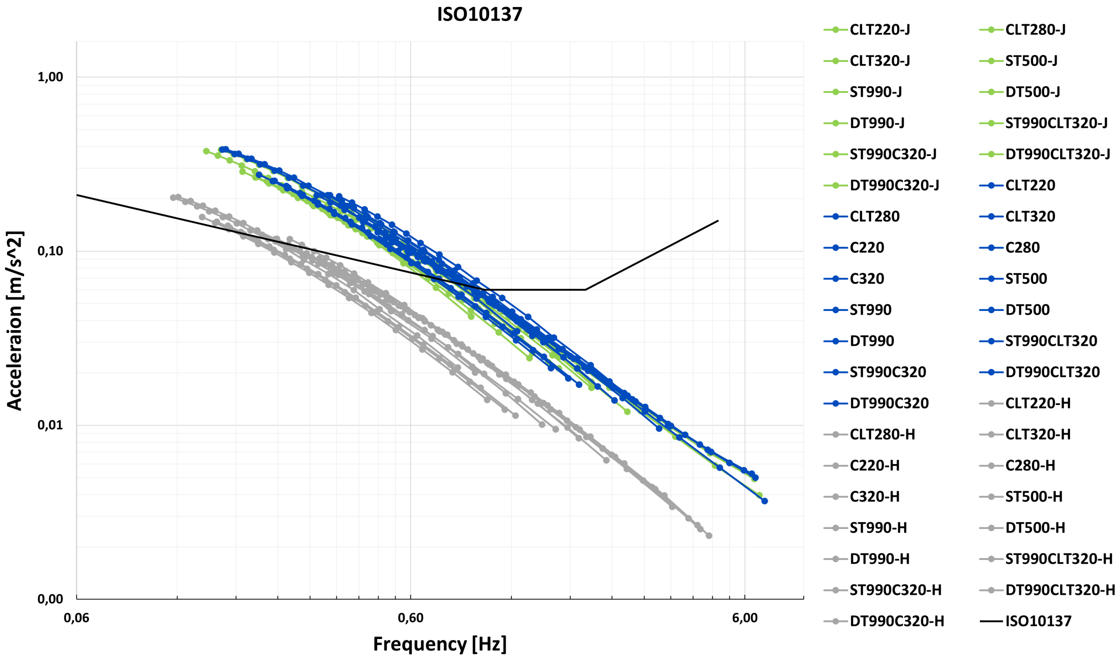


**Figure 7.5:** Effect of modifications on the acceleretion according to ISO10137 illustration

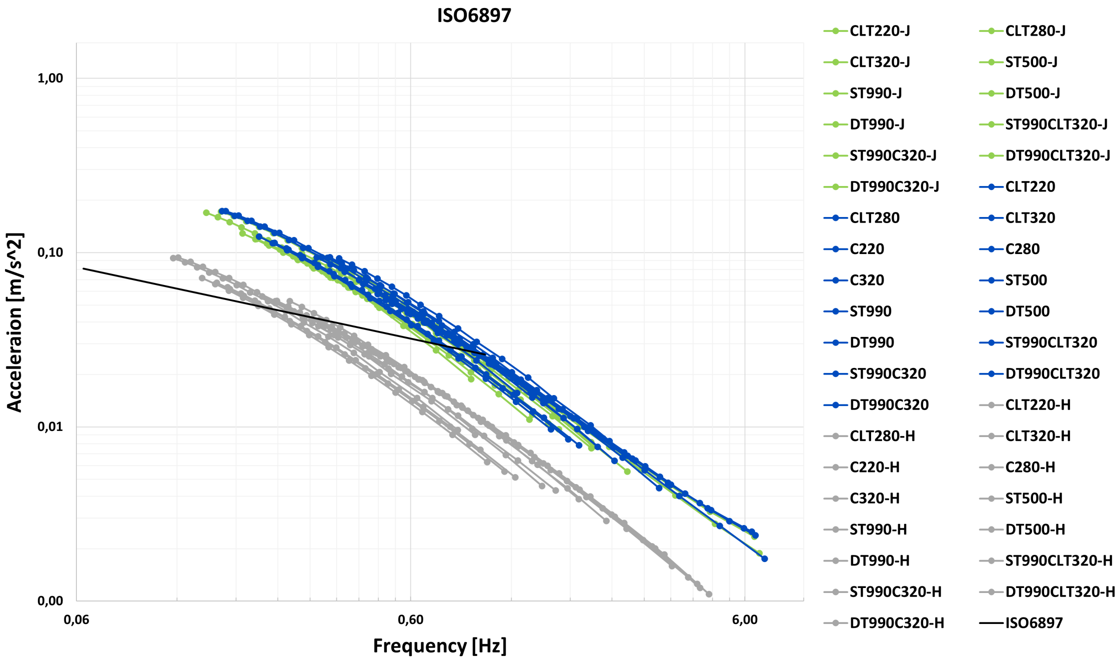


**Figure 7.6:** Effect of modifications on the acceleretion according to ISO6897 illustration

### 7.1.2 Limit based on deflection

In Figure 7.8, the height limit for the concepts with and without their modified joints is presented. Fully green stack means that there is no difference in height when joints were applied and fully blue means that no joint was applied.

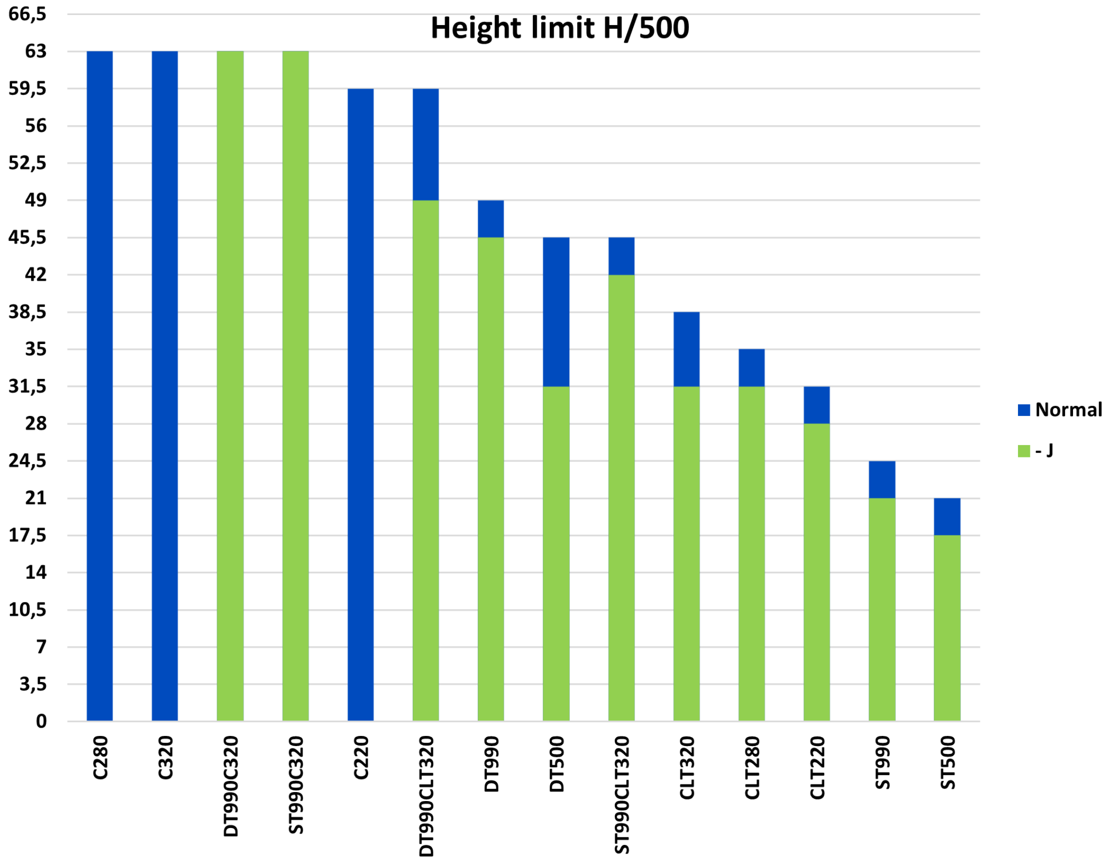


**Figure 7.7:** Height limit due to maximum deflection H/500 for concepts with their modified Joints respectively.

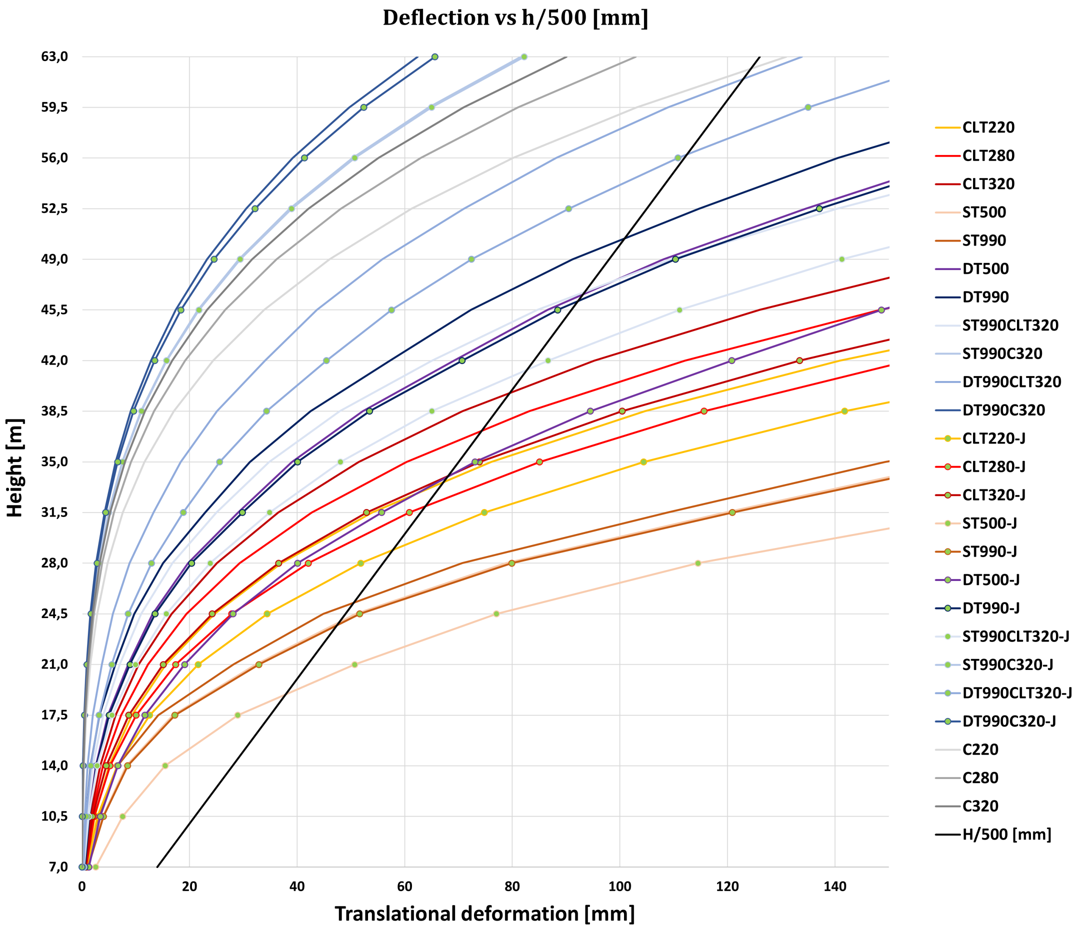


**Figure 7.8:** Graph of concepts with their modified Joints respectively and the demand of maximum deflection H/500

### 7.1.3 Overall limit

The overall limits of the concepts with and without the modifications is shown in Figure 7.9, where the maximum building height of the different concepts and modifications depends on varying demands.

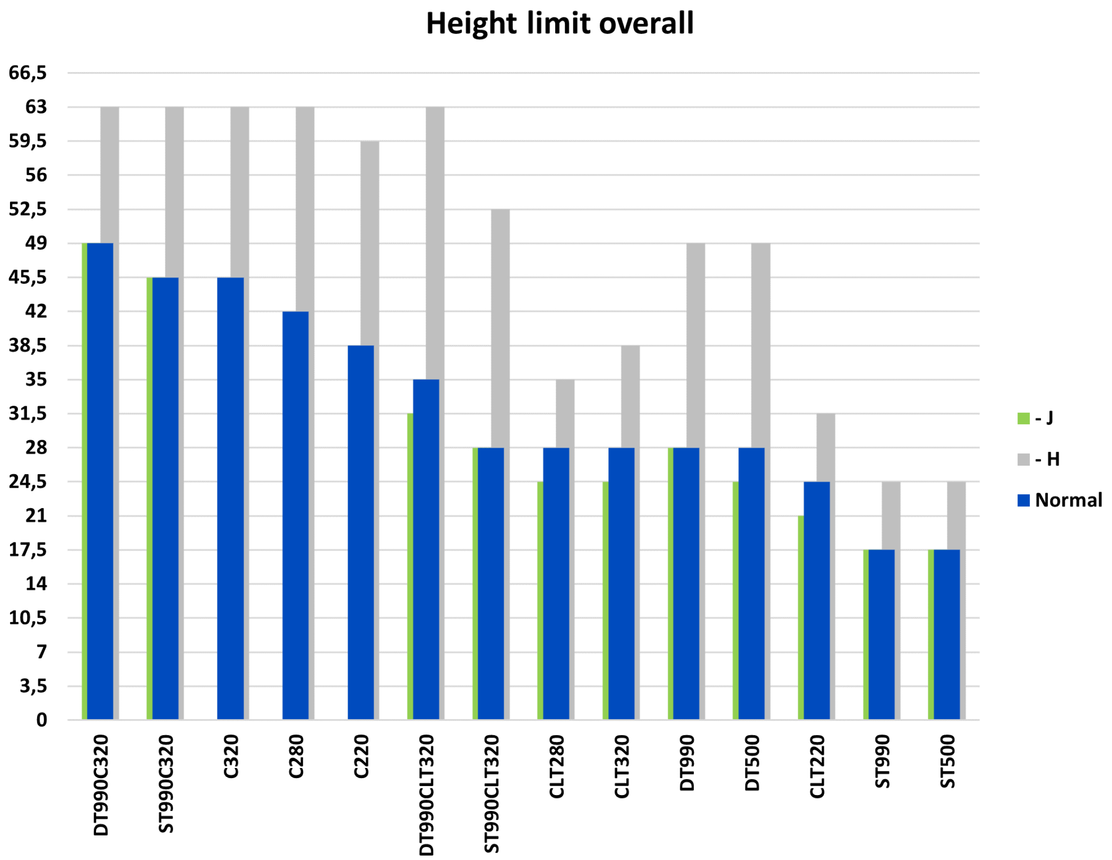


**Figure 7.9:** Height limit of the concepts and the concepts with their modifications

## 7.2 Maximum stresses of stabilizing elements

Once the height limit for the concepts has reached the maximum heights based on the stabilizing demands; transversal deformation and acceleration, presented in Figure 7.1 and 7.2, the maximum stresses in the elements was calculated with Karamba3D. The maximum stresses was calculated with a structure at the maximum height of each concept with ULS load combinations according to Table 6.1.

In the concepts including a CLT core, the CLT walls with the maximum tensile, compressive and shear stress; $\sigma_{max}$, $\sigma_{min}$ and $\sigma_{shear}$, was calculated. The calculated stresses is presented in Table 7.1.

In the concepts including a truss system, the maximum stresses of the trusses and the columns involved in the stabilizing system was calculated. The trusses and columns has either tension or compression, $\sigma_{max}$ or $\sigma_{min}$. These stresses is presented in Table 7.2.

Figure 7.10 shows the elements that is included in the stabilizing systems and where the maximum stresses occurs.

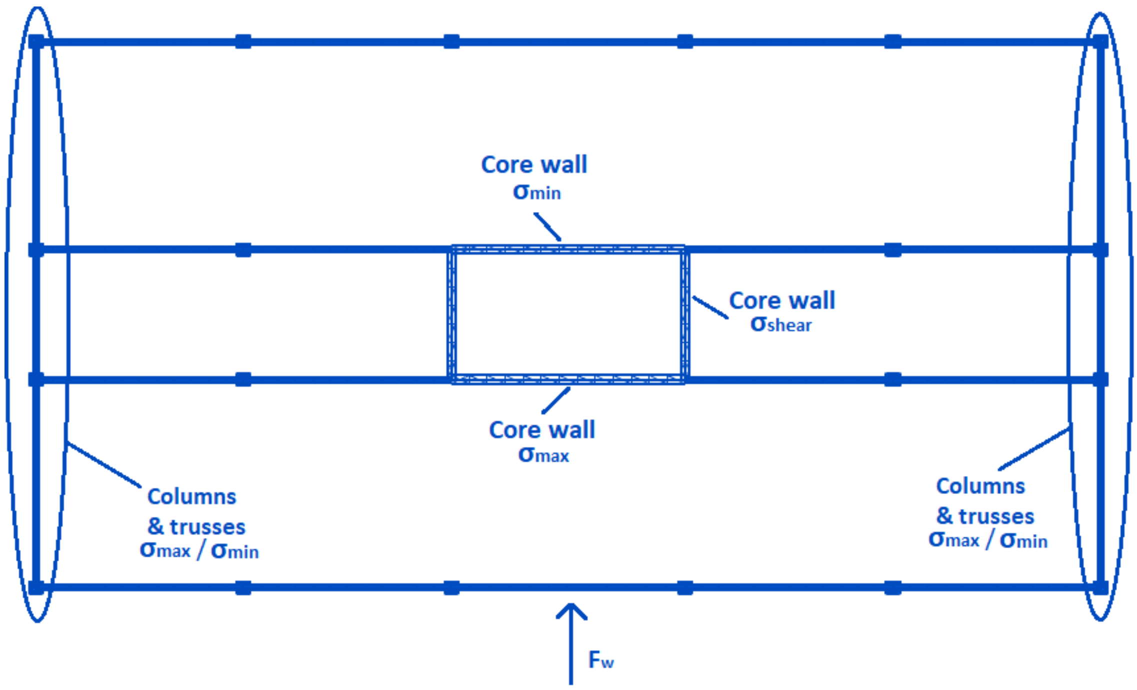


**Figure 7.10:** Stabilizing elements for which the stresses is given

**Table 7.1:** Maximum stresses in CLT core walls at maximum height of the different concepts

| Concept | Max. height $[m]$ | Core walls $(\sigma_{max}/\sigma_{min}/\sigma_{shear})$ $[MPa]$ |
|---|---|---|
| CLT220 | 24.5 | 3.01/-5.72/0.64 |
| CLT280 | 28 | 3.06/-5.49/0.57 |
| CLT320 | 28 | 2.67/-4.84/0.48 |
| CLT220-H | 31.5 | 2.93/-10.57/0.90 |
| CLT280-H | 35 | 3.04/-9.65/0.77 |
| CLT320-H | 38.5 | 3.42/-9.83/0.73 |
| ST990CLT320 | 28 | 1.22/-3.44/0.24 |
| DT990CLT320 | 35 | 0.58/-3.13/0.15 |
| ST990CLT320-H | 52.5 | 2.17/-10.79/0.54 |
| DT990CLT320-H | 63 | -0.51/-9.64/0.33 |

**Table 7.2:** Maximum stresses in trusses and columns involved in the stabilizing systems at maximum height of the different concepts

| Concept | Max. height $[m]$ | Truss $(\sigma_{max}/\sigma_{min})$ $[MPa]$ | Column $(\sigma_{max}/\sigma_{min})$ $[MPa]$ |
|---|---|---|---|
| ST500 | 17.5 | 3.59/-2.96 | 3.17/-13.32 |
| ST990 | 17.5 | 0.94/-0.77 | 2.98/-13.59 |
| DT500 | 28 | 3.09/-2.9 | 1.77/-10.22 |
| DT990 | 28 | 0.82/-0.78 | 1.40/-10.53 |
| ST500-H | 24.5 | 5.67/-5.05 | 2.79/-21.15 |
| ST990-H | 24.5 | 1.47/-1.31 | 2.52/-21.42 |
| DT500-H | 49 | 6.4/-6.4 | 1.98/-18.83 |
| DT990-H | 49 | 1.66/-1.71 | 1.50/-19.61 |
| ST990CLT320 | 28 | 3.03/-2.95 | 2.42/-12.12 |
| ST990C320 | 45.5 | 2.9/-3.15 | -0.5/-9.88 |
| DT990CLT320 | 35 | 2.25/-2.80 | 1.22/-9.87 |
| DT990C320 | 49 | 2.34/-2.79 | -0.18/-8.9 |
| ST990CLT320-H | 52.5 | 8.27/-8.66 | 1.62/-26.25 |
| ST990C320-H | 63 | 6.55/-9.2 | -1.73/-18.31 |
| DT990CLT320-H | 63 | 6.35/-7.65 | 1.00/-21.57 |
| DT990C320-H | 63 | 5.92/-7.59 | -1.39/-16.38 |

# 8
# Discussion

## 8.1 Limitations

The total height of the structure were limited to 18 floor of 3,5m height each, resulting in a total structural height of 63m. This limitation was considered reasonable since the results showed that the structures with timber were struggling to cope with the acceleration demands already at 35m of height.

The calculation of the peak acceleration (Equation 6.4) can only be applied for the fundamental flexural mode. Even though the first mode shape in some of the cases was the rotational mode shape, only the first transversal mode shape in the weak direction was considered. This limitation was done since the building that is analysed is symmetric and therefore it was considered unlikely for a rotational mode to occur as the first mode from a wind-induced force. Most likely, the accelerations in the rotational mode would also be small. To be able to ignore the rotational mode, support conditions in each outer corners of the building and core was modelled. The horisontal support conditions where set to lock the building in the strong direction, resulting in transversal mode shapes in the weak direction only. Since the building could only move in the weak direction, only the trusses that contributes to the stiffness in that direction was modelled, since trusses perpendicular to the wind direction direction does not contribute to the stiffness in the parallel direction.

$c_sc_d$ is the factor calculating wind load that takes into account the dynamical effect. In the analysis this value was set to one, meaning that no dynamical effects where taken into consideration. This was done mainly for two reasons: The first being that calculating $c_sc_d$ needs model properties such as eigenfrequency. This means that this has to be calculated first and then inserted into the model which then can be run again. For each concept, this results in a second analysis which would need computational power. The second reason is based on previous knowledge. The dynamical factor is normally close to 1 meaning that it will not effect the overall results in a significant matter. Based on these two reasons $c_sc_d$ was excluded to save on computational power.

By limiting the study to a rigid foundation, the analysis was simplified and made comparison among concepts easier. However, a rigid foundation is not always the case and it provides stiffness to the structure that maybe isn't there in the first place. Applying a weak foundation to our concepts would most likely make them perform worse than what can be seen now in the results.

The utilization of the elements that is included in the stabilizing systems was not designed in this report, only the maximum stresses of these elements where calculated in Karamba3D in ULS including the wind load. This was done not as a requirement but as an indication for how heavily loaded these elements are to guide future engineers in design.

A parameter that highly effects the outcomes of this thesis is the buildig footprint and overall geometry. The desision regardign these parameters whas done so that the results would reflect a general office building and thereby guide as many engineers as possible. A lot of things can be done in terms of geometry to improve the buildings over all deformation- and dynamical behaviour.

## 8.2 Base model

The aim for the base model was to represent a building that was as generalized as possible, giving the possibility to apply different concepts of stabilizing systems to a variation of geometries. The dimensions of the load-bearing elements included in the base model were designed in regards to the vertical loads.

## 8.3 Concepts and modifications

The choise of concepts of stabilizing systems was done to easier being able to apply these in construction, but also so that data from a big variety of concepts could be analysed to make clear conclusions. The choices were also based on stabilizing systems that is commonly used in existing timber structures, such as the ones presented in Section 2.6 and with the systems presented in Section 2.5. For a better understanding about how the dimensions of the timber elements affects the stability of the structure, different dimensions of the same types of concepts were compared.

The deflection of the concepts is reduced when applying the modification with the heavier slabs even though the mass should not have an effect on the horizontal deflection. This is because the slabs has a minor influence on the global stiffness of the structure, and therefore the stiffness increases since the concrete slab is more stiff than the CLT slab.

Unlike the modification of adding mass to the structure, the modification of introducing a stiffness of the joints at the stabilizing timber elements was done to achieve a more conservative result. The joints that was suggested in this report for the CLT and Glulam elements has a relatively low stiffness, this gives a clearer picture of the influence of the joint and one could design a more stiff joint knowing that the global deflection of the structure will be somewhere in between. What could be seen here was that the influence of reducing the stiffness of the joints in the stabilizing unit did not have substantial impact.

## 8.4 Karamba3D verification

Verification of the Karamba3D model was performed to check the accuracy of the Karamba3D model used in this study. The Karamba3D model incorporates certain uncertainties, such as manually calculated CLT material inputs and joints between elements. FEM-design is a widely utilized FEA program, therefore comparing the model from Karamba3D with a similar model in FEM-design increases the reliability.

The verification of the CLT panels presented in Table 5.2 was promising, with no difference at all in Axial stress stiffness between the models and with no difference over 5%. We think that the reason for the differences in in-plane shear stiffness of the CLT panels and the maximum displacement and eigenfrequency of the core has something to do with the in-plane shear stiffness calculation in Equations 2.1. The results of the displacement and eigenfrequency between Karamba3D and FEM-design was also below 5% and with that, the assumption of the core only being loaded axially was considered confirmed.

The verification of the entire structure was performed to increase the reliability of the model in regards to boundary conditions, mesh and such. To limit the time of analysis, the buildings tested were set to 12 floors. In the verification of the base model, the eigenfrequencies of the first seven modes was compared even though only the eigenfrequency of the first transversal mode in the weak direction was of interest in the results of this report. This was done because the eigenfrequencies depends on the stiffness and mass, as well as the boundary conditions in varying directions and mode shapes. With this, comparing the eigenfrequencies of several modes was considered as a great way to verify the modeling entire building. The verification of the base model showed very promising results, with the largest difference of 1.95% and was therefore considered verified. The same goes for the verification of the concepts with and without modifications, which was performed in a similar manner. The largest difference here was in the combined system of double truss and CLT core walls, with 2.61%.

Karamba3D is considered reliable enough for the analysis performed in this report.

## 8.5 Methods

Using a parametric design software for this type of project/analysis is a good fit. Not only is the model versitile and alterations and changes can easily be incorporated. The built in FEM program also allows for very rapid results which is highly appriciated in early design stages where alterations come often. What can be problematic however is realising misstakes. Both Grasshopper and Karamba3d always tries to run the entire script by finding a way that works, even though it might not be how you think it works. It rarely gives error messages suggesting a possible misstake in design of the code. This means that one has to be very careful with what comes out of the model and perfom suitable verifications within the program so that one can be sure that it is accually doing what you think it is. That is also why we chose to do verifications in FEM-Design to have comparable results and make sure that our model is working correctly.

## 8.6 Results

Out of the pure timber concepts, DT990CLT320 was the one reaching the highest structural height. This seems reasonable since it is the stiffest and also the heaviest out of the concepts. Interestingly, this concept only reaches 35 meters when using the normal lightweight slabs. One of the guiding structures when developing this stabilizing system was Mjöstornet at 85 meters approximately. As Abrahamsen (2018) wrote, they had to use concrete slabs to solve effects related to acceleration. This makes total sense in relation to our results. We can see that with heavier slabs we could reach at least 63 meters and possibly even further. Even though Mjöstornet doesn't have all slabs in concrete, with an optimized placement of them in the top of the building, will have a huge impact, i.e placing them on the upper floors of the building.

The concepts was initially analyzed without any modifications. There were some difficulties to pass the demands in regards to accelerations, due to the relatively low mass of the timber structure. The modification of increasing the weight of the slabs was analysed and presented as a suggested solution to pass the acceleration demands, which seemed like a realistic modification of the structure when comparing with other existing timber structures.

What is clear is that mass is of great importance when designing a building in accordance with the comfort criteria. The results of the report shows that some concepts may have its structural height increased by 28 meters or more by increasing the slab weight. The thesis also shows that by changing dimensions in the structural system, the stiffness and mass is increased, but the mass increase is relatively small compared to the mass one receives from changing the slab type. As described in Chapter 2, due to the modal shape of the fundamental mode, increasing the mass in different positions of the building has different amount of impact. If one still wants to use concrete as slab material to increase mass, its placement should be optimized so that more mass is placed in the higher parts of the building.

In this thesis, we modified the slab to one representing a concrete slab, but important remark is that it is not the material concrete that is of importance, it is its mass. Since the goal is to reduce environmental impact using concrete would be contradictory. If one could solve a slab system having layers of sand or anything else with a high density, this would be just as beneficial from a stability point of view. Another potential slab type is to use a hybrid slab consisting of both timber and concrete.

Figure 8.1 illustrates how the change of stiffness and mass affects the peak acceleration and frequency of the structure and also comparing it with the ISO10137 demand.

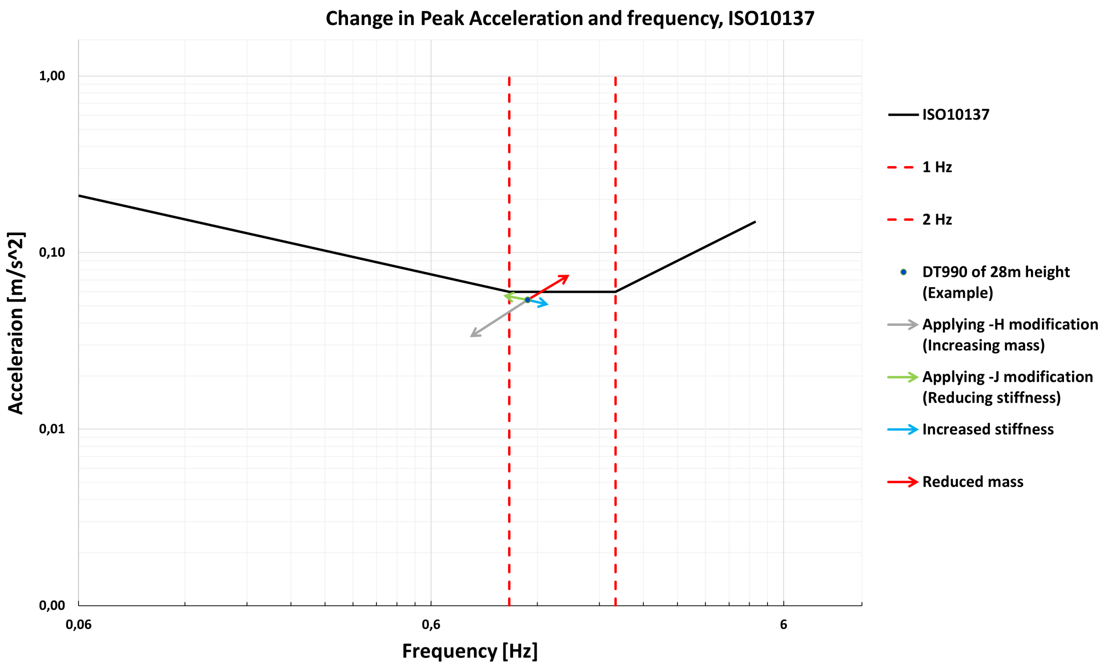


**Figure 8.1:** Illustration of change in stiffness and mass in regards to ISO10137 demands

It can be seen in Figure 8.1 that in the case of an 28m high building with DT990, the frequency is close to 1Hz. In that case, increasing the mass is recommended, since it does not only decrease the frequency but also the acceleration of the structure. By decreasing the frequency in the span between 0 and 1 Hz, the acceleration limit increases, making it easier to pass the criteria. In a case where the structure would end up closer to 2Hz, the recommended measure is to increase the stiffness of the structure. This results in an increased frequency since it increases the acceleration limit when the frequency is higher than 2Hz. Decreasing the stiffness or mass is not recommended in regards to the dynamic effects of the structure.

The difference in stiffness between concepts does not affect their chances of passing the demands from ISO6897 or ISO10137 significantly. However, it has great impact on the deflection of the building. Interestingly, reducing the joint stiffness in the stabilizing system did not have as large impact as originally thought. In the concepts with a truss one reason for this could be that most of the load in our trusses is carried in the vertical columns, which have the same dimensions in all concepts. Elements where joints where applied only handle the shear forces, which in comparasion has a relatively small impact on the overall behaviour. This would also explain why a truss with a larger dimension neither has a significant impact.

By looking at the overall engineering praxis of designing a structure with a transverse deflection of maximum H/500, this report shows that the praxis works even for accelerations if the heavier slabs is applied. Since concrete slabs is more common in todays construction, this rule of thumb holds. When trying to build more lightweight with a timber-slab similar to the one used in this thesis, H/500 is far from a rule of thumb since acceleration-demands are exceeded much earlier. The results vary between the concepts making it hard to set a rule of thumb, but a conservative choise would be close to H/1500.

## 8.7 Improvements and future studies

For future research, It would be highly interesting to see how a timber structure could behave if the position of the mass was optimized in order to maximize modal mass and thereby minimize accelerations.

Even though we can see that a CLT core provides stiffness to the structure that helps the building in terms of reaching a higher structural height, many of the existing timber structures have chosen to not use the CLT walls as a stabilizing element. It would be interesting to further evaluate why this is the case and if the possible weakness in the CLT could be improved so that it can be used more in the future.

Designing the elements included in the stabilizing systems of the concepts with the maximum stresses given in the thesis.

# 9 Conclusion

The thesis investigated how well different stabilizing systems in pure timber as well as hybrid systems performs when exposed to wind induced forces. The results of the analysis in this thesis shows that the height limit for the concepts in pure timber range from 17,5 to 35 meters, where the 35 meter structure uses two trusses in each side of the facade along with a CLT core. If the core is changed to concrete, the same concept can have an increased height of 14 meters reaching 49 meters. The height limitation of the pure timber concepts was due to human comfort in regards to dynamics.

It has also been shown that the mass of the structure has a significant impact since it reduces accelerations and therefor increases comfort. By using concrete slabs instead of timber, the maximum height of 63m that was analysed in the thesis could be achieved in some of concepts in terms of acceleration related demands.

By adding enough mass to the structure so that the demands in regard to the dynamics is fulfilled, the deflection of the building will be the governing demand. The deflection is dependent on the stiffness of the structure, where the elements and the connections between the elements contributes to the global stiffness. It is important that the stiffness of the joints is correct, by applying non-rigid joints with a stiffness based on previous research, the stiffness results changes. With the weaker joints, the height is reduced by 3,5 to 14 meters depending on concept in terms of deflection related demands.

# Bibliography

A. Alawan and J. Larsson. (2019). *Stability and dynamic properties of tall timber structures* (Master's thesis). Chalmers University of Technology.

Abrahamsen, R. (2015). World's tallest timber building - 14 storeys in bergen.

Abrahamsen, R. (2018). Mjøstårnet - construction of an 81 m tall timber building.

Abrahamsen, R. (2020). Dynamic response of tall timber buildings under service load: The dynattb research program.

Abrahamsson, T. (2019). *Structural dynamics and linear systems*. Chalmers University of Technology.

Ackerman, C., Sheerin, J., Magee, A., Blundell, S., & Mann, A. (2014). *Tall buildings-structural design of concrete buildings up to 300m tall*. MPA The Concrete Centre; Federation Internationale du beton.

Adolfsson Jörby, S. (2016). *Rätt tätt – en idéskrift om förtätning*. Boverket.

Ali, M. M., & Al-Kodmany, K. (2022). Structural systems for tall buildings. *Encyclopedia*, *2*(3), 1260–1286. https://doi.org/10.3390/encyclopedia2030085

Boverket. (2022). *Boverket föreskrifter och allmänna råd (2011:10) om tillämpning av europeiska konstruktionsstandarder (eurokoder)*.

CEN. (2002). *Eurocode 1: Actions on structures - part 1-1: General actions - densities, self-weight, imposed loads of buildings*. European Committee for Standardization.

CEN. (2005). *Eurocode 1: Actions on structures - part 1-4: General actions - wind actions*. European Committee for Standardization.

Feldmann, A., Huang, H., Chang, W., Harris, R., Dietsch, P., Gräfe, M., & Hein, C. (2016). Dynamic properties of tall timber structures under wind-induced vibration.

Feng, F. (2018). *Design and analysis of tall and complex structures*. Matthew Deans.

Forssellstrappan. (2016). Steghöjd och stegdjup [accessed 2023-02-17]. https://www.forssellstrappan.se/att-valja-trappa-2/steghojd-och-stegdjup/

Gawronski, W. K. (January 2004). *Advanced structural dynamics and active control of structures*. Springer.

Gromicko, N. (n.d.). The history of concrete [accessed 2023-03-19]. *InterNASCHI*. https://www.nachi.org/history-of-concrete.htm

Gustafsson, A., Crocetti, R., Just, A., Landel, P., Olsson, J., Pousette, A., silfverhielm, M., & Östman, B. (2019). *The CLT Handbook (E. Boström and J. Fröbel)*. Swedish Wood.

Gyllensten, S., & Modig, A. (2020). *The 200 m timber tower: A study on the possibilities of constructing a 200 meter tall timber building* (Master's thesis). Chalmers University of Technology.

Hedås, A., & Skoglund, E. (2022). *The 200 m timber tower* (Master's thesis). Chalmers University of Technology.

Hossain, A., Popovski, M., & Tannert, T. (2019). Group effects for shear connections with self-tapping screws in clt. *Journal of Structural Engineering*, *145*(8).

ISO10137. (2008). *Ss-iso 10137:2008 bases for design of structures - serviceability of buildings and walkways against vibration*. SIS Förlag AB.

ISO6897. (1984). *Guidelines for the evaluation of the response of occupants of fixed structures, especially buildings and off-shore structures, to low-frequency horizontal motion (0,063 to 1 hz)*. ISO.

Johansson, C., & Johansson, E. (2021). *Modeling of cross laminated timber in fe analysis* (Master's thesis). Chalmers University of technology.

Karoly A. Zalka. (2013). *Structural analysis of regular multi-storey buildings*. CRC Press.

Lykke Christensen, M. R. (2023). Wind return periods [Private correspondance by email].

Mass timber services. (2023). Cross laminated timber (clt) [Accessed 2023-04-17]. https://masstimberservices.com/products/clt/

Mohammad, M., Douglas, B., Rammer, D., & Pryer, S. E. (2013). *Connections in cross-laminated timber buildings*. FPInnovations; binational Softwood Lumber Council.

MTC solutions. (2020). Designing with internal knife plates [accessed 2023-06-21]. https://mtcsolutions.com/resources/tech-blogs/designing-with-internal-knife-plates/

Parlato. (2023). Structural glulam beam [Accessed 2023-04-17]. https://www.aparlato.com/products/structural-glulam-beam/

Pilkington Floatglas AB. (2015). Glasfakta [accessed 2023-02-27]. https://www.pilkington.com/~/media/Pilkington/Site%5C%20Content/Sweden/0570_Glasfakta2015_SE_1022.a

Stafford Smith, B., & Coull, A. (1991). *Tall building structures: Analysis and design*. Wiley-Interscience publication.

Stora Enso. (2015). Stiffness matrix for stora enso clt [Accessed 2023-04-17]. https://files.engineering.com/download.aspx?folder=ba8c8032-7250-422d-b804-ea359c555ea7&file=15.02.20_StiffenssMatrix.pdf

Stora Enso. (2023). Calculatis [accessed 2023-03-07]. https://calculatis.storaenso.com/

Strömmen, E. N. (2010). *Theory of bridge aerodynamics*. Springer-Verlag Berlin Heidelberg.

Swedish Wood. (2018). Stabilising systems for multi-storey buildings [accessed 2023-01-24]. https://www.swedishwood.com/publications/wood-magazine/2018-3/stabilising-systems-for-multi-storey-buildings/

Swedish Wood. (2023a). From raw material to wood product [accessed 2023-01-23]. https://www.swedishwood.com/wood-facts/about-wood/from-log-to-plank/

Swedish Wood. (2023b). Om limträ [accessed 2023-01-23]. https://www.svenskttra.se/bygg-med-tra/om-limtra/

Swedish Wood. (2023c). Why wood [accessed 2023-01-23]. https://www.swedishwood.com/building-with-wood/construction/

Swedish wood. (2016). *Limträhandboken del 3.*

Swedish wood. (2022). *Design of timber structures volume 1.*

Tacoma Narrows Bridge history. (2023). Tacoma narrows bridge history - bridge - lessons from failure [Accessed 2023-05-10]. https://wsdot.wa.gov/tnbhistory/bridges-failure.htm#6

Timber, I. (2018). Timber:the past,present and future [accessed 2023-03-19]. https://internationaltimber.com/resources/timber-the-past-present-and-future/

Tomasetti, T. (2023). Ascent [accessed 2023-01-27]. https://www.thorntontomasetti.com/project/ascent

Wang, Y., Lu, W., Dai, K., Yuan, M., & Chen, S.-E. (2018). Dynamic study of a rooftop vertical axis wind turbine tower based on an automated vibration data processing algorithm. *Journal of Civil Engineering.*

White arkitekter. (n.d.). Sara kulturhus, skellefteå [accessed 2023-03-19]. https://whitearkitekter.com/se/projekt/sara-kulturhus/

# A
# Indata Appendix

## A.1 Load calculations

# DIMENSIONING LOAD-BEARING ELEMENTS:

## Geometries:

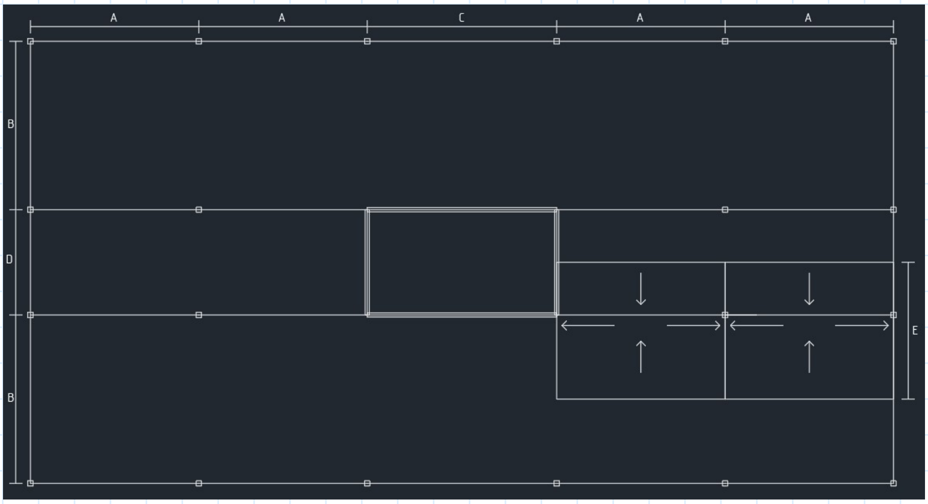


$L_A := 8\ m$ $L_B := 8\ m$ $L_C := 9\ m$ $L_D := 5\ m$

$$L_E := \frac{L_D}{2} + \frac{L_B}{2} = 6.5\ m$$

$A_{ef} := L_A \cdot L_E = 52\ m^2$ $H_{level} := 3.5\ m$

## Self-weights:

$g := 9.807\ \frac{N}{kg}$

$g_{walls} := 0.5\ \frac{kN}{m^2}$ (weight of internal non-bearing walls)

$g_{floor} := 0.15\ \frac{kN}{m^2}$ (weight of floor extension) $g_{walls} + g_{floor} = 0.65\ \frac{kN}{m^2}$

$g_{facade} := 40\ \frac{kg}{m^2} \cdot g \cdot H_{level} = 1.373\ \frac{kN}{m}$ (https://www.pilkington.com/~/media/Pilkington/Site%20Content/Sweden/0570_Glasfakta2015_SE_1022.a)

$$g_{stairs} := \frac{\left(1.375\ m^2 \cdot L_D + 0.175\ m \cdot 2\ m \cdot L_D\right) \cdot 2400\ \frac{kg}{m^3} \cdot g}{6.5\ m \cdot L_D} = 6.246\ \frac{kN}{m^2}$$

(Self-weight of stairs per floor)

$g_{elevator} := \left(1600\ kg + 0.5 \cdot 1200\ kg + 1600\ kg\right) \cdot g = 37.267\ kN$

(Self-weight for 2 elevators with car for 2.8m^2 with capacity for 1200kg, cab weight of 1600kg and counter-weight of 0.5*Capacity+cab weight (https://weightofstuff.com/how-much-does-an-elevator-weigh/)

$g_{roofing} := g_{floor} = 0.15\ \frac{kN}{m^2}$

## Self-weight and dimensions of load-bearing building parts:

$g_{slabs} := 1.5 \ \frac{kN}{m^2}$ (Self-weight of CLT 300 L8s-2 slab, from Calculatis)

$g_{beam} := 0.8 \ \frac{kN}{m}$ (Self-weight of GL32h 800x200 $mm^2$ beam, from Calculatis)

$g_{ybeam} := 0.36 \ \frac{kN}{m}$ (Self-weight of GL32h 360x200 $mm^2$ beam, from Calculatis)

$g_{column\_3} := 1.2 \ kN$ (Self-weight of one GL32h 260x260 $mm^2$ column dimensioned for 3 floors, from Calculatis)

$g_{column\_6} := 2.3 \ kN$ (Self-weight of one GL32h 360x360 $mm^2$ column dimensioned for 6 floors, from Calculatis)

$g_{column\_9} := 3.4 \ kN$ (Self-weight of one GL32h 440x440 $mm^2$ column dimensioned for 9 floors, from Calculatis)

$g_{column\_12} := 4.7 \ kN$ (Self-weight of one GL32h 520x520 $mm^2$ column dimensioned for 12 floors, from Calculatis)

$g_{column\_15} := 6.3 \ kN$ (Self-weight of one GL32h 600x600 $mm^2$ column dimensioned for 15 floors, from Calculatis)

$g_{column\_18} := 7.2 \ kN$ (Self-weight of one GL32h 640x640 $mm^2$ column dimensioned for 18 floors, from Calculatis)

$g_{core\_3} := 3.85 \ \frac{kN}{m}$ (Self-weight of CLT 220 L7s-2 core wall per meter, dimensioned for 3 floors, from Calculatis)

$g_{core\_6} := 3.85 \ \frac{kN}{m}$ (Self-weight of CLT 220 L7s-2 core wall per meter, dimensioned for 6 floors, from Calculatis)

$g_{core\_9} := 3.85 \ \frac{kN}{m}$ (Self-weight of CLT 220 L7s-2 core wall per meter, dimensioned for 9 floors, from Calculatis)

$g_{core\_12} := 4.9 \ \frac{kN}{m}$ (Self-weight of CLT 280 L7s-2 core wall per meter, dimensioned for 12 floors, from Calculatis)

$g_{core\_15} := 4.9 \ \frac{kN}{m}$ (Self-weight of CLT 280 L7s-2 core wall per meter, dimensioned for 15 floors, from Calculatis)

$g_{core\_18} := 5.6 \ \frac{kN}{m}$ (Self-weight of CLT 320 L8s-2 core wall per meter, dimensioned for 18 floors, from Calculatis)

(all core walls and columns is 3.5m)

Variable loads:

$q_k := 3 \ \frac{kN}{m^2}$ (Imposed load, category B.)

$s_k := 1.5 \ \frac{kN}{m^2}$ (Snowload, Göteborg)

Loads acting on beams:

$G_{beam} := \frac{\left(g_{walls} + g_{floor} + g_{slabs}\right) \cdot A_{ef}}{L_A} = 13.975 \ \frac{kN}{m}$ (Dead load on beam from slab)

$q_{beam} := \frac{q_k \cdot A_{ef}}{L_A} = 19.5 \ \frac{kN}{m}$ (Imposed load on beam from slab)

# Loads acting on columns:

$G_{column} := (G_{beam} + g_{beam}) \cdot L_A = 118.2\ kN$ (Dead load on column from one single floor)

$q_{column} := q_{beam} \cdot L_A = 156\ kN$ (Imposed load on column from one floor)

$q_{snowcolumn} := s_k \cdot A_{ef} = 78\ kN$ (Snow load on column from roof)

Floors includes roof with snow. Self-weight of the closest 2 columns above the dimensioned column is neglected.

For 3 floors: $n := 3$

$G_{column\_3} := G_{column} \cdot n = 354.6\ kN$

$q_{column\_3} := q_{column} \cdot (n-1) = 312\ kN$

For 6 floors: $n := 6$

$G_{column\_6} := G_{column} \cdot 3 + G_{column\_3} + g_{column\_3} \cdot 3 = 712.8\ kN$

$q_{column\_6} := q_{column} \cdot (n-1) = 780\ kN$

For 9 floors: $n := 9$

$G_{column\_9} := G_{column} \cdot 3 + G_{column\_6} + g_{column\_6} \cdot 3 = (1.074 \cdot 10^3)\ kN$

$q_{column\_9} := q_{column} \cdot (n-1) = (1.248 \cdot 10^3)\ kN$

For 12 floors: $n := 12$

$G_{column\_12} := G_{column} \cdot 3 + G_{column\_9} + g_{column\_9} \cdot 3 = (1.439 \cdot 10^3)\ kN$

$q_{column\_12} := q_{column} \cdot (n-1) = (1.716 \cdot 10^3)\ kN$

For 15 floors: $n := 15$

$G_{column\_15} := G_{column} \cdot 3 + G_{column\_12} + g_{column\_12} \cdot 3 = (1.808 \cdot 10^3)\ kN$

$q_{column\_15} := q_{column} \cdot (n-1) = (2.184 \cdot 10^3)\ kN$

For 18 floors: $n := 18$

$G_{column\_18} := G_{column} \cdot 3 + G_{column\_15} + g_{column\_15} \cdot 3 = (2.181 \cdot 10^3)\ kN$

$q_{column\_18} := q_{column} \cdot (n-1) = (2.652 \cdot 10^3)\ kN$

## Loads on Core walls:

## FLOOR INDEPENDENT LOADS (Not stacking up):

Applied as uniform load all except at door opening (7.1m):

$$G_{elevator} := \frac{\left(g_{elevator} + 1200\ kg \cdot g\right)}{7.1\ m} = 6.906\ \frac{kN}{m}$$

(Dead load elevator spread out, maximum loaded)

$$q_{snowcore} := s_k \cdot \left(\frac{L_D}{2} + \frac{L_B}{2}\right) \cdot \frac{9\ m}{7.1\ m} = 12.359\ \frac{kN}{m}$$

(Snow load)

$$Q_{snowcore} := \frac{\left(s_k \cdot \left(\frac{L_B}{2} + \frac{L_D}{2}\right) \cdot \frac{L_A}{2}\right) \cdot 2}{7.1\ m} = 10.986\ \frac{kN}{m}$$

(Snow spread from 2 point loads)

$$q_{totsnow} := q_{snowcore} + Q_{snowcore} = 23.345\ \frac{kN}{m}$$

(Total snow load spread out)

Load applied as uniform load on entire wall:

$$G_{core} := \left(g_{slabs} + g_{floor}\right) \cdot \frac{L_B}{2} + g_{stairs} \cdot \frac{L_D}{2} = 22.216\ \frac{kN}{m}$$

(Dead load of slabs and stairs on the core wall)

$$q_{core} := q_k \cdot \left(\frac{L_B}{2} + \frac{L_D}{2}\right) = 19.5\ \frac{kN}{m}$$

(Imposed load from the slabs and stairs on the core wall)

Point loads applied in upper corners of wall:

$$G_{pointcore} := \left(G_{beam} + g_{beam}\right) \cdot \frac{L_A}{2} = 59.1\ kN$$

(Dead load of beam and slab)

$$Q_{pointcore} := q_{beam} \cdot \frac{L_A}{2} = 78\ kN$$

(Imposed load from beam and slab)

Loads Adding up per floor (FOR CALCULATION BELOW):

$$G_{spreadcore} := \frac{G_{pointcore} \cdot 2 + G_{core} \cdot 9\ m}{7.1\ m} = 44.809\ \frac{kN}{m}$$

(Loads from one wall spread out over all except door opening)

$$Q_{spreadcore} := \frac{Q_{pointcore} \cdot 2 + q_{core} \cdot 9\ m}{7.1\ m} = 46.69\ \frac{kN}{m}$$

# FLOOR DEPENDENT LOAD(INCREASES):

Self-weight of the closest 2 walls above the dimensioned wall is neglected. Loads coming from walls above only, spread out and uniformly distributed on all except door openings.

For 3 floors:

$$G_{core\_3} := G_{spreadcore} \cdot 2 = 89.617\ \frac{kN}{m}$$

$$q_{core\_3} := Q_{spreadcore} \cdot 1 = 46.69\ \frac{kN}{m}$$

For 6 floors:

$$G_{core\_6} := G_{spreadcore} \cdot 3 + G_{core\_3} + g_{core\_3} \cdot \frac{9\ m}{7.1\ m} \cdot 3 = 238.684\ \frac{kN}{m}$$

$$q_{core\_6} := Q_{spreadcore} \cdot 3 + q_{core\_3} = 186.761\ \frac{kN}{m}$$

For 9 floors:

$$G_{core\_9} := G_{spreadcore} \cdot 3 + G_{core\_6} + g_{core\_6} \cdot \frac{9\ m}{7.1\ m} \cdot 3 = 387.751\ \frac{kN}{m}$$

$$q_{core\_9} := Q_{spreadcore} \cdot 3 + q_{core\_6} = 326.831\ \frac{kN}{m}$$

For 12 floors:

$$G_{core\_12} := G_{spreadcore} \cdot 3 + G_{core\_9} + g_{core\_9} \cdot \frac{9\ m}{7.1\ m} \cdot 3 = 536.818\ \frac{kN}{m}$$

$$q_{core\_12} := Q_{spreadcore} \cdot 3 + q_{core\_9} = 466.901\ \frac{kN}{m}$$

For 15 floors:

$$G_{core\_15} := G_{spreadcore} \cdot 3 + G_{core\_12} + g_{core\_12} \cdot \frac{9\ m}{7.1\ m} \cdot 3 = 689.878\ \frac{kN}{m}$$

$$q_{core\_15} := Q_{spreadcore} \cdot 3 + q_{core\_12} = 606.972\ \frac{kN}{m}$$

For 18 floors:

$$G_{core\_18} := G_{spreadcore} \cdot 3 + G_{core\_15} + g_{core\_15} \cdot \frac{9\ m}{7.1\ m} \cdot 3 = 842.938\ \frac{kN}{m}$$

$$q_{core\_18} := Q_{spreadcore} \cdot 3 + q_{core\_15} = 747.042\ \frac{kN}{m}$$

## A.2 Slabs

Civil Engineer Student
Oliver Wennerholm

Chalmers

Designer OW

Checker OW


## System

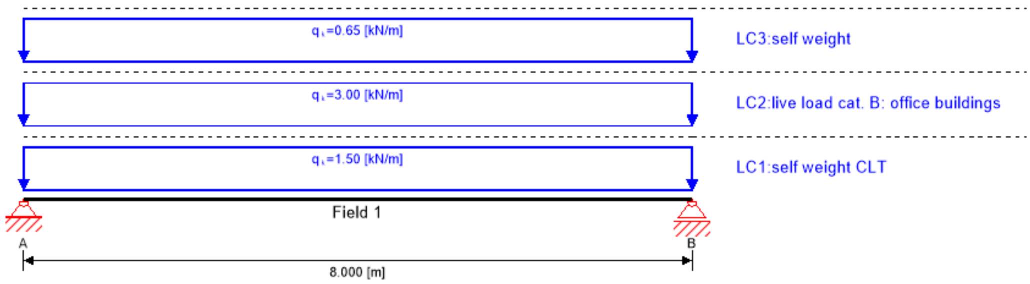


## Global utilization ratio

57 %

| ULS | 25 % | ULS Fire | 16 % | SLS | 57 % | SLS Vibration | 55 % | Support | -1 % |
|---|---|---|---|---|---|---|---|---|---|

## Section: CLT 300 L8s - 2

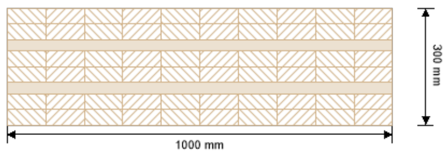


| Layer | Thickness | Orientation | Material |
|---|---|---|---|
| 1 | 40.0 mm | 0° | C24 spruce ETA (2019) |
| 2 | 40.0 mm | 0° | C24 spruce ETA (2019) |
| 3 | 30.0 mm | 90° | C24 spruce ETA (2019) |
| 4 | 40.0 mm | 0° | C24 spruce ETA (2019) |
| 5 | 40.0 mm | 0° | C24 spruce ETA (2019) |
| 6 | 30.0 mm | 90° | C24 spruce ETA (2019) |
| 7 | 40.0 mm | 0° | C24 spruce ETA (2019) |
| 8 | 40.0 mm | 0° | C24 spruce ETA (2019) |
| $t_{CLT}$ | **300.0 mm** | | |

## Material values

| Material | $f_{m,k}$ [N/mm²] | $f_{t,0,k}$ [N/mm²] | $f_{t,90,k}$ [N/mm²] | $f_{c,0,k}$ [N/mm²] | $f_{c,90,k}$ [N/mm²] | $f_{v,k}$ [N/mm²] | $f_{r,k\ min}$ [N/mm²] | $E_{0,mean}$ [N/mm²] | $G_{mean}$ [N/mm²] | $G_{r,mean}$ [N/mm²] |
|---|---|---|---|---|---|---|---|---|---|---|
| C24 spruce ETA (2019) | 24.00 | 14.00 | 0.12 | 21.00 | 2.50 | 4.00 | 1.25 | 12,000.00 | 690.00 | 50.00 |

## ULS Combinations

| | Combination rule |
|---|---|
| LCO1 | 1.35/1.00 * LC1 + 1.35/1.00 * LC3 |
| LCO2 | 1.35/1.00 * LC1 + 1.35/1.00 * LC3 + 1.50/0.00 * LC2 |

## ULS Combinations Fire

| | Combination rule |
|---|---|
| LCO3 | 1.00/1.00 * LC1 + 1.00/1.00 * LC3 |
| LCO4 | 1.00/1.00 * LC1 + 1.00/1.00 * LC3 + 1.00/0.00 * 0.50 * LC2 |

## SLS Characteristic Combination

| | Combination rule |
|---|---|
| LCO5 | 1.00/1.00 * LC1 + 1.00/1.00 * LC3 |
| LCO6 | 1.00/1.00 * LC1 + 1.00/1.00 * LC3 + 1.00/0.00 * LC2 |

**SLS Quasi-permanent Combination**

| | Combination rule |
|---|---|
| LCO7 | 1.00/1.00 * LC1 + 1.00/1.00 * LC3 |
| LCO8 | 1.00/1.00 * LC1 + 1.00/1.00 * LC3 + 1.00/0.00 * 0.30 * LC2 |

**Disclaimer**

## A.3 Beams

Civil Engineer Student Oliver Wennerholm | Chalmers | Designer OW | Checker OW

## System

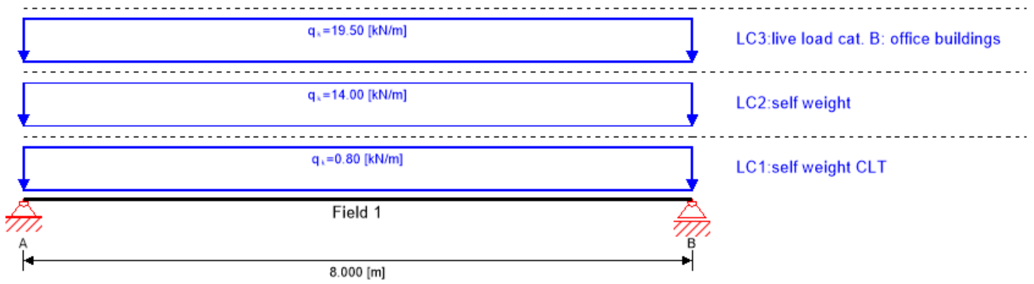


## Global utilization ratio

93 %

| ULS | 92 % | ULS Fire | 93 % | SLS | 64 % | SLS Vibration | 65 % | Support | -1 % | Void | -1 % |
|---|---|---|---|---|---|---|---|---|---|---|---|

## Section: Wooden beam 20/80

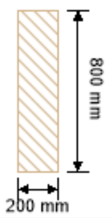


| Section width [cm] | Section height [cm] | Area [mm²] | Iy [mm⁴] | Iz [mm⁴] |
|---|---|---|---|---|
| 20 | 80 | 160,000 | 8,533,334,000 | 533,333,300 |

## Material values

| Material | $f_{m,k}$ [N/mm²] | $f_{t,0,k}$ [N/mm²] | $f_{t,90,k}$ [N/mm²] | $f_{c,0,k}$ [N/mm²] | $f_{c,90,k}$ [N/mm²] | $f_{v,k}$ [N/mm²] | $f_{r,k\ min}$ [N/mm²] | $E_{0,mean}$ [N/mm²] | $G_{mean}$ [N/mm²] | $E_{0,5}$ [N/mm²] |
|---|---|---|---|---|---|---|---|---|---|---|
| GL 32h | 32.00 | 25.60 | 0.50 | 32.00 | 2.50 | 2.50 | 1.20 | 14,200.00 | 350.00 | 11,800.00 |

## ULS Combinations

| | Combination rule |
|---|---|
| LCO1 | 1.35/1.00 * LC1 + 1.35/1.00 * LC2 |
| LCO2 | 1.35/1.00 * LC1 + 1.35/1.00 * LC2 + 1.50/0.00 * LC3 |

## ULS Combinations Fire

| | Combination rule |
|---|---|
| LCO3 | 1.00/1.00 * LC1 + 1.00/1.00 * LC2 |
| LCO4 | 1.00/1.00 * LC1 + 1.00/1.00 * LC2 + 1.00/0.00 * 0.30 * LC3 |

## SLS Characteristic Combination

| | Combination rule |
|---|---|
| LCO5 | 1.00/1.00 * LC1 + 1.00/1.00 * LC2 |
| LCO6 | 1.00/1.00 * LC1 + 1.00/1.00 * LC2 + 1.00/0.00 * LC3 |

## SLS Quasi-permanent Combination

| | Combination rule |
|---|---|
| LCO7 | 1.00/1.00 * LC1 + 1.00/1.00 * LC2 |
| LCO8 | 1.00/1.00 * LC1 + 1.00/1.00 * LC2 + 1.00/0.00 * 0.30 * LC3 |

## Reference documents for this analysis

| English title | Description |
|---|---|
| CERTIFICATE NO. EUFI29-20000564-C | Product certificate |
| LVL G by Stora Enso_Structural design manual column&beam_ V01 | Design manual |

**Reference documents for this analysis**

| English title | Description |
|---|---|
| ETA 20_0291 LVL G by Stora Enso | ETA |

**Disclaimer**

The software was created to assist engineers in their daily business. The software is an engineering software that is dealing with a very complex matter of structural analysis and building physics analysis. Therefore, this software shall only be operated by skilled, experienced engineers, with a deep understanding of structural engineering and building physics related to timber structures. The user of the software is obliged to check all input values, no matter if they were given by the user or given by default by the software and all results for plausibility.
The use of the results of the software should not be relied upon as the basis for any decision or action. Any use of results of the software is only allowed, if the results have been verified and approved regarding completeness and correctness by a project structural/building physics engineer. The user has the possibility to make print-outs from the software. Any modification of those are not allowed.
Stora Enso Wood Products GmbH does not assume any warranty regarding the software. The software has been developed with utmost diligence, nevertheless Stora Enso Wood Products GmbH, neither expressly nor implicitly, provides any warranty in terms of accuracy, validity, timeliness and completeness of information and data created by the software. Stora Enso Wood Products GmbH does also not assume any warranty for the general usability of the software, its suitability for a special purpose or for the compatibility of the software with the ones of third party producers or providers.
Stora Enso Wood Products GmbH is only liable for damages caused by gross negligence or intent through Stora Enso Wood Products GmbH; the liability for slight negligence is excluded. This does not apply to personal injury. Under the aforementioned conditions Stora Enso Wood Products GmbH is as well not liable for operational failures or the loss of programs and/or data of the user's data processing system.
Applicable Law: These terms of use shall be governed by the laws of Austria excluding however any conflict of laws rules and any laws regarding the Convention of the International Sale of Goods (CISG).

## System

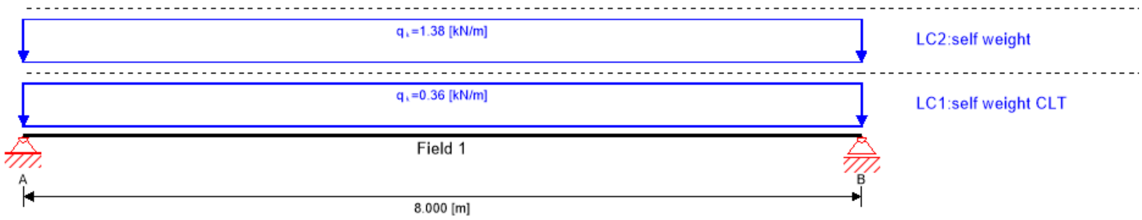


## Global utilization ratio 73 %

| ULS | | ULS Fire | | SLS | | SLS Vibration | | Support | | Void | |
|---|---|---|---|---|---|---|---|---|---|---|---|
| ULS | 27 % | ULS Fire | 42 % | SLS | 50 % | SLS Vibration | 73 % | Support | -1 % | Void | -1 % |

## Section: Wooden beam 20/36

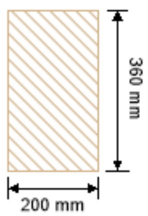


| Section width [cm] | Section height [cm] | Area [mm²] | Iy [mm⁴] | Iz [mm⁴] |
|---|---|---|---|---|
| 20 | 36 | 72,000 | 777,600,100 | 240,000,000 |

## Material values

| Material | $f_{m,k}$ [N/mm²] | $f_{t,0,k}$ [N/mm²] | $f_{t,90,k}$ [N/mm²] | $f_{c,0,k}$ [N/mm²] | $f_{c,90,k}$ [N/mm²] | $f_{v,k}$ [N/mm²] | $f_{r,k\ min}$ [N/mm²] | $E_{0,mean}$ [N/mm²] | $G_{mean}$ [N/mm²] | $E_{0,5}$ [N/mm²] |
|---|---|---|---|---|---|---|---|---|---|---|
| GL 32h | 32.00 | 25.60 | 0.50 | 32.00 | 2.50 | 2.50 | 1.20 | 14,200.00 | 350.00 | 11,800.00 |

## ULS Combinations

| | Combination rule |
|---|---|
| LCO1 | 1.35/1.00 * LC1 + 1.35/1.00 * LC2 |

## ULS Combinations Fire

| | Combination rule |
|---|---|
| LCO2 | 1.00/1.00 * LC1 + 1.00/1.00 * LC2 |

## SLS Characteristic Combination

| | Combination rule |
|---|---|
| LCO3 | 1.00/1.00 * LC1 + 1.00/1.00 * LC2 |

## SLS Quasi-permanent Combination

| | Combination rule |
|---|---|
| LCO4 | 1.00/1.00 * LC1 + 1.00/1.00 * LC2 |

## Reference documents for this analysis

| English title | Description |
|---|---|
| CERTIFICATE NO. EUFI29-20000564-C | Product certificate |
| LVL G by Stora Enso_Structural design manual column&beam_ V01 | Design manual |
| ETA 20_0291 LVL G by Stora Enso | ETA |

## Disclaimer

The software was created to assist engineers in their daily business. The software is an engineering software that is dealing with a very complex matter of structural analysis and building physics analysis. Therefore, this software shall only be operated by skilled, experienced engineers, with a deep understanding of structural engineering and building physics related to timber structures. The user of the software is obliged to check all input values, no matter if they were given by the user or given by default by the software and all results for plausibility.
The use of the results of the software should not be relied upon as the basis for any decision or action. Any use of results of the software is only allowed, if the results have been verified and approved regarding completeness and correctness by a project structural/building physics engineer. The user has the possibility to make print-outs from the software. Any modification of those are not allowed.
Stora Enso Wood Products GmbH does not assume any warranty regarding the software. The software has been developed with utmost diligence, nevertheless Stora Enso Wood Products GmbH, neither expressly nor implicitly, provides any warranty in terms of accuracy, validity, timeliness and completeness of information and data created by the software. Stora Enso Wood Products GmbH does also not assume any warranty for the general usability of the software, its suitability for a special purpose or for the compatibility of the software with the ones of third party producers or providers.
Stora Enso Wood Products GmbH is only liable for damages caused by gross negligence or intent through Stora Enso Wood Products GmbH; the liability for slight negligence is excluded. This does not apply to personal injury. Under the aforementioned conditions Stora Enso Wood Products GmbH is as well not liable for operational failures or the loss of programs and/or data of the user's data processing system.
Applicable Law: These terms of use shall be governed by the laws of Austria excluding however any conflict of laws rules and any laws regarding the Convention of the International Sale of Goods (CISG).

## A.4 Columns

Civil Engineer Student
Oliver Wennerholm
Chalmers
Designer OW
Checker OW

## System

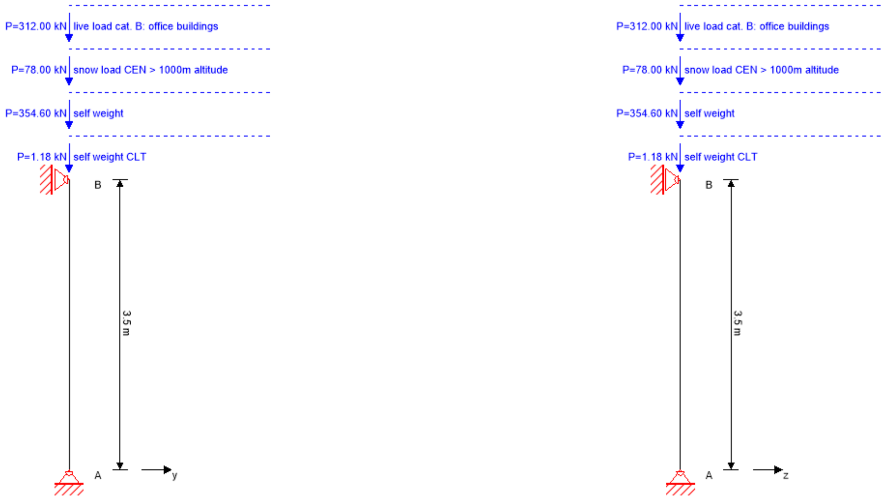


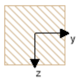


## Global utilization ratio 85 %

| | | | |
|---|---|---|---|
| ULS | 82 % | ULS Fire | 85 % |

## Section: Wooden beam 26/26

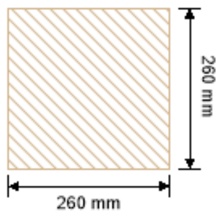


| Section width | Section height | Area | Iy | Iz |
|---|---|---|---|---|
| [cm] | [cm] | [mm²] | [mm⁴] | [mm⁴] |
| 26 | 26 | 67,600 | 380,813,200 | 380,813,200 |

## Material values

| Material | $f_{m,k}$ | $f_{t,0,k}$ | $f_{t,90,k}$ | $f_{c,0,k}$ | $f_{c,90,k}$ | $f_{v,k}$ | $f_{r,k\ min}$ | $E_{0,mean}$ | $G_{mean}$ | $E_{0,5}$ |
|---|---|---|---|---|---|---|---|---|---|---|
| | [N/mm²] | [N/mm²] | [N/mm²] | [N/mm²] | [N/mm²] | [N/mm²] | [N/mm²] | [N/mm²] | [N/mm²] | [N/mm²] |
| GL 32h | 32.00 | 25.60 | 0.50 | 32.00 | 2.50 | 2.50 | 1.20 | 14,200.00 | 350.00 | 11,800.00 |

## ULS Combinations

| | Combination rule |
|---|---|
| LCO1 | 1.35/1.00 * LC1 + 1.35/1.00 * LC2 |
| LCO2 | 1.35/1.00 * LC1 + 1.35/1.00 * LC2 + 1.50/0.00 * LC3 |
| LCO3 | 1.35/1.00 * LC1 + 1.35/1.00 * LC2 + 1.50/0.00 * LC3 + 1.50/0.00 * 0.70 * LC4 |
| LCO4 | 1.35/1.00 * LC1 + 1.35/1.00 * LC2 + 1.50/0.00 * LC4 |
| LCO5 | 1.35/1.00 * LC1 + 1.35/1.00 * LC2 + 1.50/0.00 * LC4 + 1.50/0.00 * 0.70 * LC3 |

## ULS Combinations Fire

| | Combination rule |
|---|---|
| LCO1 | 1.00/1.00 * LC1 + 1.00/1.00 * LC2 |
| LCO2 | 1.00/1.00 * LC1 + 1.00/1.00 * LC2 + 1.00/0.00 * 0.20 * LC3 |

**ULS Combinations Fire**

| | Combination rule |
|---|---|
| LCO3 | 1.00/1.00 * LC1 + 1.00/1.00 * LC2 + 1.00/0.00 * 0.20 * LC3 + 1.00/0.00 * 0.30 * LC4 |
| LCO4 | 1.00/1.00 * LC1 + 1.00/1.00 * LC2 + 1.00/0.00 * 0.30 * LC4 |
| LCO5 | 1.00/1.00 * LC1 + 1.00/1.00 * LC2 + 1.00/0.00 * 0.30 * LC4 + 1.00/0.00 * 0.20 * LC3 |

**Reference documents for this analysis**

| English title | Description |
|---|---|
| CERTIFICATE NO. EUFI29-20000564-C | Product certificate |
| LVL G by Stora Enso_Structural design manual column&beam_ V01 | Design manual |
| ETA 20_0291 LVL G by Stora Enso | ETA |

**Disclaimer**

Civil Engineer Student
Oliver Wennerholm
Chalmers
Designer OW
Checker OW

## System

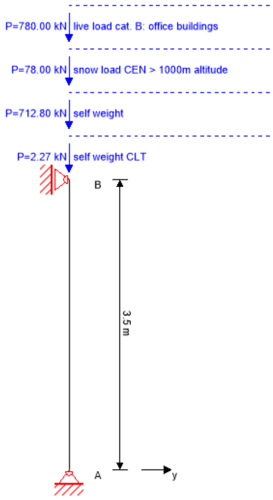


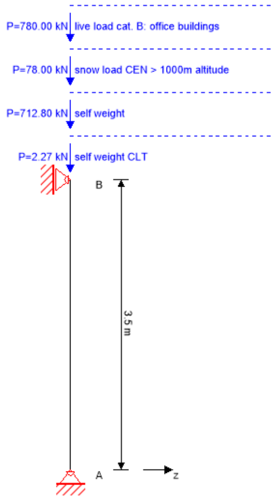


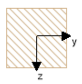


## Global utilization ratio 87 %

| ULS | 87 % | ULS Fire | 42 % |
|---|---|---|---|

## Section: Wooden beam 36/36

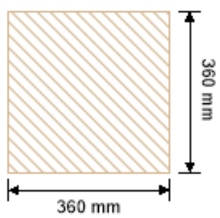


| Section width | Section height | Area | Iy | Iz |
|---|---|---|---|---|
| [cm] | [cm] | [mm²] | [mm⁴] | [mm⁴] |
| 36 | 36 | 129,600 | 1,399,680,000 | 1,399,680,000 |

## Material values

| Material | $f_{m,k}$ | $f_{t,0,k}$ | $f_{t,90,k}$ | $f_{c,0,k}$ | $f_{c,90,k}$ | $f_{v,k}$ | $f_{r,k\ min}$ | $E_{0,mean}$ | $G_{mean}$ | $E_{0,5}$ |
|---|---|---|---|---|---|---|---|---|---|---|
| | [N/mm²] | [N/mm²] | [N/mm²] | [N/mm²] | [N/mm²] | [N/mm²] | [N/mm²] | [N/mm²] | [N/mm²] | [N/mm²] |
| GL 32h | 32.00 | 25.60 | 0.50 | 32.00 | 2.50 | 2.50 | 1.20 | 14,200.00 | 350.00 | 11,800.00 |

## ULS Combinations

| | Combination rule |
|---|---|
| LCO1 | 1.35/1.00 * LC1 + 1.35/1.00 * LC2 |
| LCO2 | 1.35/1.00 * LC1 + 1.35/1.00 * LC2 + 1.50/0.00 * LC3 |
| LCO3 | 1.35/1.00 * LC1 + 1.35/1.00 * LC2 + 1.50/0.00 * LC3 + 1.50/0.00 * 0.70 * LC4 |
| LCO4 | 1.35/1.00 * LC1 + 1.35/1.00 * LC2 + 1.50/0.00 * LC4 |
| LCO5 | 1.35/1.00 * LC1 + 1.35/1.00 * LC2 + 1.50/0.00 * LC4 + 1.50/0.00 * 0.70 * LC3 |

## ULS Combinations Fire

| | Combination rule |
|---|---|
| LCO1 | 1.00/1.00 * LC1 + 1.00/1.00 * LC2 |
| LCO2 | 1.00/1.00 * LC1 + 1.00/1.00 * LC2 + 1.00/0.00 * 0.20 * LC3 |

Civil Engineer Student Oliver Wennerholm | Chalmers | Designer OW | Checker OW

## ULS Combinations Fire

| | Combination rule |
|---|---|
| LCO3 | 1.00/1.00 * LC1 + 1.00/1.00 * LC2 + 1.00/0.00 * 0.20 * LC3 + 1.00/0.00 * 0.30 * LC4 |
| LCO4 | 1.00/1.00 * LC1 + 1.00/1.00 * LC2 + 1.00/0.00 * 0.30 * LC4 |
| LCO5 | 1.00/1.00 * LC1 + 1.00/1.00 * LC2 + 1.00/0.00 * 0.30 * LC4 + 1.00/0.00 * 0.20 * LC3 |

## Reference documents for this analysis

| English title | Description |
|---|---|
| CERTIFICATE NO. EUFI29-20000564-C | Product certificate |
| LVL G by Stora Enso_Structural design manual column&beam_ V01 | Design manual |
| ETA 20_0291 LVL G by Stora Enso | ETA |

## Disclaimer

## System

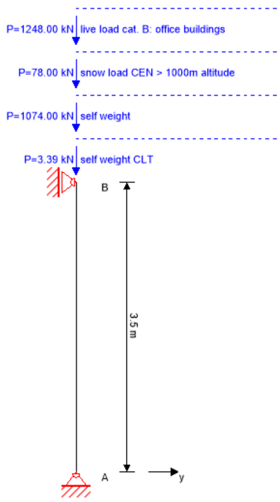


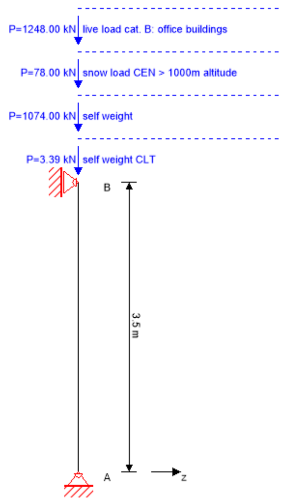


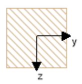


## Global utilization ratio 88 %

| | | | |
|---|---|---|---|
| ULS | 88 % | ULS Fire | 36 % |

## Section: Wooden beam 44/44

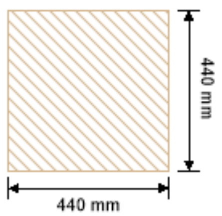


| Section width | Section height | Area | Iy | Iz |
|---|---|---|---|---|
| [cm] | [cm] | [mm²] | [mm⁴] | [mm⁴] |
| 44 | 44 | 193,600 | 3,123,414,000 | 3,123,414,000 |

## Material values

| Material | $f_{m,k}$ | $f_{t,0,k}$ | $f_{t,90,k}$ | $f_{c,0,k}$ | $f_{c,90,k}$ | $f_{v,k}$ | $f_{r,k\ min}$ | $E_{0,mean}$ | $G_{mean}$ | $E_{0,5}$ |
|---|---|---|---|---|---|---|---|---|---|---|
| | [N/mm²] | [N/mm²] | [N/mm²] | [N/mm²] | [N/mm²] | [N/mm²] | [N/mm²] | [N/mm²] | [N/mm²] | [N/mm²] |
| GL 32h | 32.00 | 25.60 | 0.50 | 32.00 | 2.50 | 2.50 | 1.20 | 14,200.00 | 350.00 | 11,800.00 |

## ULS Combinations

| | Combination rule |
|---|---|
| LCO1 | 1.35/1.00 * LC1 + 1.35/1.00 * LC2 |
| LCO2 | 1.35/1.00 * LC1 + 1.35/1.00 * LC2 + 1.50/0.00 * LC3 |
| LCO3 | 1.35/1.00 * LC1 + 1.35/1.00 * LC2 + 1.50/0.00 * LC3 + 1.50/0.00 * 0.70 * LC4 |
| LCO4 | 1.35/1.00 * LC1 + 1.35/1.00 * LC2 + 1.50/0.00 * LC4 |
| LCO5 | 1.35/1.00 * LC1 + 1.35/1.00 * LC2 + 1.50/0.00 * LC4 + 1.50/0.00 * 0.70 * LC3 |

## ULS Combinations Fire

| | Combination rule |
|---|---|
| LCO1 | 1.00/1.00 * LC1 + 1.00/1.00 * LC2 |
| LCO2 | 1.00/1.00 * LC1 + 1.00/1.00 * LC2 + 1.00/0.00 * 0.20 * LC3 |

**ULS Combinations Fire**

| | Combination rule |
|---|---|
| LCO3 | 1.00/1.00 * LC1 + 1.00/1.00 * LC2 + 1.00/0.00 * 0.20 * LC3 + 1.00/0.00 * 0.30 * LC4 |
| LCO4 | 1.00/1.00 * LC1 + 1.00/1.00 * LC2 + 1.00/0.00 * 0.30 * LC4 |
| LCO5 | 1.00/1.00 * LC1 + 1.00/1.00 * LC2 + 1.00/0.00 * 0.30 * LC4 + 1.00/0.00 * 0.20 * LC3 |

**Reference documents for this analysis**

| English title | Description |
|---|---|
| CERTIFICATE NO. EUFI29-20000564-C | Product certificate |
| LVL G by Stora Enso_Structural design manual column&beam_ V01 | Design manual |
| ETA 20_0291 LVL G by Stora Enso | ETA |

**Disclaimer**

Civil Engineer Student
Oliver Wennerholm
Chalmers
Designer OW
Checker OW

## System

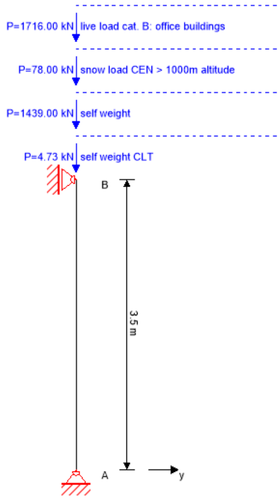


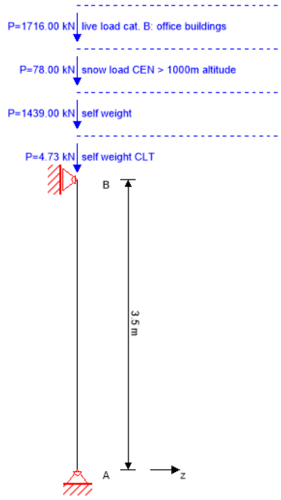


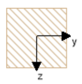


## Global utilization ratio 84 %

| ULS | 84 % | ULS Fire | 38 % |
|---|---|---|---|

## Section: Wooden beam 52/52

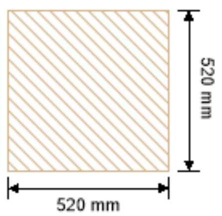


| Section width | Section height | Area | Iy | Iz |
|---|---|---|---|---|
| [cm] | [cm] | [mm²] | [mm⁴] | [mm⁴] |
| 52 | 52 | 270,400 | 6,093,012,000 | 6,093,012,000 |

## Material values

| Material | $f_{m,k}$ | $f_{t,0,k}$ | $f_{t,90,k}$ | $f_{c,0,k}$ | $f_{c,90,k}$ | $f_{v,k}$ | $f_{r,k\ min}$ | $E_{0,mean}$ | $G_{mean}$ | $E_{0,5}$ |
|---|---|---|---|---|---|---|---|---|---|---|
| | [N/mm²] | [N/mm²] | [N/mm²] | [N/mm²] | [N/mm²] | [N/mm²] | [N/mm²] | [N/mm²] | [N/mm²] | [N/mm²] |
| GL 32h | 32.00 | 25.60 | 0.50 | 32.00 | 2.50 | 2.50 | 1.20 | 14,200.00 | 350.00 | 11,800.00 |

## ULS Combinations

| | Combination rule |
|---|---|
| LCO1 | 1.35/1.00 * LC1 + 1.35/1.00 * LC2 |
| LCO2 | 1.35/1.00 * LC1 + 1.35/1.00 * LC2 + 1.50/0.00 * LC3 |
| LCO3 | 1.35/1.00 * LC1 + 1.35/1.00 * LC2 + 1.50/0.00 * LC3 + 1.50/0.00 * 0.70 * LC4 |
| LCO4 | 1.35/1.00 * LC1 + 1.35/1.00 * LC2 + 1.50/0.00 * LC4 |
| LCO5 | 1.35/1.00 * LC1 + 1.35/1.00 * LC2 + 1.50/0.00 * LC4 + 1.50/0.00 * 0.70 * LC3 |

## ULS Combinations Fire

| | Combination rule |
|---|---|
| LCO1 | 1.00/1.00 * LC1 + 1.00/1.00 * LC2 |
| LCO2 | 1.00/1.00 * LC1 + 1.00/1.00 * LC2 + 1.00/0.00 * 0.20 * LC3 |

## ULS Combinations Fire

| | Combination rule |
|---|---|
| LCO3 | 1.00/1.00 * LC1 + 1.00/1.00 * LC2 + 1.00/0.00 * 0.20 * LC3 + 1.00/0.00 * 0.30 * LC4 |
| LCO4 | 1.00/1.00 * LC1 + 1.00/1.00 * LC2 + 1.00/0.00 * 0.30 * LC4 |
| LCO5 | 1.00/1.00 * LC1 + 1.00/1.00 * LC2 + 1.00/0.00 * 0.30 * LC4 + 1.00/0.00 * 0.20 * LC3 |

## Reference documents for this analysis

| English title | Description |
|---|---|
| CERTIFICATE NO. EUFI29-20000564-C | Product certificate |
| LVL G by Stora Enso_Structural design manual column&beam_ V01 | Design manual |
| ETA 20_0291 LVL G by Stora Enso | ETA |

## Disclaimer

## System

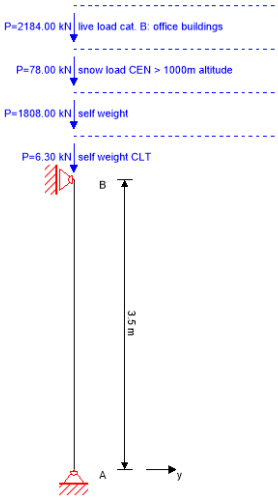


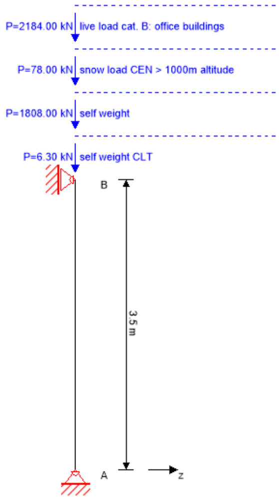


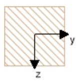


## Global utilization ratio 79 %

| ULS | 79 % | ULS Fire | 32 % |
|---|---|---|---|

## Section: Wooden beam 60/60

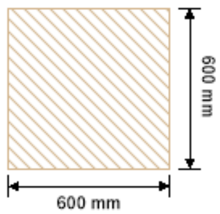


| Section width | Section height | Area | Iy | Iz |
|---|---|---|---|---|
| [cm] | [cm] | [mm²] | [mm⁴] | [mm⁴] |
| 60 | 60 | 360,000 | 10,800,000,000 | 10,800,000,000 |

## Material values

| Material | $f_{m,k}$ | $f_{t,0,k}$ | $f_{t,90,k}$ | $f_{c,0,k}$ | $f_{c,90,k}$ | $f_{v,k}$ | $f_{r,k\ min}$ | $E_{0,mean}$ | $G_{mean}$ | $E_{0,5}$ |
|---|---|---|---|---|---|---|---|---|---|---|
| | [N/mm²] | [N/mm²] | [N/mm²] | [N/mm²] | [N/mm²] | [N/mm²] | [N/mm²] | [N/mm²] | [N/mm²] | [N/mm²] |
| GL 32h | 32.00 | 25.60 | 0.50 | 32.00 | 2.50 | 2.50 | 1.20 | 14,200.00 | 350.00 | 11,800.00 |

## ULS Combinations

| | Combination rule |
|---|---|
| LCO1 | 1.35/1.00 * LC1 + 1.35/1.00 * LC2 |
| LCO2 | 1.35/1.00 * LC1 + 1.35/1.00 * LC2 + 1.50/0.00 * LC3 |
| LCO3 | 1.35/1.00 * LC1 + 1.35/1.00 * LC2 + 1.50/0.00 * LC3 + 1.50/0.00 * 0.70 * LC4 |
| LCO4 | 1.35/1.00 * LC1 + 1.35/1.00 * LC2 + 1.50/0.00 * LC4 |
| LCO5 | 1.35/1.00 * LC1 + 1.35/1.00 * LC2 + 1.50/0.00 * LC4 + 1.50/0.00 * 0.70 * LC3 |

## ULS Combinations Fire

| | Combination rule |
|---|---|
| LCO1 | 1.00/1.00 * LC1 + 1.00/1.00 * LC2 |
| LCO2 | 1.00/1.00 * LC1 + 1.00/1.00 * LC2 + 1.00/0.00 * 0.20 * LC3 |

## ULS Combinations Fire

| | Combination rule |
|---|---|
| LCO3 | 1.00/1.00 * LC1 + 1.00/1.00 * LC2 + 1.00/0.00 * 0.20 * LC3 + 1.00/0.00 * 0.30 * LC4 |
| LCO4 | 1.00/1.00 * LC1 + 1.00/1.00 * LC2 + 1.00/0.00 * 0.30 * LC4 |
| LCO5 | 1.00/1.00 * LC1 + 1.00/1.00 * LC2 + 1.00/0.00 * 0.30 * LC4 + 1.00/0.00 * 0.20 * LC3 |

## Reference documents for this analysis

| English title | Description |
|---|---|
| CERTIFICATE NO. EUFI29-20000564-C | Product certificate |
| LVL G by Stora Enso_Structural design manual column&beam_ V01 | Design manual |
| ETA 20_0291 LVL G by Stora Enso | ETA |

## Disclaimer

## System

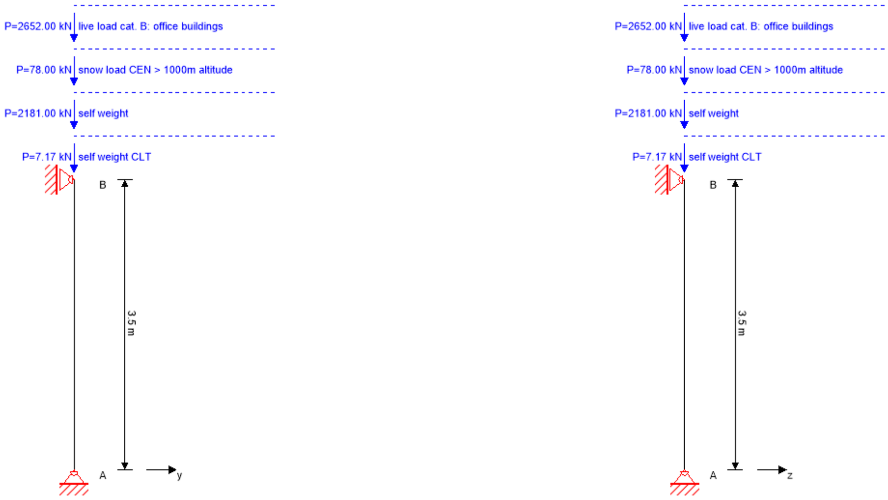


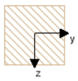

## Global utilization ratio 84 %

| ULS | 84 % | ULS Fire | 33 % |
|---|---|---|---|

## Section: Wooden beam 64/64

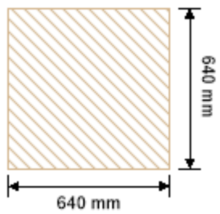


| Section width [cm] | Section height [cm] | Area [mm²] | Iy [mm⁴] | Iz [mm⁴] |
|---|---|---|---|---|
| 64 | 64 | 409,600 | 13,981,010,000 | 13,981,010,000 |

## Material values

| Material | $f_{m,k}$ [N/mm²] | $f_{t,0,k}$ [N/mm²] | $f_{t,90,k}$ [N/mm²] | $f_{c,0,k}$ [N/mm²] | $f_{c,90,k}$ [N/mm²] | $f_{v,k}$ [N/mm²] | $f_{r,k\ min}$ [N/mm²] | $E_{0,mean}$ [N/mm²] | $G_{mean}$ [N/mm²] | $E_{0,5}$ [N/mm²] |
|---|---|---|---|---|---|---|---|---|---|---|
| GL 32h | 32.00 | 25.60 | 0.50 | 32.00 | 2.50 | 2.50 | 1.20 | 14,200.00 | 350.00 | 11,800.00 |

## ULS Combinations

| | Combination rule |
|---|---|
| LCO1 | 1.35/1.00 * LC1 + 1.35/1.00 * LC2 |
| LCO2 | 1.35/1.00 * LC1 + 1.35/1.00 * LC2 + 1.50/0.00 * LC3 |
| LCO3 | 1.35/1.00 * LC1 + 1.35/1.00 * LC2 + 1.50/0.00 * LC3 + 1.50/0.00 * 0.70 * LC4 |
| LCO4 | 1.35/1.00 * LC1 + 1.35/1.00 * LC2 + 1.50/0.00 * LC4 |
| LCO5 | 1.35/1.00 * LC1 + 1.35/1.00 * LC2 + 1.50/0.00 * LC4 + 1.50/0.00 * 0.70 * LC3 |

## ULS Combinations Fire

| | Combination rule |
|---|---|
| LCO1 | 1.00/1.00 * LC1 + 1.00/1.00 * LC2 |
| LCO2 | 1.00/1.00 * LC1 + 1.00/1.00 * LC2 + 1.00/0.00 * 0.20 * LC3 |

### ULS Combinations Fire

| | Combination rule |
|---|---|
| LCO3 | 1.00/1.00 * LC1 + 1.00/1.00 * LC2 + 1.00/0.00 * 0.20 * LC3 + 1.00/0.00 * 0.30 * LC4 |
| LCO4 | 1.00/1.00 * LC1 + 1.00/1.00 * LC2 + 1.00/0.00 * 0.30 * LC4 |
| LCO5 | 1.00/1.00 * LC1 + 1.00/1.00 * LC2 + 1.00/0.00 * 0.30 * LC4 + 1.00/0.00 * 0.20 * LC3 |

### Reference documents for this analysis

| English title | Description |
|---|---|
| CERTIFICATE NO. EUFI29-20000564-C | Product certificate |
| LVL G by Stora Enso_Structural design manual column&beam_ V01 | Design manual |
| ETA 20_0291 LVL G by Stora Enso | ETA |

### Disclaimer

## A.5 Core walls

| | | |
|---|---|---|
| **MasterThesis** | | Page 1/2 |
| Core wall 3 floors | | 09.03.2023 |

| | | | |
|---|---|---|---|
| Civil Engineer Student<br>Oliver Wennerholm | Chalmers | Designer OW | Checker OW |

## System

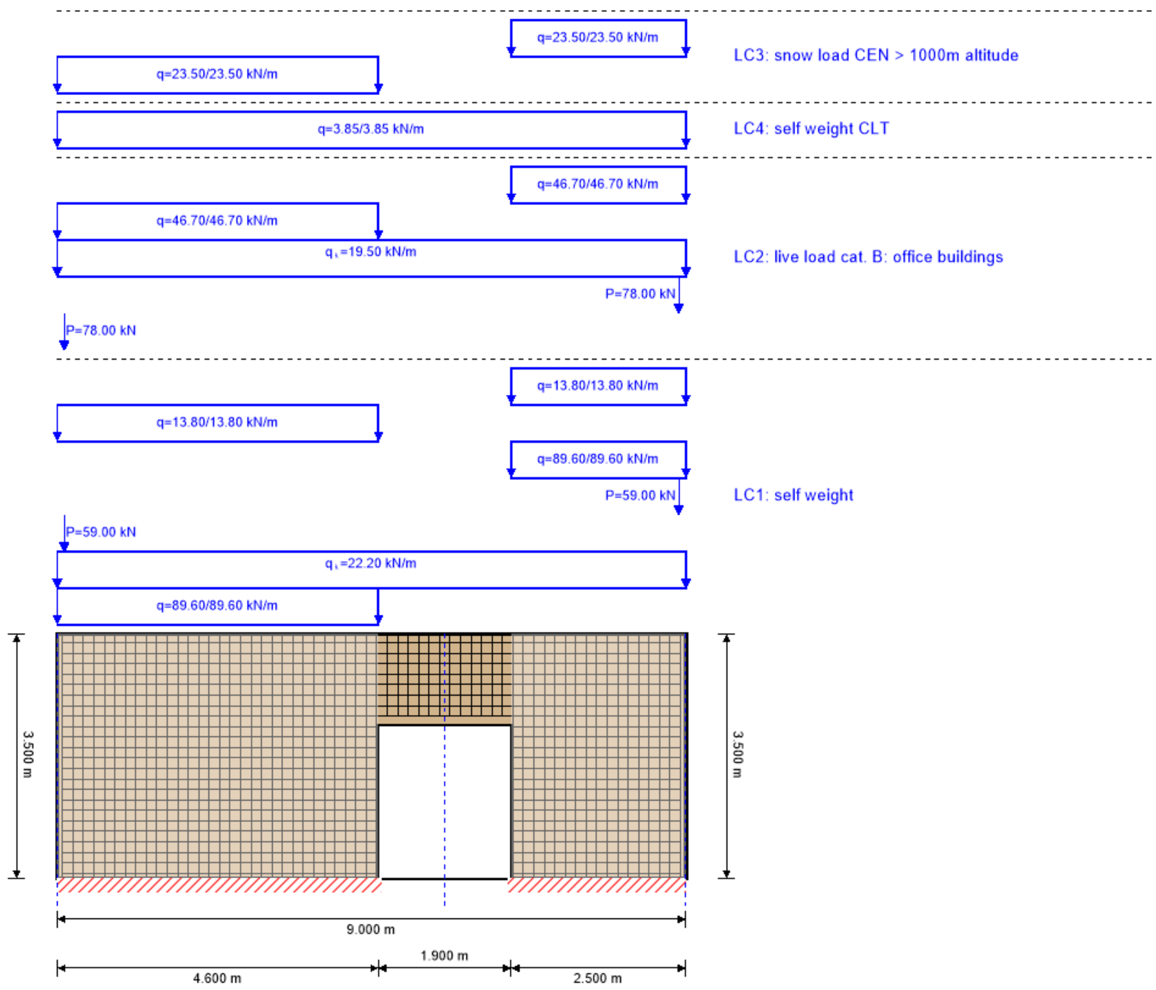


## Global utilization ratio 45 %

| ULS | 45 % | ULS Fire | 39 % | SLS | 5 % |
|---|---|---|---|---|---|

## Section: CLT 220 L7s - 2

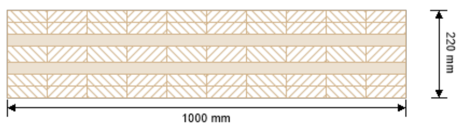


| Layer | Thickness | Orientation | Material |
|---|---|---|---|
| 1 | 30.0 mm | 0° | C24 spruce ETA (2019) |
| 2 | 30.0 mm | 0° | C24 spruce ETA (2019) |
| 3 | 30.0 mm | 90° | C24 spruce ETA (2019) |
| 4 | 40.0 mm | 0° | C24 spruce ETA (2019) |
| 5 | 30.0 mm | 90° | C24 spruce ETA (2019) |
| 6 | 30.0 mm | 0° | C24 spruce ETA (2019) |
| 7 | 30.0 mm | 0° | C24 spruce ETA (2019) |
| $t_{CLT}$ | **220.0 mm** | | |

## Material values

| Material | $f_{m,k}$ [N/mm²] | $f_{t,0,k}$ [N/mm²] | $f_{t,90,k}$ [N/mm²] | $f_{c,0,k}$ [N/mm²] | $f_{c,90,k}$ [N/mm²] | $f_{v,k}$ [N/mm²] | $f_{r,k\,min}$ [N/mm²] | $E_{0,mean}$ [N/mm²] | $G_{mean}$ [N/mm²] | $G_{r,mean}$ [N/mm²] |
|---|---|---|---|---|---|---|---|---|---|---|
| C24 spruce ETA (2019) | 24.00 | 14.00 | 0.12 | 21.00 | 2.50 | 4.00 | 1.25 | 12,000.00 | 690.00 | 50.00 |

## ULS Combinations

| | Combination rule |
|---|---|
| LCO1 | 1.12/1.00 * LC1 + 1.12/1.00 * LC4 |
| LCO2 | 1.12/1.00 * LC1 + 1.12/1.00 * LC4 + 1.25/0.00 * LC2 |
| LCO3 | 1.12/1.00 * LC1 + 1.12/1.00 * LC4 + 1.25/0.00 * LC2 + 1.25/0.00 * 0.70 * LC3 |
| LCO4 | 1.12/1.00 * LC1 + 1.12/1.00 * LC4 + 1.25/0.00 * LC3 |
| LCO5 | 1.12/1.00 * LC1 + 1.12/1.00 * LC4 + 1.25/0.00 * LC3 + 1.25/0.00 * 0.70 * LC2 |

## ULS Combinations Fire

| | Combination rule |
|---|---|
| LCO1 | 1.00/1.00 * LC1 + 1.00/1.00 * LC4 |
| LCO2 | 1.00/1.00 * LC1 + 1.00/1.00 * LC4 + 1.00/0.00 * 0.30 * LC2 |
| LCO3 | 1.00/1.00 * LC1 + 1.00/1.00 * LC4 + 1.00/0.00 * 0.30 * LC2 + 1.00/0.00 * 0.20 * LC3 |
| LCO4 | 1.00/1.00 * LC1 + 1.00/1.00 * LC4 + 1.00/0.00 * 0.20 * LC3 |
| LCO5 | 1.00/1.00 * LC1 + 1.00/1.00 * LC4 + 1.00/0.00 * 0.20 * LC3 + 1.00/0.00 * 0.30 * LC2 |

## System

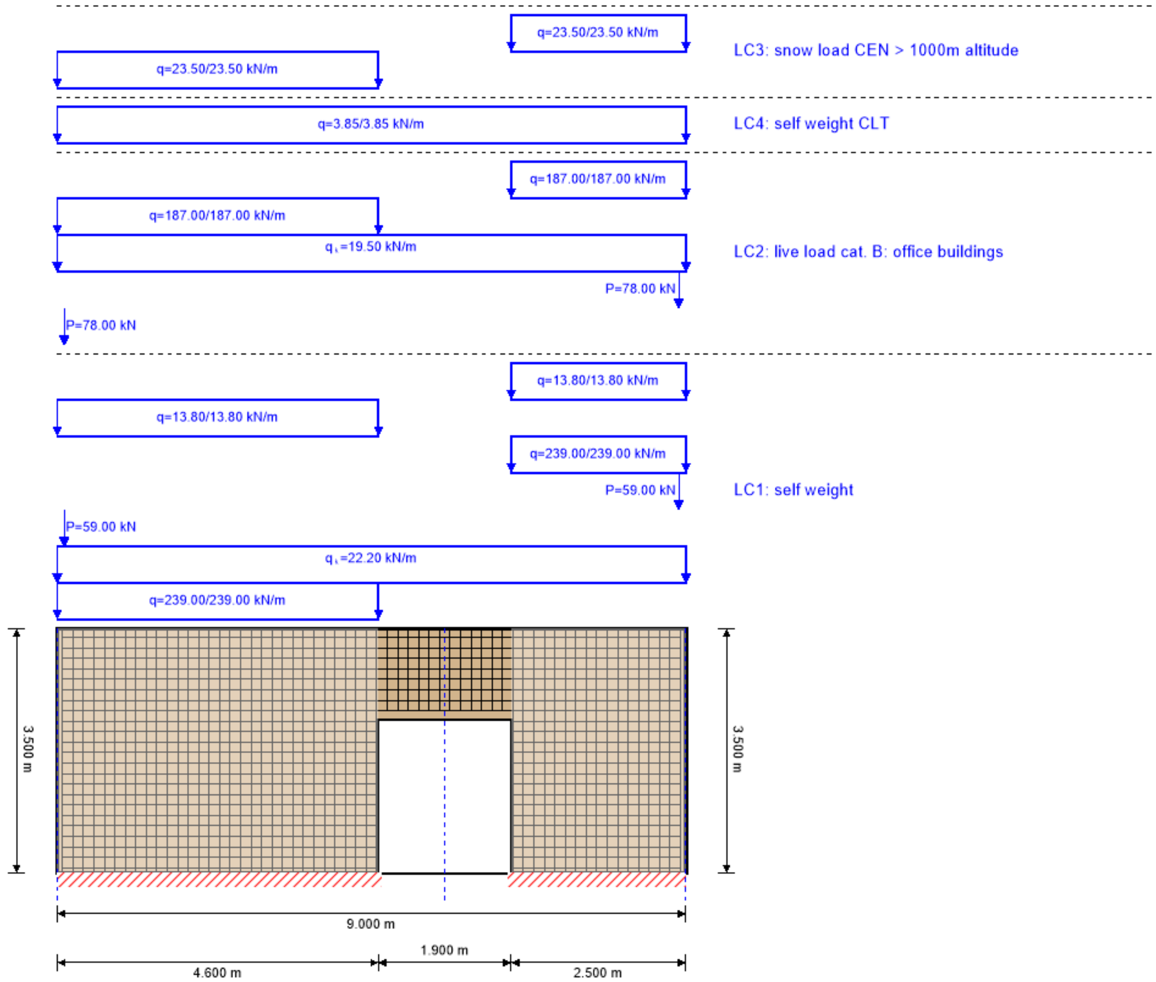


## Global utilization ratio 64 %

| ULS | 64 % | ULS Fire | 57 % | SLS | 5 % |
|---|---|---|---|---|---|

## Section: CLT 220 L7s - 2

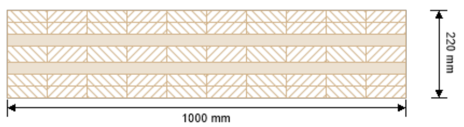


| Layer | Thickness | Orientation | Material |
|---|---|---|---|
| 1 | 30.0 mm | 0° | C24 spruce ETA (2019) |
| 2 | 30.0 mm | 0° | C24 spruce ETA (2019) |
| 3 | 30.0 mm | 90° | C24 spruce ETA (2019) |
| 4 | 40.0 mm | 0° | C24 spruce ETA (2019) |
| 5 | 30.0 mm | 90° | C24 spruce ETA (2019) |
| 6 | 30.0 mm | 0° | C24 spruce ETA (2019) |
| 7 | 30.0 mm | 0° | C24 spruce ETA (2019) |
| $t_{CLT}$ | **220.0 mm** | | |

### Material values

| Material | $f_{m,k}$ [N/mm²] | $f_{t,0,k}$ [N/mm²] | $f_{t,90,k}$ [N/mm²] | $f_{c,0,k}$ [N/mm²] | $f_{c,90,k}$ [N/mm²] | $f_{v,k}$ [N/mm²] | $f_{r,k\,min}$ [N/mm²] | $E_{0,mean}$ [N/mm²] | $G_{mean}$ [N/mm²] | $G_{r,mean}$ [N/mm²] |
|---|---|---|---|---|---|---|---|---|---|---|
| C24 spruce ETA (2019) | 24.00 | 14.00 | 0.12 | 21.00 | 2.50 | 4.00 | 1.25 | 12,000.00 | 690.00 | 50.00 |

### ULS Combinations

| | Combination rule |
|---|---|
| LCO1 | 1.12/1.00 * LC1 + 1.12/1.00 * LC4 |
| LCO2 | 1.12/1.00 * LC1 + 1.12/1.00 * LC4 + 1.25/0.00 * LC2 |
| LCO3 | 1.12/1.00 * LC1 + 1.12/1.00 * LC4 + 1.25/0.00 * LC2 + 1.25/0.00 * 0.70 * LC3 |
| LCO4 | 1.12/1.00 * LC1 + 1.12/1.00 * LC4 + 1.25/0.00 * LC3 |
| LCO5 | 1.12/1.00 * LC1 + 1.12/1.00 * LC4 + 1.25/0.00 * LC3 + 1.25/0.00 * 0.70 * LC2 |

### ULS Combinations Fire

| | Combination rule |
|---|---|
| LCO1 | 1.00/1.00 * LC1 + 1.00/1.00 * LC4 |
| LCO2 | 1.00/1.00 * LC1 + 1.00/1.00 * LC4 + 1.00/0.00 * 0.30 * LC2 |
| LCO3 | 1.00/1.00 * LC1 + 1.00/1.00 * LC4 + 1.00/0.00 * 0.30 * LC2 + 1.00/0.00 * 0.20 * LC3 |
| LCO4 | 1.00/1.00 * LC1 + 1.00/1.00 * LC4 + 1.00/0.00 * 0.20 * LC3 |
| LCO5 | 1.00/1.00 * LC1 + 1.00/1.00 * LC4 + 1.00/0.00 * 0.20 * LC3 + 1.00/0.00 * 0.30 * LC2 |

Civil Engineer Student Oliver Wennerholm | Chalmers | Designer OW | Checker OW


## System

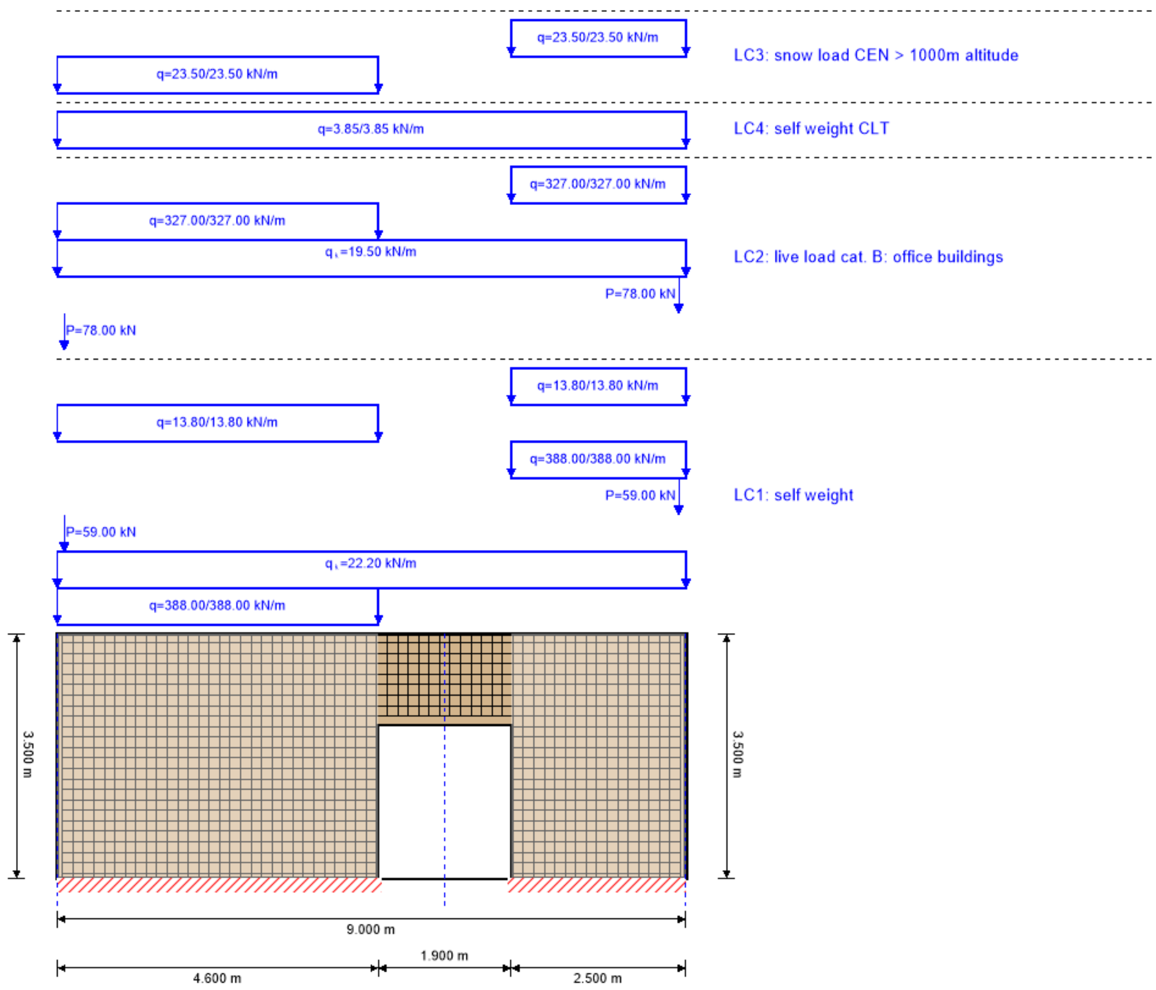


## Global utilization ratio 83 %

| ULS | 83 % | ULS Fire | 74 % | SLS | 5 % |
|---|---|---|---|---|---|

## Section: CLT 220 L7s - 2

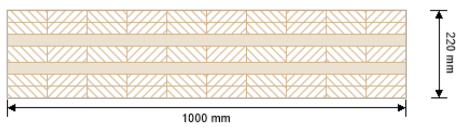


| Layer | Thickness | Orientation | Material |
|---|---|---|---|
| 1 | 30.0 mm | 0° | C24 spruce ETA (2019) |
| 2 | 30.0 mm | 0° | C24 spruce ETA (2019) |
| 3 | 30.0 mm | 90° | C24 spruce ETA (2019) |
| 4 | 40.0 mm | 0° | C24 spruce ETA (2019) |
| 5 | 30.0 mm | 90° | C24 spruce ETA (2019) |
| 6 | 30.0 mm | 0° | C24 spruce ETA (2019) |
| 7 | 30.0 mm | 0° | C24 spruce ETA (2019) |
| $t_{CLT}$ | **220.0 mm** | | |

### Material values

| Material | $f_{m,k}$ [N/mm²] | $f_{t,0,k}$ [N/mm²] | $f_{t,90,k}$ [N/mm²] | $f_{c,0,k}$ [N/mm²] | $f_{c,90,k}$ [N/mm²] | $f_{v,k}$ [N/mm²] | $f_{r,k\ min}$ [N/mm²] | $E_{0,mean}$ [N/mm²] | $G_{mean}$ [N/mm²] | $G_{r,mean}$ [N/mm²] |
|---|---|---|---|---|---|---|---|---|---|---|
| C24 spruce ETA (2019) | 24.00 | 14.00 | 0.12 | 21.00 | 2.50 | 4.00 | 1.25 | 12,000.00 | 690.00 | 50.00 |

### ULS Combinations

| | Combination rule |
|---|---|
| LCO1 | 1.12/1.00 * LC1 + 1.12/1.00 * LC4 |
| LCO2 | 1.12/1.00 * LC1 + 1.12/1.00 * LC4 + 1.25/0.00 * LC2 |
| LCO3 | 1.12/1.00 * LC1 + 1.12/1.00 * LC4 + 1.25/0.00 * LC2 + 1.25/0.00 * 0.70 * LC3 |
| LCO4 | 1.12/1.00 * LC1 + 1.12/1.00 * LC4 + 1.25/0.00 * LC3 |
| LCO5 | 1.12/1.00 * LC1 + 1.12/1.00 * LC4 + 1.25/0.00 * LC3 + 1.25/0.00 * 0.70 * LC2 |

### ULS Combinations Fire

| | Combination rule |
|---|---|
| LCO1 | 1.00/1.00 * LC1 + 1.00/1.00 * LC4 |
| LCO2 | 1.00/1.00 * LC1 + 1.00/1.00 * LC4 + 1.00/0.00 * 0.30 * LC2 |
| LCO3 | 1.00/1.00 * LC1 + 1.00/1.00 * LC4 + 1.00/0.00 * 0.30 * LC2 + 1.00/0.00 * 0.20 * LC3 |
| LCO4 | 1.00/1.00 * LC1 + 1.00/1.00 * LC4 + 1.00/0.00 * 0.20 * LC3 |
| LCO5 | 1.00/1.00 * LC1 + 1.00/1.00 * LC4 + 1.00/0.00 * 0.20 * LC3 + 1.00/0.00 * 0.30 * LC2 |

Civil Engineer Student
Oliver Wennerholm

Chalmers

Designer OW

Checker OW


## System

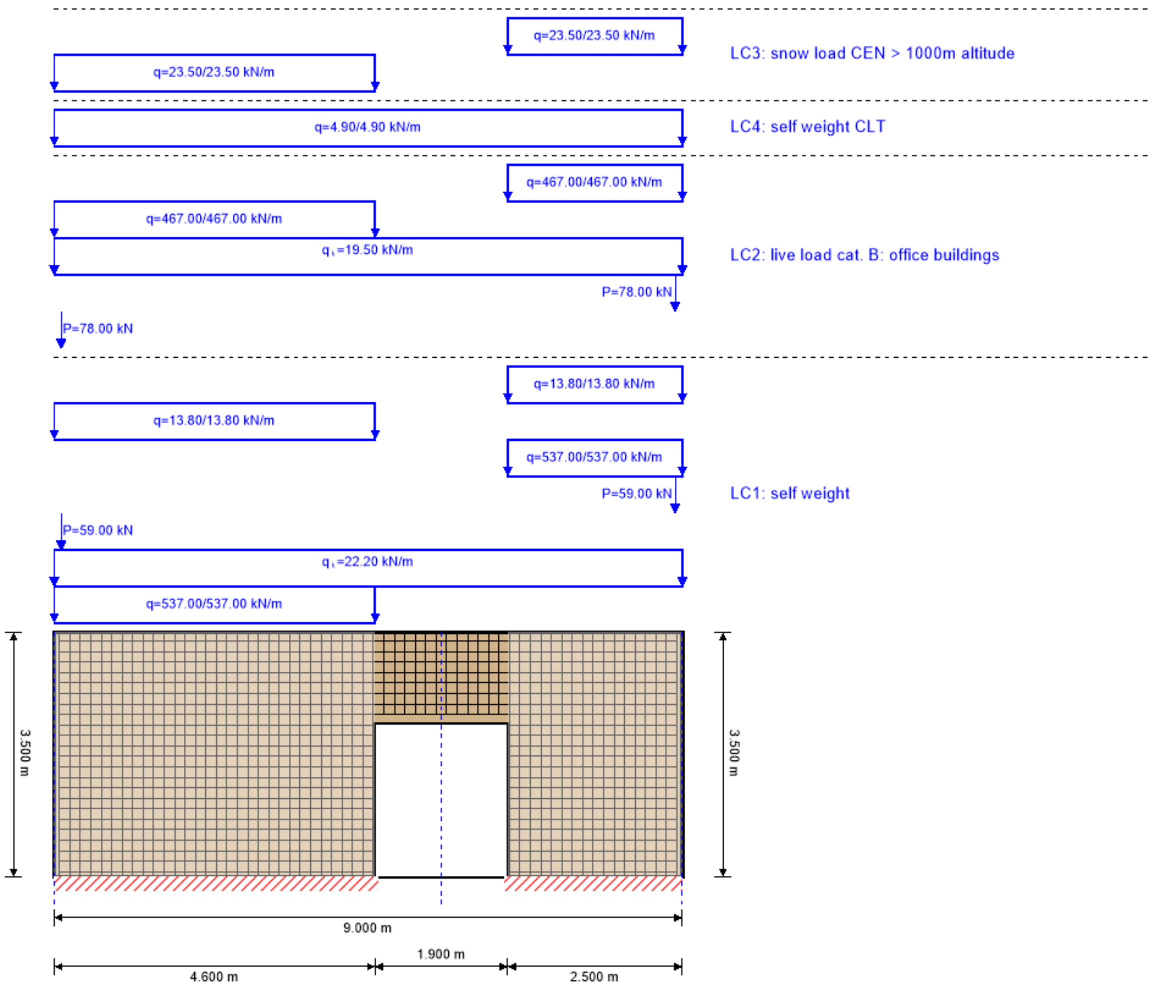


| Global utilization ratio | | | | | | 74 % |
|---|---|---|---|---|---|---|
| ULS | 74 % | ULS Fire | 43 % | SLS | 4 % | |

## Section: CLT 280 L7s - 2

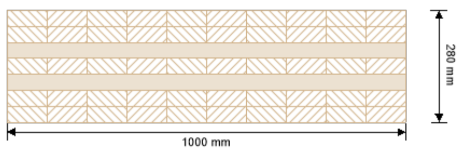


| Layer | Thickness | Orientation | Material |
|---|---|---|---|
| 1 | 40.0 mm | 0° | C24 spruce ETA (2019) |
| 2 | 40.0 mm | 0° | C24 spruce ETA (2019) |
| 3 | 40.0 mm | 90° | C24 spruce ETA (2019) |
| 4 | 40.0 mm | 0° | C24 spruce ETA (2019) |
| 5 | 40.0 mm | 90° | C24 spruce ETA (2019) |
| 6 | 40.0 mm | 0° | C24 spruce ETA (2019) |
| 7 | 40.0 mm | 0° | C24 spruce ETA (2019) |
| $t_{CLT}$ | **280.0 mm** | | |

**Material values**

| Material | $f_{m,k}$ [N/mm²] | $f_{t,0,k}$ [N/mm²] | $f_{t,90,k}$ [N/mm²] | $f_{c,0,k}$ [N/mm²] | $f_{c,90,k}$ [N/mm²] | $f_{v,k}$ [N/mm²] | $f_{r,k\ min}$ [N/mm²] | $E_{0,mean}$ [N/mm²] | $G_{mean}$ [N/mm²] | $G_{r,mean}$ [N/mm²] |
|---|---|---|---|---|---|---|---|---|---|---|
| C24 spruce ETA (2019) | 24.00 | 14.00 | 0.12 | 21.00 | 2.50 | 4.00 | 1.25 | 12,000.00 | 690.00 | 50.00 |

**ULS Combinations**

| | Combination rule |
|---|---|
| LCO1 | 1.12/1.00 * LC1 + 1.12/1.00 * LC4 |
| LCO2 | 1.12/1.00 * LC1 + 1.12/1.00 * LC4 + 1.25/0.00 * LC2 |
| LCO3 | 1.12/1.00 * LC1 + 1.12/1.00 * LC4 + 1.25/0.00 * LC2 + 1.25/0.00 * 0.70 * LC3 |
| LCO4 | 1.12/1.00 * LC1 + 1.12/1.00 * LC4 + 1.25/0.00 * LC3 |
| LCO5 | 1.12/1.00 * LC1 + 1.12/1.00 * LC4 + 1.25/0.00 * LC3 + 1.25/0.00 * 0.70 * LC2 |

**ULS Combinations Fire**

| | Combination rule |
|---|---|
| LCO1 | 1.00/1.00 * LC1 + 1.00/1.00 * LC4 |
| LCO2 | 1.00/1.00 * LC1 + 1.00/1.00 * LC4 + 1.00/0.00 * 0.30 * LC2 |
| LCO3 | 1.00/1.00 * LC1 + 1.00/1.00 * LC4 + 1.00/0.00 * 0.30 * LC2 + 1.00/0.00 * 0.20 * LC3 |
| LCO4 | 1.00/1.00 * LC1 + 1.00/1.00 * LC4 + 1.00/0.00 * 0.20 * LC3 |
| LCO5 | 1.00/1.00 * LC1 + 1.00/1.00 * LC4 + 1.00/0.00 * 0.20 * LC3 + 1.00/0.00 * 0.30 * LC2 |

## System

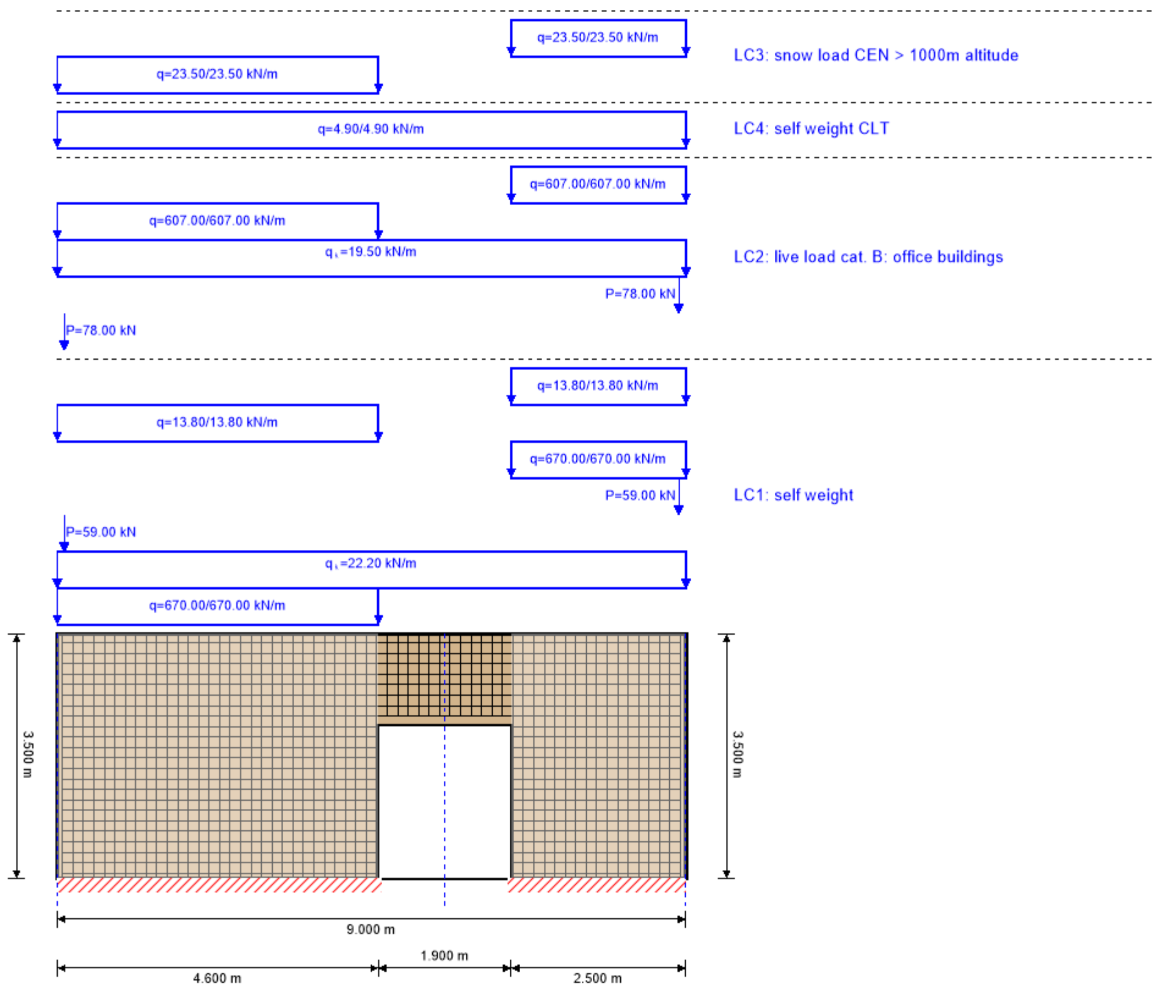


| **Global utilization ratio** | | | | | | | **87 %** |
|---|---|---|---|---|---|---|---|
| ULS | 87 % | ULS Fire | 51 % | SLS | 4 % | | |

## Section: CLT 280 L7s - 2

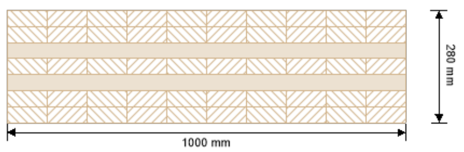


| Layer | Thickness | Orientation | Material |
|---|---|---|---|
| 1 | 40.0 mm | 0° | C24 spruce ETA (2019) |
| 2 | 40.0 mm | 0° | C24 spruce ETA (2019) |
| 3 | 40.0 mm | 90° | C24 spruce ETA (2019) |
| 4 | 40.0 mm | 0° | C24 spruce ETA (2019) |
| 5 | 40.0 mm | 90° | C24 spruce ETA (2019) |
| 6 | 40.0 mm | 0° | C24 spruce ETA (2019) |
| 7 | 40.0 mm | 0° | C24 spruce ETA (2019) |
| $t_{CLT}$ | **280.0 mm** | | |

### Material values

| Material | $f_{m,k}$ [N/mm²] | $f_{t,0,k}$ [N/mm²] | $f_{t,90,k}$ [N/mm²] | $f_{c,0,k}$ [N/mm²] | $f_{c,90,k}$ [N/mm²] | $f_{v,k}$ [N/mm²] | $f_{r,k\,min}$ [N/mm²] | $E_{0,mean}$ [N/mm²] | $G_{mean}$ [N/mm²] | $G_{r,mean}$ [N/mm²] |
|---|---|---|---|---|---|---|---|---|---|---|
| C24 spruce ETA (2019) | 24.00 | 14.00 | 0.12 | 21.00 | 2.50 | 4.00 | 1.25 | 12,000.00 | 690.00 | 50.00 |

### ULS Combinations

| | Combination rule |
|---|---|
| LCO1 | 1.12/1.00 * LC1 + 1.12/1.00 * LC4 |
| LCO2 | 1.12/1.00 * LC1 + 1.12/1.00 * LC4 + 1.25/0.00 * LC2 |
| LCO3 | 1.12/1.00 * LC1 + 1.12/1.00 * LC4 + 1.25/0.00 * LC2 + 1.25/0.00 * 0.70 * LC3 |
| LCO4 | 1.12/1.00 * LC1 + 1.12/1.00 * LC4 + 1.25/0.00 * LC3 |
| LCO5 | 1.12/1.00 * LC1 + 1.12/1.00 * LC4 + 1.25/0.00 * LC3 + 1.25/0.00 * 0.70 * LC2 |

### ULS Combinations Fire

| | Combination rule |
|---|---|
| LCO1 | 1.00/1.00 * LC1 + 1.00/1.00 * LC4 |
| LCO2 | 1.00/1.00 * LC1 + 1.00/1.00 * LC4 + 1.00/0.00 * 0.30 * LC2 |
| LCO3 | 1.00/1.00 * LC1 + 1.00/1.00 * LC4 + 1.00/0.00 * 0.30 * LC2 + 1.00/0.00 * 0.20 * LC3 |
| LCO4 | 1.00/1.00 * LC1 + 1.00/1.00 * LC4 + 1.00/0.00 * 0.20 * LC3 |
| LCO5 | 1.00/1.00 * LC1 + 1.00/1.00 * LC4 + 1.00/0.00 * 0.20 * LC3 + 1.00/0.00 * 0.30 * LC2 |

## System

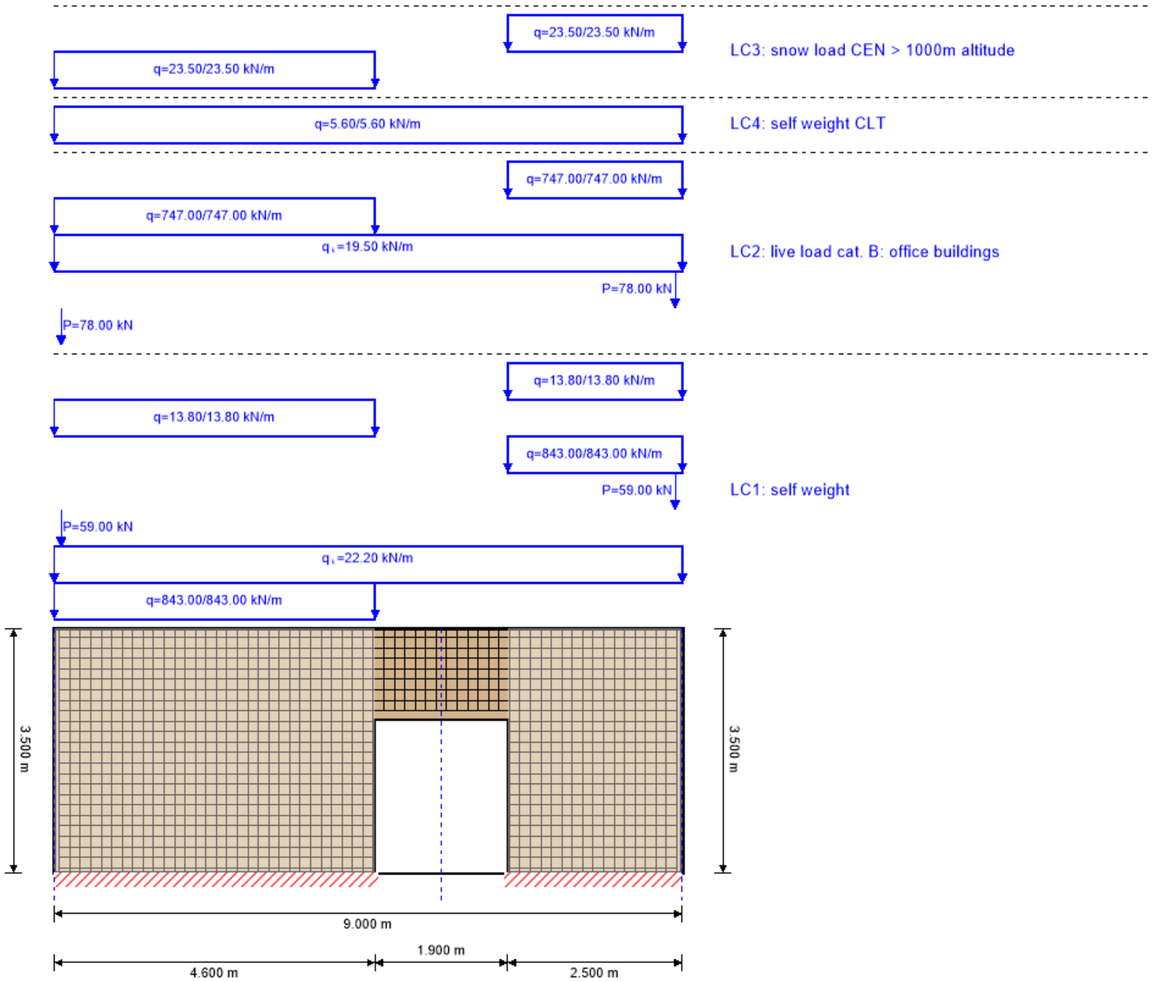


| Global utilization ratio | | | | | | 83 % |
|---|---|---|---|---|---|---|
| ULS | 83 % | ULS Fire | 41 % | SLS | 4 % | |

**Section: CLT 320 L8s - 2**

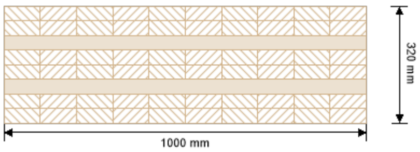


| Layer | Thickness | Orientation | Material |
|---|---|---|---|
| 1 | 40.0 mm | 0° | C24 spruce ETA (2019) |
| 2 | 40.0 mm | 0° | C24 spruce ETA (2019) |
| 3 | 40.0 mm | 90° | C24 spruce ETA (2019) |
| 4 | 40.0 mm | 0° | C24 spruce ETA (2019) |
| 5 | 40.0 mm | 0° | C24 spruce ETA (2019) |
| 6 | 40.0 mm | 90° | C24 spruce ETA (2019) |
| 7 | 40.0 mm | 0° | C24 spruce ETA (2019) |
| 8 | 40.0 mm | 0° | C24 spruce ETA (2019) |
| $t_{CLT}$ | **320.0 mm** | | |

**Material values**

| Material | $f_{m,k}$ [N/mm²] | $f_{t,0,k}$ [N/mm²] | $f_{t,90,k}$ [N/mm²] | $f_{c,0,k}$ [N/mm²] | $f_{c,90,k}$ [N/mm²] | $f_{v,k}$ [N/mm²] | $f_{r,k\ min}$ [N/mm²] | $E_{0,mean}$ [N/mm²] | $G_{mean}$ [N/mm²] | $G_{r,mean}$ [N/mm²] |
|---|---|---|---|---|---|---|---|---|---|---|
| C24 spruce ETA (2019) | 24.00 | 14.00 | 0.12 | 21.00 | 2.50 | 4.00 | 1.25 | 12,000.00 | 690.00 | 50.00 |

**ULS Combinations**

| | Combination rule |
|---|---|
| LCO1 | 1.12/1.00 * LC1 + 1.12/1.00 * LC4 |
| LCO2 | 1.12/1.00 * LC1 + 1.12/1.00 * LC4 + 1.25/0.00 * LC2 |
| LCO3 | 1.12/1.00 * LC1 + 1.12/1.00 * LC4 + 1.25/0.00 * LC2 + 1.25/0.00 * 0.70 * LC3 |
| LCO4 | 1.12/1.00 * LC1 + 1.12/1.00 * LC4 + 1.25/0.00 * LC3 |
| LCO5 | 1.12/1.00 * LC1 + 1.12/1.00 * LC4 + 1.25/0.00 * LC3 + 1.25/0.00 * 0.70 * LC2 |

**ULS Combinations Fire**

| | Combination rule |
|---|---|
| LCO1 | 1.00/1.00 * LC1 + 1.00/1.00 * LC4 |
| LCO2 | 1.00/1.00 * LC1 + 1.00/1.00 * LC4 + 1.00/0.00 * 0.30 * LC2 |
| LCO3 | 1.00/1.00 * LC1 + 1.00/1.00 * LC4 + 1.00/0.00 * 0.30 * LC2 + 1.00/0.00 * 0.20 * LC3 |
| LCO4 | 1.00/1.00 * LC1 + 1.00/1.00 * LC4 + 1.00/0.00 * 0.20 * LC3 |
| LCO5 | 1.00/1.00 * LC1 + 1.00/1.00 * LC4 + 1.00/0.00 * 0.20 * LC3 + 1.00/0.00 * 0.30 * LC2 |

## A.6 Modified material properties of CLT

**Table A.1:** The material properties of C24 and factors used for calculation of CLT panels, from Stora Enso (2015)

| | |
|---|---|
| $E_{0,mean}$ [MPa] | 12500 |
| $E_{90,mean}$ [MPa] | 0 |
| $G_{0,mean}$ [MPa] | 690 |
| $G_R$ [MPa] | 50 |
| $\rho$ $[N/m^3]$ | 4200 |
| $f_{m,k}$ [MPa] | 24 |
| $f_{t,0,k}$ [MPa] | $14,5$ |
| $f_{t,90,k}$ [MPa] | $0,4$ |
| $f_{c,0,k}$ [MPa] | 21 |
| $f_{c,90,k}$ [MPa] | $2,5$ |
| $f_{v,k}$ [MPa] | 4 |
| $f_{r,k}$ [MPa] | $0,8$ |
| $K_{shear}$ | $0,7$ |
| $K_{twist}$ | $0,65$ |

### A.6.1 CLT 320 L8s-2

| CLT 320 L8s-2 | | | | | | | | | | | | |
|---|---|---|---|---|---|---|---|---|---|---|---|---|
| | | | | | | | For axial loading: | | For flexural loading: | | | |
| layers: | t | b | A | z | Direction | A_main | E1*A | E2*A | G31*k*A | G32*k*A | E1*Ief | E2*Ief |
| 1 | 40 | 1000 | 40000 | 20 | 0 | 40000 | 500000000 | 0 | 5740800 | 280000 | 9,86667E+12 | 0 |
| 2 | 40 | 1000 | 40000 | 60 | 0 | 40000 | 500000000 | 0 | 5740800 | 280000 | 5,06667E+12 | 0 |
| 3 | 40 | 1000 | 40000 | 100 | 90 | 0 | 0 | 500000000 | 416000 | 3864000 | 0 | 1,86667E+12 |
| 4 | 40 | 1000 | 40000 | 140 | 0 | 40000 | 500000000 | 0 | 5740800 | 280000 | 2,66667E+11 | 0 |
| 5 | 40 | 1000 | 40000 | 180 | 0 | 40000 | 500000000 | 0 | 5740800 | 280000 | 2,66667E+11 | 0 |
| 6 | 40 | 1000 | 40000 | 220 | 90 | 0 | 0 | 500000000 | 416000 | 3864000 | 0 | 1,86667E+12 |
| 7 | 40 | 1000 | 40000 | 260 | 0 | 40000 | 500000000 | 0 | 5740800 | 280000 | 5,06667E+12 | 0 |
| 8 | 40 | 1000 | 40000 | 300 | 0 | 40000 | 500000000 | 0 | 5740800 | 280000 | 9,86667E+12 | 0 |
| | | | | | | | 3E+09 | 1000000000 | 35276800 | 9408000 | 3,04E+13 | 3,73333E+12 |
| h_clt | 320 | | | | | | | | | | | |
| z_na | 160 | | | | | | | | | | | |
| A_ref | 320000 | | | | | | | | | | | |
| I_ref | 2730666667 | | | | | | | | | | | |
| k0 | 0,208 | | | | | | | | | | | |
| k90 | 0,14 | | | | | | | | | | | |
| A_main | 240000 | | | | | | | | | | | |
| % | 0,75 | | | | | | | | | | | |
| | | | | | | | | | | | | |
| Modified: | Axial | Bending | | | | | | | | | | |
| E1 | 3125 | 1367,188 | | | | | | | | | | |
| E2 | 9375 | 11132,81 | | | | | | | | | | |
| G12 | 483 | 448,5 | | | | | | | | | | |
| nue12 | 0 | | | | | | | | | | | |
| G31 | 29,4 | | | | | | | | | | | |
| G32 | 110,24 | | | | | | | | | | | |
| gamma | 3500 | | | | | | | | | | | |
| alphaT1 | 5,00E-06 | | | | | | | | | | | |
| alphaT2 | 5,00E-06 | | | | | | | | | | | |
| ft1 | 3,925 | | | | | | | | | | | |
| ft2 | 10,975 | | | | | | | | | | | |
| fc1 | 7,125 | | | | | | | | | | | |
| fc2 | 16,375 | | | | | | | Gzx=G32 | | | | |
| t12 | 4 | | | | | | | Gzy=G31 | | | | |
| F12 | 0 | | | | | | | Gxy=G12 | | | | |
| S-Hypo | Rankine | | | | | | | Ex=E2 | | | | |
| | | | | | | | | Ey=E1 | | | | |

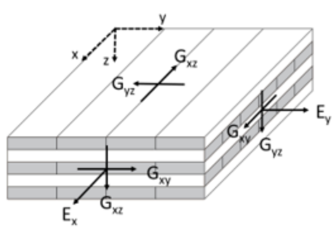

### A.6.2 CLT 280 L7s-2

| CLT 280 L7s-2 | | | | | | | | | | | | |
|---|---|---|---|---|---|---|---|---|---|---|---|---|
| | | | | | | | For axial loading: | | For flexural loading: | | | |
| layers: | t | b | A | z | Direction | A_main | E1*A | E2*A | G31*k*A | G32*k*A | E1*Ief | E2*Ief |
| 1 | 40 | 1000 | 40000 | 20 | 0 | 40000 | 500000000 | 0 | 4940400 | 272000 | 7,267E+12 | 0 |
| 2 | 40 | 1000 | 40000 | 60 | 0 | 40000 | 500000000 | 0 | 4940400 | 272000 | 3,267E+12 | 0 |
| 3 | 40 | 1000 | 40000 | 100 | 90 | 0 | 0 | 500000000 | 358000 | 3753600 | 0 | 8,6667E+11 |
| 4 | 40 | 1000 | 40000 | 140 | 0 | 40000 | 500000000 | 0 | 4940400 | 272000 | 6,667E+10 | 0 |
| 5 | 40 | 1000 | 40000 | 180 | 90 | 0 | 0 | 0 | 358000 | 3753600 | 0 | 8,6667E+11 |
| 6 | 40 | 1000 | 40000 | 220 | 0 | 40000 | 500000000 | 500000000 | 4940400 | 272000 | 3,267E+12 | 0 |
| 7 | 40 | 1000 | 40000 | 260 | 0 | 40000 | 500000000 | 0 | 4940400 | 272000 | 7,267E+12 | 0 |
| 8 | 0 | 1000 | 0 | 280 | 0 | 0 | 0 | 0 | 0 | 0 | 0 | 0 |
| | | | | | | | 2500000000 | 1000000000 | 25418000 | 8867200 | 2,113E+13 | 1,7333E+12 |

| | | |
|---|---|---|
| h_clt | 280 | |
| z_na | 140 | |
| A_ref | 280000 | |
| I_ref | 1829333333 | |
| k0 | 0,179 | |
| k90 | 0,136 | |
| A_main | 200000 | |
| % | 0,714285714 | |
| | | |
| Modified: | Axial | Bending |
| E1 | 3571,428571 | 947,5218659 |
| E2 | 8928,571429 | 11552,47813 |
| G12 | 483 | 448,5 |
| nue12 | 0 | |
| G31 | 31,66857143 | |
| G32 | 90,77857143 | |
| gamma | 3500 | |
| alphaT1 | 5,00E-06 | |
| alphaT2 | 5,00E-06 | |
| ft1 | 4,428571429 | |
| ft2 | 10,47142857 | |
| fc1 | 7,785714286 | |
| fc2 | 15,71428571 | |
| t12 | 4 | |
| F12 | 0 | |
| S-Hypo | Rankine | |

### A.6.3 CLT 220 L7s-2

| CLT 220 L7s-2 | | | | | | | | | | | | |
|---|---|---|---|---|---|---|---|---|---|---|---|---|
| | | | | | | | For axial loading: | | For flexural loading: | | | |
| layers: | t | b | A | z | Direction | A_main | E1*A | E2*A | G31*k*A | G32*k*A | E1*Ief | E2*Ief |
| 1 | 30 | 1000 | 30000 | 15 | 0 | 30000 | 375000000 | 0 | 3891600 | 228000 | 3,41E+12 | 0 |
| 2 | 30 | 1000 | 30000 | 45 | 0 | 30000 | 375000000 | 0 | 3891600 | 228000 | 1,61E+12 | 0 |
| 3 | 30 | 1000 | 30000 | 75 | 90 | 0 | 0 | 375000000 | 282000 | 3146400 | 0 | 4,88E+11 |
| 4 | 40 | 1000 | 40000 | 110 | 0 | 40000 | 500000000 | 0 | 5188800 | 304000 | 6,67E+10 | 0 |
| 5 | 30 | 1000 | 30000 | 145 | 90 | 0 | 0 | 0 | 282000 | 3146400 | 0 | 4,88E+11 |
| 6 | 30 | 1000 | 30000 | 175 | 0 | 30000 | 375000000 | 375000000 | 3891600 | 228000 | 1,61E+12 | 0 |
| 7 | 30 | 1000 | 30000 | 205 | 0 | 30000 | 375000000 | 0 | 3891600 | 228000 | 3,41E+12 | 0 |
| 8 | 0 | 1000 | 0 | 220 | 0 | 0 | 0 | 0 | 0 | 0 | 0 | 0 |
| | | | | | | | 2000000000 | 750000000 | 21319200 | 7508800 | 1,01E+13 | 9,75E+11 |

| | |
|---|---|
| h_clt | 220 |
| z_na | 110 |
| A_ref | 220000 |
| I_ref | 887333333 |
| k0 | 0,188 |
| k90 | 0,152 |
| A_main | 160000 |
| % | 0,72727273 |

| Modified: | Axial | Bending |
|---|---|---|
| E1 | 3409,09091 | 1098,798 |
| E2 | 9090,90909 | 11401,2 |
| G12 | 483 | 448,5 |
| nue12 | 0 | |
| G31 | 34,1309091 | |
| G32 | 96,9054545 | |
| gamma | 3500 | |
| alphaT1 | 5,00E-06 | |
| alphaT2 | 5,00E-06 | |
| ft1 | 4,24545455 | |
| ft2 | 10,6545455 | |
| fc1 | 7,54545455 | |
| fc2 | 15,9545455 | |
| t12 | 4 | |
| F12 | 0 | |
| S-Hypo | Rankine | |

# B

# Results Appendix

## B.1 Data from analysis

| | ISO10137 $[m/s^2]$ | ISO6897 $[m/s^2]$ | Frequency $[Hz]$ | Height $[m]$ | Deflection $[mm]$ |
|---|---|---|---|---|---|
| CLT220 | 0,0071 | 0,0032 | 3,002 | 7,0 | 0,86 |
| Max height: | 0,0134 | 0,0061 | 2,100 | 10,5 | 2,35 |
| ISO10137 | 0,0213 | 0,0097 | 1,577 | 14,0 | 5,02 |
| 28 | 0,0308 | 0,0139 | 1,240 | 17,5 | 9,26 |
| ISO6897 | 0,0419 | 0,0189 | 1,006 | 21,0 | 15,59 |
| 24,5 | 0,0548 | 0,0247 | 0,835 | 24,5 | 24,63 |
| Deflection | 0,0694 | 0,0312 | 0,705 | 28,0 | 37,11 |
| 31,5 | 0,0856 | 0,0384 | 0,603 | 31,5 | 53,92 |
| | 0,1033 | 0,0463 | 0,521 | 35,0 | 76,04 |
| | 0,1224 | 0,0548 | 0,455 | 38,5 | 104,62 |
| | 0,1426 | 0,0638 | 0,400 | 42,0 | 140,91 |
| | 0,1638 | 0,0732 | 0,355 | 45,5 | 186,33 |
| | 0,1857 | 0,0830 | 0,316 | 49,0 | 242,41 |
| | 0,2080 | 0,0930 | 0,284 | 52,5 | 310,83 |
| | 0,2305 | 0,1032 | 0,256 | 56,0 | 393,40 |
| | 0,2530 | 0,1134 | 0,232 | 59,5 | 492,07 |
| | 0,2753 | 0,1236 | 0,211 | 63,0 | 608,92 |
| CLT280 | 0,0063 | 0,0029 | 3,405 | 7,0 | 0,66 |
| Max height: | 0,0117 | 0,0054 | 2,373 | 10,5 | 1,83 |
| ISO10137 | 0,0186 | 0,0085 | 1,778 | 14,0 | 3,93 |
| 28 | 0,0269 | 0,0122 | 1,395 | 17,5 | 7,27 |
| ISO6897 | 0,0368 | 0,0167 | 1,130 | 21,0 | 12,28 |
| 28 | 0,0482 | 0,0218 | 0,937 | 24,5 | 19,44 |
| Deflection | 0,0613 | 0,0276 | 0,790 | 28,0 | 29,35 |
| 35 | 0,0759 | 0,0341 | 0,675 | 31,5 | 42,72 |
| | 0,0920 | 0,0413 | 0,583 | 35,0 | 60,34 |
| | 0,1094 | 0,0490 | 0,509 | 38,5 | 83,13 |
| | 0,1280 | 0,0573 | 0,447 | 42,0 | 112,11 |
| | 0,1477 | 0,0661 | 0,396 | 45,5 | 148,42 |
| | 0,1681 | 0,0752 | 0,353 | 49,0 | 193,30 |

| | | | | | |
|---|---|---|---|---|---|
| | 0,1890 | 0,0846 | 0,317 | 52,5 | 248,11 |
| | 0,2104 | 0,0942 | 0,285 | 56,0 | 314,34 |
| | 0,2319 | 0,1039 | 0,258 | 59,5 | 393,54 |
| | 0,2534 | 0,1136 | 0,235 | 63,0 | 487,45 |
| CLT320 | 0,0059 | 0,0027 | 3,662 | 7,0 | 0,57 |
| Max height: | 0,0109 | 0,0050 | 2,553 | 10,5 | 1,57 |
| ISO10137 | 0,0171 | 0,0078 | 1,913 | 14,0 | 3,37 |
| 28 | 0,0247 | 0,0113 | 1,502 | 17,5 | 6,25 |
| ISO6897 | 0,0337 | 0,0153 | 1,217 | 21,0 | 10,53 |
| 28 | 0,0442 | 0,0200 | 1,009 | 24,5 | 16,66 |
| Deflection | 0,0561 | 0,0253 | 0,851 | 28,0 | 25,10 |
| 38,5 | 0,0695 | 0,0313 | 0,728 | 31,5 | 36,47 |
| | 0,0843 | 0,0379 | 0,630 | 35,0 | 51,42 |
| | 0,1004 | 0,0451 | 0,550 | 38,5 | 70,74 |
| | 0,1177 | 0,0528 | 0,484 | 42,0 | 95,26 |
| | 0,1360 | 0,0609 | 0,429 | 45,5 | 125,96 |
| | 0,1551 | 0,0694 | 0,382 | 49,0 | 163,88 |
| | 0,1749 | 0,0783 | 0,343 | 52,5 | 210,16 |
| | 0,1952 | 0,0874 | 0,309 | 56,0 | 266,04 |
| | 0,2157 | 0,0966 | 0,280 | 59,5 | 332,86 |
| | 0,2363 | 0,1059 | 0,255 | 63,0 | 412,07 |
| C220 | 0,0462 | 0,0218 | 8,022 | 7,0 | 0,05 |
| Max height: | 0,0044 | 0,0021 | 7,549 | 10,5 | 0,15 |
| ISO10137 | 0,0061 | 0,0029 | 5,397 | 14,0 | 0,37 |
| 42 | 0,0088 | 0,0041 | 3,974 | 17,5 | 0,81 |
| ISO6897 | 0,0127 | 0,0059 | 3,019 | 21,0 | 1,57 |
| 38,5 | 0,0178 | 0,0083 | 2,360 | 24,5 | 2,83 |
| Deflection | 0,0242 | 0,0112 | 1,888 | 28,0 | 4,76 |
| 59,5 | 0,0318 | 0,0147 | 1,542 | 31,5 | 7,59 |
| | 0,0407 | 0,0187 | 1,281 | 35,0 | 11,60 |
| | 0,0507 | 0,0232 | 1,080 | 38,5 | 17,07 |
| | 0,0619 | 0,0282 | 0,922 | 42,0 | 24,38 |
| | 0,0740 | 0,0336 | 0,796 | 45,5 | 33,87 |
| | 0,0872 | 0,0395 | 0,694 | 49,0 | 46,02 |
| | 0,1011 | 0,0457 | 0,610 | 52,5 | 61,24 |
| | 0,1159 | 0,0522 | 0,541 | 56,0 | 80,12 |
| | 0,1311 | 0,0590 | 0,482 | 59,5 | 103,10 |
| | 0,1469 | 0,0660 | 0,433 | 63,0 | 130,93 |
| C280 | 0,0463 | 0,0219 | 8,022 | 7,0 | 0,04 |
| Max height: | 0,0401 | 0,0191 | 7,713 | 10,5 | 0,11 |
| ISO10137 | 0,0055 | 0,0026 | 5,964 | 14,0 | 0,29 |
| 42 | 0,0077 | 0,0037 | 4,399 | 17,5 | 0,63 |
| ISO6897 | 0,0110 | 0,0052 | 3,343 | 21,0 | 1,23 |
| 42 | 0,0153 | 0,0071 | 2,614 | 24,5 | 2,22 |

| | | | | | |
|---|---|---|---|---|---|
| Deflection | 0,0207 | 0,0096 | 2,091 | 28,0 | 3,74 |
| 63 | 0,0272 | 0,0126 | 1,708 | 31,5 | 5,96 |
| | 0,0348 | 0,0160 | 1,418 | 35,0 | 9,11 |
| | 0,0435 | 0,0199 | 1,196 | 38,5 | 13,41 |
| | 0,0531 | 0,0243 | 1,020 | 42,0 | 19,15 |
| | 0,0637 | 0,0290 | 0,881 | 45,5 | 26,61 |
| | 0,0752 | 0,0342 | 0,768 | 49,0 | 36,16 |
| | 0,0875 | 0,0396 | 0,675 | 52,5 | 48,13 |
| | 0,1005 | 0,0454 | 0,598 | 56,0 | 62,98 |
| | 0,1141 | 0,0514 | 0,533 | 59,5 | 81,06 |
| | 0,1282 | 0,0577 | 0,478 | 63,0 | 102,95 |
| C320 | 0,0463 | 0,0219 | 8,022 | 7,0 | 0,03 |
| Max height: | 0,0402 | 0,0191 | 7,713 | 10,5 | 0,10 |
| ISO10137 | 0,0053 | 0,0025 | 6,292 | 14,0 | 0,25 |
| 45,5 | 0,0072 | 0,0034 | 4,647 | 17,5 | 0,55 |
| ISO6897 | 0,0102 | 0,0048 | 3,532 | 21,0 | 1,08 |
| 45,5 | 0,0141 | 0,0066 | 2,761 | 24,5 | 1,94 |
| Deflection | 0,0190 | 0,0088 | 2,209 | 28,0 | 3,27 |
| 63 | 0,0249 | 0,0115 | 1,804 | 31,5 | 5,21 |
| | 0,0319 | 0,0147 | 1,498 | 35,0 | 7,97 |
| | 0,0398 | 0,0183 | 1,263 | 38,5 | 11,73 |
| | 0,0487 | 0,0223 | 1,077 | 42,0 | 16,75 |
| | 0,0585 | 0,0267 | 0,930 | 45,5 | 23,28 |
| | 0,0691 | 0,0314 | 0,810 | 49,0 | 31,63 |
| | 0,0805 | 0,0365 | 0,712 | 52,5 | 42,10 |
| | 0,0926 | 0,0419 | 0,631 | 56,0 | 55,10 |
| | 0,1053 | 0,0475 | 0,563 | 59,5 | 70,92 |
| | 0,1185 | 0,0534 | 0,505 | 63,0 | 90,09 |
| CLT220-H | 0,0045 | 0,0020 | 1,927 | 7,0 | 0,85 |
| Max height: | 0,0088 | 0,0039 | 1,349 | 10,5 | 2,32 |
| ISO10137 | 0,0140 | 0,0063 | 1,016 | 14,0 | 4,93 |
| 52,5 | 0,0201 | 0,0090 | 0,800 | 17,5 | 9,05 |
| ISO6897 | 0,0272 | 0,0122 | 0,651 | 21,0 | 15,17 |
| 45,5 | 0,0352 | 0,0157 | 0,541 | 24,5 | 23,84 |
| Deflection | 0,0441 | 0,0197 | 0,458 | 28,0 | 35,73 |
| 31,5 | 0,0538 | 0,0240 | 0,393 | 31,5 | 51,61 |
| | 0,0642 | 0,0287 | 0,341 | 35,0 | 72,31 |
| | 0,0751 | 0,0336 | 0,298 | 38,5 | 98,79 |
| | 0,0865 | 0,0388 | 0,263 | 42,0 | 132,10 |
| | 0,0982 | 0,0441 | 0,234 | 45,5 | 173,25 |
| | 0,1100 | 0,0495 | 0,210 | 49,0 | 223,49 |
| | 0,1219 | 0,0551 | 0,189 | 52,5 | 284,08 |
| | 0,1338 | 0,0606 | 0,171 | 56,0 | 356,26 |
| | 0,1455 | 0,0661 | 0,156 | 59,5 | 441,48 |

| | | | | | |
|---|---|---|---|---|---|
| | 0,1570 | 0,0715 | 0,143 | 63,0 | 541,23 |
| CLT280-H | 0,0039 | 0,0018 | 2,192 | 7,0 | 0,66 |
| Max height: | 0,0077 | 0,0035 | 1,528 | 10,5 | 1,81 |
| ISO10137 | 0,0123 | 0,0055 | 1,146 | 14,0 | 3,86 |
| 56 | 0,0178 | 0,0080 | 0,901 | 17,5 | 7,13 |
| ISO6897 | 0,0242 | 0,0108 | 0,731 | 21,0 | 11,99 |
| 49 | 0,0315 | 0,0141 | 0,607 | 24,5 | 18,91 |
| Deflection | 0,0396 | 0,0177 | 0,513 | 28,0 | 28,43 |
| 35 | 0,0485 | 0,0217 | 0,439 | 31,5 | 41,19 |
| | 0,0582 | 0,0260 | 0,381 | 35,0 | 57,86 |
| | 0,0685 | 0,0306 | 0,333 | 38,5 | 79,27 |
| | 0,0792 | 0,0355 | 0,294 | 42,0 | 106,27 |
| | 0,0903 | 0,0405 | 0,261 | 45,5 | 139,74 |
| | 0,1017 | 0,0457 | 0,233 | 49,0 | 180,74 |
| | 0,1132 | 0,0510 | 0,210 | 52,5 | 230,33 |
| | 0,1248 | 0,0564 | 0,190 | 56,0 | 289,60 |
| | 0,1363 | 0,0617 | 0,173 | 59,5 | 359,78 |
| | 0,1477 | 0,0671 | 0,158 | 63,0 | 442,18 |
| CLT320-H | 0,0036 | 0,0016 | 2,361 | 7,0 | 0,57 |
| Max height: | 0,0071 | 0,0032 | 1,646 | 10,5 | 1,56 |
| ISO10137 | 0,0114 | 0,0051 | 1,234 | 14,0 | 3,33 |
| 56 | 0,0164 | 0,0074 | 0,970 | 17,5 | 6,14 |
| ISO6897 | 0,0223 | 0,0100 | 0,788 | 21,0 | 10,31 |
| 52,5 | 0,0291 | 0,0130 | 0,654 | 24,5 | 16,25 |
| Deflection | 0,0366 | 0,0164 | 0,553 | 28,0 | 24,40 |
| 38,5 | 0,0449 | 0,0201 | 0,474 | 31,5 | 35,31 |
| | 0,0540 | 0,0241 | 0,411 | 35,0 | 49,58 |
| | 0,0636 | 0,0285 | 0,359 | 38,5 | 67,88 |
| | 0,0738 | 0,0330 | 0,317 | 42,0 | 90,97 |
| | 0,0844 | 0,0378 | 0,282 | 45,5 | 119,61 |
| | 0,0953 | 0,0428 | 0,252 | 49,0 | 154,71 |
| | 0,1064 | 0,0479 | 0,227 | 52,5 | 197,21 |
| | 0,1176 | 0,0530 | 0,205 | 56,0 | 248,06 |
| | 0,1287 | 0,0582 | 0,186 | 59,5 | 308,33 |
| | 0,1399 | 0,0634 | 0,170 | 63,0 | 379,18 |
| C220-H | 0,0054 | 0,0025 | 5,361 | 7,0 | 0,05 |
| Max height: | 0,0067 | 0,0031 | 4,928 | 10,5 | 0,15 |
| ISO10137 | 0,0034 | 0,0016 | 3,634 | 14,0 | 0,37 |
| 63 | 0,0056 | 0,0026 | 2,658 | 17,5 | 0,80 |
| ISO6897 | 0,0086 | 0,0040 | 2,014 | 21,0 | 1,56 |
| 59,5 | 0,0123 | 0,0057 | 1,574 | 24,5 | 2,80 |
| Deflection | 0,0169 | 0,0077 | 1,259 | 28,0 | 4,71 |
| 59,5 | 0,0223 | 0,0102 | 1,029 | 31,5 | 7,50 |
| | 0,0285 | 0,0129 | 0,856 | 35,0 | 11,43 |

| | | | | | |
|---|---|---|---|---|---|
| | 0,0354 | 0,0160 | 0,723 | 38,5 | 16,78 |
| | 0,0429 | 0,0194 | 0,618 | 42,0 | 23,90 |
| | 0,0510 | 0,0230 | 0,534 | 45,5 | 33,12 |
| | 0,0596 | 0,0268 | 0,467 | 49,0 | 44,87 |
| | 0,0686 | 0,0308 | 0,411 | 52,5 | 59,53 |
| | 0,0779 | 0,0350 | 0,365 | 56,0 | 77,65 |
| | 0,0874 | 0,0393 | 0,326 | 59,5 | 99,62 |
| | 0,0972 | 0,0437 | 0,293 | 63,0 | 126,10 |
| C280-H | 0,0054 | 0,0025 | 5,363 | 7,0 | 0,04 |
| Max height: | 0,0067 | 0,0032 | 4,931 | 10,5 | 0,11 |
| ISO10137 | 0,0029 | 0,0014 | 4,066 | 14,0 | 0,29 |
| 63 | 0,0048 | 0,0022 | 2,974 | 17,5 | 0,63 |
| ISO6897 | 0,0074 | 0,0034 | 2,253 | 21,0 | 1,23 |
| 63 | 0,0106 | 0,0049 | 1,760 | 24,5 | 2,20 |
| Deflection | 0,0146 | 0,0067 | 1,408 | 28,0 | 3,71 |
| 63 | 0,0193 | 0,0088 | 1,151 | 31,5 | 5,90 |
| | 0,0247 | 0,0112 | 0,956 | 35,0 | 9,00 |
| | 0,0308 | 0,0140 | 0,807 | 38,5 | 13,23 |
| | 0,0375 | 0,0169 | 0,690 | 42,0 | 18,85 |
| | 0,0447 | 0,0202 | 0,596 | 45,5 | 26,14 |
| | 0,0524 | 0,0236 | 0,520 | 49,0 | 35,44 |
| | 0,0605 | 0,0272 | 0,458 | 52,5 | 47,06 |
| | 0,0690 | 0,0310 | 0,406 | 56,0 | 61,43 |
| | 0,0778 | 0,0350 | 0,363 | 59,5 | 78,87 |
| | 0,0868 | 0,0390 | 0,326 | 63,0 | 99,92 |
| C320-H | 0,0054 | 0,0025 | 5,364 | 7,0 | 0,03 |
| Max height: | 0,0068 | 0,0032 | 4,932 | 10,5 | 0,10 |
| ISO10137 | 0,0027 | 0,0013 | 4,323 | 14,0 | 0,25 |
| 63 | 0,0044 | 0,0021 | 3,164 | 17,5 | 0,55 |
| ISO6897 | 0,0068 | 0,0031 | 2,397 | 21,0 | 1,07 |
| 63 | 0,0098 | 0,0045 | 1,871 | 24,5 | 1,93 |
| Deflection | 0,0134 | 0,0062 | 1,497 | 28,0 | 3,24 |
| 63 | 0,0178 | 0,0081 | 1,223 | 31,5 | 5,17 |
| | 0,0228 | 0,0104 | 1,016 | 35,0 | 7,88 |
| | 0,0284 | 0,0129 | 0,858 | 38,5 | 11,59 |
| | 0,0347 | 0,0157 | 0,733 | 42,0 | 16,52 |
| | 0,0414 | 0,0187 | 0,633 | 45,5 | 22,91 |
| | 0,0487 | 0,0220 | 0,553 | 49,0 | 31,08 |
| | 0,0563 | 0,0254 | 0,486 | 52,5 | 41,28 |
| | 0,0644 | 0,0290 | 0,431 | 56,0 | 53,90 |
| | 0,0727 | 0,0327 | 0,385 | 59,5 | 69,24 |
| | 0,0812 | 0,0365 | 0,346 | 63,0 | 87,75 |
| ST990C320-H | 0,0083 | 0,0039 | 5,435 | 7,0 | 0,03 |
| Max height: | 0,0081 | 0,0038 | 5,012 | 10,5 | 0,10 |

| | | | | | |
|---|---|---|---|---|---|
| ISO10137 | 0,0025 | 0,0012 | 4,410 | 14,0 | 0,24 |
| 63 | 0,0043 | 0,0020 | 3,236 | 17,5 | 0,52 |
| ISO6897 | 0,0066 | 0,0031 | 2,450 | 21,0 | 1,02 |
| 63 | 0,0094 | 0,0044 | 1,921 | 24,5 | 1,82 |
| Deflection | 0,0130 | 0,0060 | 1,539 | 28,0 | 3,05 |
| 63 | 0,0172 | 0,0079 | 1,259 | 31,5 | 4,85 |
| | 0,0219 | 0,0100 | 1,051 | 35,0 | 7,34 |
| | 0,0273 | 0,0124 | 0,889 | 38,5 | 10,73 |
| | 0,0332 | 0,0150 | 0,761 | 42,0 | 15,24 |
| | 0,0395 | 0,0179 | 0,661 | 45,5 | 20,96 |
| | 0,0464 | 0,0209 | 0,578 | 49,0 | 28,24 |
| | 0,0535 | 0,0241 | 0,510 | 52,5 | 37,31 |
| | 0,0611 | 0,0275 | 0,454 | 56,0 | 48,39 |
| | 0,0688 | 0,0310 | 0,407 | 59,5 | 61,81 |
| | 0,0768 | 0,0346 | 0,366 | 63,0 | 77,97 |
| ST990C320 | 0,0840 | 0,0397 | 8,109 | 7,0 | 0,03 |
| Max height: | 0,0536 | 0,0255 | 7,804 | 10,5 | 0,09 |
| ISO10137 | 0,0050 | 0,0024 | 6,456 | 14,0 | 0,23 |
| 45,5 | 0,0070 | 0,0033 | 4,752 | 17,5 | 0,52 |
| ISO6897 | 0,0099 | 0,0047 | 3,603 | 21,0 | 1,02 |
| 45,5 | 0,0137 | 0,0064 | 2,823 | 24,5 | 1,83 |
| Deflection | 0,0184 | 0,0086 | 2,260 | 28,0 | 3,09 |
| 63 | 0,0241 | 0,0112 | 1,846 | 31,5 | 4,92 |
| | 0,0308 | 0,0142 | 1,538 | 35,0 | 7,48 |
| | 0,0383 | 0,0176 | 1,299 | 38,5 | 10,97 |
| | 0,0468 | 0,0214 | 1,110 | 42,0 | 15,63 |
| | 0,0560 | 0,0256 | 0,962 | 45,5 | 21,56 |
| | 0,0661 | 0,0301 | 0,840 | 49,0 | 29,15 |
| | 0,0768 | 0,0349 | 0,740 | 52,5 | 38,65 |
| | 0,0882 | 0,0400 | 0,657 | 56,0 | 50,30 |
| | 0,1001 | 0,0453 | 0,588 | 59,5 | 64,46 |
| | 0,1126 | 0,0508 | 0,528 | 63,0 | 81,59 |
| ST990CLT320-H | 0,0025 | 0,0011 | 3,295 | 7,0 | 0,03 |
| Max height: | 0,0057 | 0,0026 | 2,129 | 10,5 | 0,10 |
| ISO10137 | 0,0095 | 0,0043 | 1,630 | 14,0 | 0,24 |
| 56 | 0,0142 | 0,0064 | 1,257 | 17,5 | 0,52 |
| ISO6897 | 0,0197 | 0,0089 | 0,994 | 21,0 | 1,02 |
| 52,5 | 0,0257 | 0,0116 | 0,831 | 24,5 | 1,82 |
| Deflection | 0,0325 | 0,0146 | 0,697 | 28,0 | 3,05 |
| 63 | 0,0401 | 0,0180 | 0,590 | 31,5 | 4,85 |
| | 0,0481 | 0,0216 | 0,515 | 35,0 | 7,34 |
| | 0,0567 | 0,0254 | 0,450 | 38,5 | 10,73 |
| | 0,0658 | 0,0295 | 0,395 | 42,0 | 15,24 |
| | 0,0750 | 0,0336 | 0,354 | 45,5 | 20,96 |

| | | | | | |
|---|---|---|---|---|---|
| | 0,0846 | 0,0379 | 0,318 | 49,0 | 28,24 |
| | 0,0944 | 0,0424 | 0,286 | 52,5 | 37,31 |
| | 0,1043 | 0,0469 | 0,259 | 56,0 | 48,39 |
| | 0,1142 | 0,0514 | 0,236 | 59,5 | 61,81 |
| | 0,1242 | 0,0560 | 0,216 | 63,0 | 77,97 |
| ST990CLT320 | 0,0039 | 0,0018 | 4,900 | 7,0 | 0,30 |
| Max height: | 0,0082 | 0,0038 | 3,212 | 10,5 | 0,97 |
| ISO10137 | 0,0139 | 0,0064 | 2,444 | 14,0 | 2,04 |
| 31,5 | 0,0212 | 0,0097 | 1,889 | 17,5 | 3,95 |
| ISO6897 | 0,0300 | 0,0137 | 1,497 | 21,0 | 7,02 |
| 28 | 0,0395 | 0,0180 | 1,249 | 24,5 | 10,99 |
| Deflection | 0,0505 | 0,0229 | 1,047 | 28,0 | 16,82 |
| 45,5 | 0,0628 | 0,0284 | 0,885 | 31,5 | 25,01 |
| | 0,0758 | 0,0342 | 0,770 | 35,0 | 34,79 |
| | 0,0901 | 0,0406 | 0,671 | 38,5 | 47,92 |
| | 0,1055 | 0,0475 | 0,588 | 42,0 | 65,07 |
| | 0,1214 | 0,0545 | 0,525 | 45,5 | 84,69 |
| | 0,1381 | 0,0620 | 0,469 | 49,0 | 109,51 |
| | 0,1554 | 0,0697 | 0,421 | 52,5 | 140,36 |
| | 0,1731 | 0,0776 | 0,381 | 56,0 | 176,21 |
| | 0,1912 | 0,0857 | 0,345 | 59,5 | 219,63 |
| | 0,2095 | 0,0939 | 0,314 | 63,0 | 271,55 |
| DT990C320-H | 0,0040 | 0,0019 | 5,502 | 7,0 | 0,03 |
| Max height: | 0,0058 | 0,0027 | 5,054 | 10,5 | 0,09 |
| ISO10137 | 0,0023 | 0,0011 | 4,689 | 14,0 | 0,21 |
| 63 | 0,0040 | 0,0019 | 3,447 | 17,5 | 0,46 |
| ISO6897 | 0,0060 | 0,0028 | 2,614 | 21,0 | 0,89 |
| 63 | 0,0086 | 0,0040 | 2,067 | 24,5 | 1,56 |
| Deflection | 0,0117 | 0,0054 | 1,668 | 28,0 | 2,58 |
| 63 | 0,0154 | 0,0071 | 1,371 | 31,5 | 4,06 |
| | 0,0195 | 0,0089 | 1,156 | 35,0 | 6,02 |
| | 0,0241 | 0,0110 | 0,986 | 38,5 | 8,66 |
| | 0,0292 | 0,0133 | 0,850 | 42,0 | 12,12 |
| | 0,0344 | 0,0156 | 0,746 | 45,5 | 16,32 |
| | 0,0401 | 0,0181 | 0,659 | 49,0 | 21,57 |
| | 0,0460 | 0,0208 | 0,586 | 52,5 | 28,04 |
| | 0,0522 | 0,0235 | 0,526 | 56,0 | 35,71 |
| | 0,0585 | 0,0264 | 0,475 | 59,5 | 44,87 |
| | 0,0651 | 0,0293 | 0,431 | 63,0 | 55,77 |
| DT990C320 | 0,0377 | 0,0178 | 8,248 | 7,0 | 0,02 |
| Max height: | 0,0454 | 0,0216 | 7,892 | 10,5 | 0,08 |
| ISO10137 | 0,0037 | 0,0018 | 6,879 | 14,0 | 0,20 |
| 49 | 0,0057 | 0,0027 | 5,046 | 17,5 | 0,45 |
| ISO6897 | 0,0085 | 0,0040 | 3,819 | 21,0 | 0,89 |

| | | | | | |
|---|---|---|---|---|---|
| 49 | 0,0120 | 0,0056 | 3,011 | 24,5 | 1,58 |
| Deflection | 0,0164 | 0,0076 | 2,422 | 28,0 | 2,64 |
| 63 | 0,0216 | 0,0100 | 1,984 | 31,5 | 4,19 |
| | 0,0274 | 0,0127 | 1,665 | 35,0 | 6,27 |
| | 0,0341 | 0,0157 | 1,415 | 38,5 | 9,09 |
| | 0,0416 | 0,0191 | 1,215 | 42,0 | 12,84 |
| | 0,0495 | 0,0227 | 1,061 | 45,5 | 17,43 |
| | 0,0582 | 0,0266 | 0,934 | 49,0 | 23,25 |
| | 0,0674 | 0,0307 | 0,827 | 52,5 | 30,51 |
| | 0,0771 | 0,0350 | 0,739 | 56,0 | 39,20 |
| | 0,0873 | 0,0396 | 0,664 | 59,5 | 49,73 |
| | 0,0981 | 0,0444 | 0,599 | 63,0 | 62,42 |
| DT990CLT320-H | 0,0015 | 0,0007 | 4,846 | 7,0 | 0,13 |
| Max height: | 0,0037 | 0,0017 | 3,040 | 10,5 | 0,45 |
| ISO10137 | 0,0063 | 0,0029 | 2,311 | 14,0 | 0,95 |
| 63 | 0,0097 | 0,0044 | 1,769 | 17,5 | 1,88 |
| ISO6897 | 0,0140 | 0,0064 | 1,384 | 21,0 | 3,42 |
| 63 | 0,0184 | 0,0084 | 1,159 | 24,5 | 5,32 |
| Deflection | 0,0236 | 0,0107 | 0,973 | 28,0 | 8,10 |
| 63 | 0,0294 | 0,0133 | 0,823 | 31,5 | 12,01 |
| | 0,0353 | 0,0159 | 0,723 | 35,0 | 16,38 |
| | 0,0416 | 0,0188 | 0,636 | 38,5 | 22,16 |
| | 0,0484 | 0,0218 | 0,561 | 42,0 | 29,62 |
| | 0,0551 | 0,0248 | 0,507 | 45,5 | 37,56 |
| | 0,0620 | 0,0279 | 0,459 | 49,0 | 47,43 |
| | 0,0692 | 0,0311 | 0,415 | 52,5 | 59,49 |
| | 0,0764 | 0,0343 | 0,380 | 56,0 | 72,92 |
| | 0,0837 | 0,0376 | 0,349 | 59,5 | 88,90 |
| | 0,0911 | 0,0409 | 0,320 | 63,0 | 107,71 |
| DT990CLT320 | 0,0033 | 0,0015 | 6,066 | 7,0 | 0,18 |
| Max height: | 0,0061 | 0,0028 | 4,269 | 10,5 | 0,52 |
| ISO10137 | 0,0096 | 0,0045 | 3,323 | 14,0 | 1,05 |
| 35 | 0,0143 | 0,0067 | 2,586 | 17,5 | 2,03 |
| ISO6897 | 0,0206 | 0,0095 | 2,037 | 21,0 | 3,69 |
| 35 | 0,0274 | 0,0126 | 1,706 | 24,5 | 5,76 |
| Deflection | 0,0355 | 0,0163 | 1,430 | 28,0 | 8,86 |
| 59,5 | 0,0450 | 0,0205 | 1,206 | 31,5 | 13,29 |
| | 0,0547 | 0,0249 | 1,055 | 35,0 | 18,33 |
| | 0,0655 | 0,0298 | 0,923 | 38,5 | 25,11 |
| | 0,0774 | 0,0351 | 0,810 | 42,0 | 34,01 |
| | 0,0892 | 0,0404 | 0,729 | 45,5 | 43,66 |
| | 0,1018 | 0,0460 | 0,655 | 49,0 | 55,83 |
| | 0,1151 | 0,0520 | 0,590 | 52,5 | 70,97 |
| | 0,1286 | 0,0580 | 0,537 | 56,0 | 88,13 |

| | | | | | |
|---|---|---|---|---|---|
| | 0,1426 | 0,0642 | 0,489 | 59,5 | 108,91 |
| | 0,1571 | 0,0706 | 0,446 | 63,0 | 133,83 |
| ST990-H | 0,0041 | 0,0019 | 2,252 | 7,0 | 0,62 |
| Max height: | 0,0114 | 0,0051 | 1,256 | 10,5 | 2,74 |
| ISO10137 | 0,0201 | 0,0090 | 0,935 | 14,0 | 6,01 |
| 35 | 0,0315 | 0,0141 | 0,693 | 17,5 | 12,74 |
| ISO6897 | 0,0452 | 0,0201 | 0,525 | 21,0 | 24,89 |
| 31,5 | 0,0587 | 0,0261 | 0,437 | 24,5 | 39,13 |
| Deflection | 0,0733 | 0,0326 | 0,364 | 28,0 | 60,74 |
| 24,5 | 0,0886 | 0,0395 | 0,305 | 31,5 | 91,95 |
| | 0,1029 | 0,0460 | 0,268 | 35,0 | 124,61 |
| | 0,1174 | 0,0526 | 0,236 | 38,5 | 168,30 |
| | 0,1317 | 0,0592 | 0,208 | 42,0 | 225,28 |
| | 0,1451 | 0,0654 | 0,189 | 45,5 | 282,36 |
| | 0,1581 | 0,0714 | 0,172 | 49,0 | 353,73 |
| | 0,1707 | 0,0774 | 0,156 | 52,5 | 441,57 |
| | 0,1826 | 0,0830 | 0,143 | 56,0 | 537,11 |
| | 0,1939 | 0,0885 | 0,132 | 59,5 | 651,63 |
| | 0,2047 | 0,0937 | 0,121 | 63,0 | 787,40 |
| ST500-H | 0,0050 | 0,0023 | 1,831 | 7,0 | 0,96 |
| Max height: | 0,0126 | 0,0056 | 1,101 | 10,5 | 3,59 |
| ISO10137 | 0,0214 | 0,0096 | 0,829 | 14,0 | 7,65 |
| 35 | 0,0328 | 0,0146 | 0,627 | 17,5 | 15,50 |
| ISO6897 | 0,0464 | 0,0207 | 0,484 | 21,0 | 29,10 |
| 31,5 | 0,0597 | 0,0266 | 0,406 | 24,5 | 45,13 |
| Deflection | 0,0740 | 0,0330 | 0,340 | 28,0 | 68,90 |
| 24,5 | 0,0891 | 0,0398 | 0,287 | 31,5 | 102,66 |
| | 0,1031 | 0,0461 | 0,254 | 35,0 | 138,25 |
| | 0,1173 | 0,0526 | 0,224 | 38,5 | 185,28 |
| | 0,1314 | 0,0591 | 0,199 | 42,0 | 246,02 |
| | 0,1445 | 0,0652 | 0,181 | 45,5 | 307,28 |
| | 0,1572 | 0,0711 | 0,165 | 49,0 | 383,25 |
| | 0,1695 | 0,0770 | 0,150 | 52,5 | 476,14 |
| | 0,1812 | 0,0825 | 0,138 | 56,0 | 577,17 |
| | 0,1924 | 0,0879 | 0,127 | 59,5 | 697,64 |
| | 0,2030 | 0,0930 | 0,117 | 63,0 | 839,82 |
| DT990-H | 0,0019 | 0,0009 | 4,230 | 7,0 | 0,17 |
| Max height: | 0,0048 | 0,0022 | 2,536 | 10,5 | 0,66 |
| ISO10137 | 0,0084 | 0,0038 | 1,912 | 14,0 | 1,41 |
| 56 | 0,0133 | 0,0061 | 1,439 | 17,5 | 2,90 |
| ISO6897 | 0,0196 | 0,0089 | 1,104 | 21,0 | 5,52 |
| 49 | 0,0259 | 0,0117 | 0,923 | 24,5 | 8,61 |
| Deflection | 0,0331 | 0,0149 | 0,772 | 28,0 | 13,25 |
| 52,5 | 0,0413 | 0,0186 | 0,650 | 31,5 | 19,89 |

| | | | | | |
|---|---|---|---|---|---|
| | 0,0490 | 0,0220 | 0,574 | 35,0 | 26,88 |
| | 0,0573 | 0,0257 | 0,506 | 38,5 | 36,18 |
| | 0,0661 | 0,0296 | 0,447 | 42,0 | 48,26 |
| | 0,0744 | 0,0333 | 0,406 | 45,5 | 60,43 |
| | 0,0829 | 0,0372 | 0,369 | 49,0 | 75,59 |
| | 0,0916 | 0,0411 | 0,335 | 52,5 | 94,21 |
| | 0,1001 | 0,0449 | 0,308 | 56,0 | 114,48 |
| | 0,1086 | 0,0488 | 0,283 | 59,5 | 138,74 |
| | 0,1172 | 0,0527 | 0,261 | 63,0 | 167,46 |
| DT500-H | 0,0027 | 0,0012 | 2,959 | 7,0 | 0,36 |
| Max height: | 0,0061 | 0,0028 | 1,937 | 10,5 | 1,15 |
| ISO10137 | 0,0101 | 0,0046 | 1,484 | 14,0 | 2,36 |
| 59,5 | 0,0153 | 0,0069 | 1,155 | 17,5 | 4,48 |
| ISO6897 | 0,0216 | 0,0098 | 0,917 | 21,0 | 7,93 |
| 52,5 | 0,0280 | 0,0126 | 0,776 | 24,5 | 12,05 |
| Deflection | 0,0353 | 0,0159 | 0,660 | 28,0 | 17,92 |
| 49 | 0,0434 | 0,0194 | 0,564 | 31,5 | 26,01 |
| | 0,0510 | 0,0229 | 0,501 | 35,0 | 34,69 |
| | 0,0592 | 0,0265 | 0,446 | 38,5 | 45,90 |
| | 0,0678 | 0,0304 | 0,397 | 42,0 | 60,13 |
| | 0,0758 | 0,0340 | 0,363 | 45,5 | 74,69 |
| | 0,0841 | 0,0377 | 0,331 | 49,0 | 92,49 |
| | 0,0926 | 0,0415 | 0,303 | 52,5 | 113,99 |
| | 0,1009 | 0,0453 | 0,280 | 56,0 | 137,41 |
| | 0,1092 | 0,0491 | 0,258 | 59,5 | 165,08 |
| | 0,1176 | 0,0529 | 0,239 | 63,0 | 197,47 |
| ST990 | 0,0076 | 0,0035 | 3,077 | 7,0 | 0,75 |
| Max height: | 0,0188 | 0,0086 | 1,846 | 10,5 | 3,03 |
| ISO10137 | 0,0326 | 0,0148 | 1,388 | 14,0 | 6,61 |
| 17,5 | 0,0514 | 0,0232 | 1,029 | 17,5 | 14,15 |
| ISO6897 | 0,0752 | 0,0337 | 0,775 | 21,0 | 28,15 |
| 17,5 | 0,0989 | 0,0442 | 0,642 | 24,5 | 44,85 |
| Deflection | 0,1255 | 0,0560 | 0,531 | 28,0 | 70,68 |
| 24,5 | 0,1544 | 0,0688 | 0,442 | 31,5 | 108,83 |
| | 0,1815 | 0,0809 | 0,387 | 35,0 | 149,29 |
| | 0,2095 | 0,0934 | 0,339 | 38,5 | 204,18 |
| | 0,2380 | 0,1061 | 0,297 | 42,0 | 276,95 |
| | 0,2642 | 0,1179 | 0,268 | 45,5 | 350,56 |
| | 0,2901 | 0,1296 | 0,242 | 49,0 | 443,56 |
| | 0,3156 | 0,1412 | 0,219 | 52,5 | 559,45 |
| | 0,3397 | 0,1522 | 0,200 | 56,0 | 686,75 |
| | 0,3629 | 0,1629 | 0,183 | 59,5 | 841,05 |
| | 0,3851 | 0,1733 | 0,168 | 63,0 | 1026,16 |
| ST500 | 0,0087 | 0,0040 | 2,618 | 7,0 | 1,08 |

| | | | | | |
|---|---|---|---|---|---|
| Max height: | 0,0204 | 0,0093 | 1,645 | 10,5 | 3,88 |
| ISO10137 | 0,0346 | 0,0156 | 1,249 | 14,0 | 8,26 |
| 17,5 | 0,0536 | 0,0241 | 0,944 | 17,5 | 16,91 |
| ISO6897 | 0,0773 | 0,0346 | 0,723 | 21,0 | 32,36 |
| 17,5 | 0,1009 | 0,0451 | 0,603 | 24,5 | 50,85 |
| Deflection | 0,1274 | 0,0568 | 0,503 | 28,0 | 78,85 |
| 21 | 0,1561 | 0,0695 | 0,421 | 31,5 | 119,54 |
| | 0,1829 | 0,0815 | 0,370 | 35,0 | 162,93 |
| | 0,2106 | 0,0938 | 0,325 | 38,5 | 221,17 |
| | 0,2387 | 0,1065 | 0,286 | 42,0 | 297,68 |
| | 0,2646 | 0,1181 | 0,259 | 45,5 | 375,47 |
| | 0,2903 | 0,1297 | 0,235 | 49,0 | 473,08 |
| | 0,3155 | 0,1412 | 0,213 | 52,5 | 594,01 |
| | 0,3393 | 0,1521 | 0,195 | 56,0 | 726,81 |
| | 0,3623 | 0,1628 | 0,179 | 59,5 | 887,05 |
| | 0,3843 | 0,1730 | 0,164 | 63,0 | 1078,57 |
| DT990 | 0,0049 | 0,0023 | 4,616 | 7,0 | 0,28 |
| Max height: | 0,0094 | 0,0043 | 3,358 | 10,5 | 0,81 |
| ISO10137 | 0,0148 | 0,0068 | 2,674 | 14,0 | 1,63 |
| 28 | 0,0221 | 0,0102 | 2,073 | 17,5 | 3,26 |
| ISO6897 | 0,0319 | 0,0146 | 1,608 | 21,0 | 6,20 |
| 28 | 0,0420 | 0,0192 | 1,348 | 24,5 | 9,72 |
| Deflection | 0,0539 | 0,0245 | 1,127 | 28,0 | 15,08 |
| 49 | 0,0677 | 0,0307 | 0,945 | 31,5 | 22,91 |
| | 0,0810 | 0,0367 | 0,832 | 35,0 | 31,24 |
| | 0,0956 | 0,0432 | 0,731 | 38,5 | 42,48 |
| | 0,1114 | 0,0502 | 0,642 | 42,0 | 57,28 |
| | 0,1262 | 0,0568 | 0,582 | 45,5 | 72,32 |
| | 0,1418 | 0,0638 | 0,527 | 49,0 | 91,23 |
| | 0,1581 | 0,0710 | 0,477 | 52,5 | 114,72 |
| | 0,1740 | 0,0781 | 0,437 | 56,0 | 140,52 |
| | 0,1903 | 0,0854 | 0,400 | 59,5 | 171,72 |
| | 0,2070 | 0,0928 | 0,367 | 63,0 | 209,07 |
| DT500 | 0,0056 | 0,0026 | 3,780 | 7,0 | 0,47 |
| Max height: | 0,0107 | 0,0049 | 2,744 | 10,5 | 1,30 |
| ISO10137 | 0,0167 | 0,0077 | 2,176 | 14,0 | 2,57 |
| 28 | 0,0246 | 0,0113 | 1,721 | 17,5 | 4,84 |
| ISO6897 | 0,0348 | 0,0158 | 1,373 | 21,0 | 8,61 |
| 28 | 0,0452 | 0,0205 | 1,163 | 24,5 | 13,15 |
| Deflection | 0,0573 | 0,0260 | 0,987 | 28,0 | 19,75 |
| 45,5 | 0,0712 | 0,0322 | 0,841 | 31,5 | 29,03 |
| | 0,0846 | 0,0382 | 0,745 | 35,0 | 39,05 |
| | 0,0992 | 0,0447 | 0,660 | 38,5 | 52,19 |
| | 0,1149 | 0,0517 | 0,585 | 42,0 | 69,14 |

| | | | | | |
|---|---|---|---|---|---|
| | 0,1296 | 0,0582 | 0,533 | 45,5 | 86,57 |
| | 0,1451 | 0,0651 | 0,485 | 49,0 | 108,12 |
| | 0,1612 | 0,0723 | 0,441 | 52,5 | 134,49 |
| | 0,1770 | 0,0793 | 0,406 | 56,0 | 163,44 |
| | 0,1931 | 0,0866 | 0,373 | 59,5 | 198,04 |
| | 0,2096 | 0,0939 | 0,344 | 63,0 | 239,05 |
| CLT220-J | 0,0077 | 0,0035 | 2,801 | 7,0 | 0,98 |
| Max height: | 0,0156 | 0,0071 | 1,894 | 10,5 | 2,90 |
| ISO10137 | 0,0260 | 0,0118 | 1,386 | 14,0 | 6,55 |
| 24,5 | 0,0384 | 0,0173 | 1,071 | 17,5 | 12,56 |
| ISO6897 | 0,0525 | 0,0236 | 0,860 | 21,0 | 21,61 |
| 21 | 0,0681 | 0,0305 | 0,710 | 24,5 | 34,42 |
| Deflection | 0,0849 | 0,0380 | 0,598 | 28,0 | 51,85 |
| 28 | 0,1028 | 0,0459 | 0,513 | 31,5 | 74,81 |
| | 0,1215 | 0,0543 | 0,445 | 35,0 | 104,43 |
| | 0,1411 | 0,0630 | 0,390 | 38,5 | 141,82 |
| | 0,1612 | 0,0720 | 0,345 | 42,0 | 188,44 |
| | 0,1818 | 0,0812 | 0,308 | 45,5 | 245,60 |
| | 0,2028 | 0,0907 | 0,276 | 49,0 | 315,05 |
| | 0,2238 | 0,1002 | 0,249 | 52,5 | 398,32 |
| | 0,2449 | 0,1098 | 0,226 | 56,0 | 497,58 |
| | 0,2659 | 0,1194 | 0,206 | 59,5 | 614,51 |
| | 0,2866 | 0,1289 | 0,188 | 63,0 | 751,49 |
| CLT280-J | 0,0068 | 0,0031 | 3,168 | 7,0 | 0,76 |
| Max height: | 0,0138 | 0,0063 | 2,128 | 10,5 | 2,28 |
| ISO10137 | 0,0230 | 0,0104 | 1,550 | 14,0 | 5,21 |
| 24,5 | 0,0342 | 0,0155 | 1,193 | 17,5 | 10,07 |
| ISO6897 | 0,0470 | 0,0212 | 0,955 | 21,0 | 17,42 |
| 24,5 | 0,0612 | 0,0275 | 0,787 | 24,5 | 27,86 |
| Deflection | 0,0766 | 0,0344 | 0,662 | 28,0 | 42,09 |
| 31,5 | 0,0931 | 0,0417 | 0,567 | 31,5 | 60,85 |
| | 0,1105 | 0,0494 | 0,491 | 35,0 | 85,06 |
| | 0,1286 | 0,0575 | 0,431 | 38,5 | 115,64 |
| | 0,1474 | 0,0659 | 0,381 | 42,0 | 153,78 |
| | 0,1668 | 0,0745 | 0,339 | 45,5 | 200,53 |
| | 0,1865 | 0,0834 | 0,304 | 49,0 | 257,36 |
| | 0,2065 | 0,0924 | 0,275 | 52,5 | 325,49 |
| | 0,2266 | 0,1015 | 0,249 | 56,0 | 406,72 |
| | 0,2468 | 0,1107 | 0,227 | 59,5 | 502,39 |
| | 0,2668 | 0,1198 | 0,208 | 63,0 | 614,53 |
| CLT320-J | 0,0064 | 0,0029 | 3,410 | 7,0 | 0,65 |
| Max height: | 0,0128 | 0,0058 | 2,290 | 10,5 | 1,96 |
| ISO10137 | 0,0212 | 0,0097 | 1,665 | 14,0 | 4,49 |
| 24,5 | 0,0316 | 0,0143 | 1,280 | 17,5 | 8,71 |

| | | | | | |
|---|---|---|---|---|---|
| ISO6897 | 0,0436 | 0,0197 | 1,024 | 21,0 | 15,11 |
| 24,5 | 0,0569 | 0,0256 | 0,843 | 24,5 | 24,20 |
| Deflection | 0,0713 | 0,0320 | 0,709 | 28,0 | 36,58 |
| 31,5 | 0,0867 | 0,0389 | 0,607 | 31,5 | 52,89 |
| | 0,1031 | 0,0462 | 0,526 | 35,0 | 73,91 |
| | 0,1201 | 0,0538 | 0,461 | 38,5 | 100,41 |
| | 0,1379 | 0,0617 | 0,408 | 42,0 | 133,40 |
| | 0,1562 | 0,0698 | 0,364 | 45,5 | 173,78 |
| | 0,1749 | 0,0782 | 0,326 | 49,0 | 222,78 |
| | 0,1939 | 0,0868 | 0,294 | 52,5 | 281,46 |
| | 0,2131 | 0,0954 | 0,267 | 56,0 | 351,31 |
| | 0,2324 | 0,1042 | 0,243 | 59,5 | 433,51 |
| | 0,2517 | 0,1129 | 0,223 | 63,0 | 529,74 |
| CLT220-H-J | 0,0047 | 0,0021 | 1,857 | 7,0 | 0,92 |
| Max height: | 0,0094 | 0,0042 | 1,285 | 10,5 | 2,57 |
| ISO10137 | 0,0151 | 0,0068 | 0,960 | 14,0 | 5,53 |
| 52,5 | 0,0217 | 0,0097 | 0,754 | 17,5 | 10,22 |
| ISO6897 | 0,0292 | 0,0131 | 0,612 | 21,0 | 17,15 |
| 45,5 | 0,0376 | 0,0168 | 0,509 | 24,5 | 26,90 |
| Deflection | 0,0467 | 0,0208 | 0,432 | 28,0 | 40,14 |
| 31,5 | 0,0564 | 0,0252 | 0,371 | 31,5 | 57,70 |
| | 0,0668 | 0,0298 | 0,323 | 35,0 | 80,34 |
| | 0,0776 | 0,0347 | 0,283 | 38,5 | 109,10 |
| | 0,0889 | 0,0399 | 0,251 | 42,0 | 145,07 |
| | 0,1003 | 0,0451 | 0,224 | 45,5 | 189,21 |
| | 0,1120 | 0,0505 | 0,201 | 49,0 | 242,76 |
| | 0,1236 | 0,0559 | 0,181 | 52,5 | 307,08 |
| | 0,1352 | 0,0613 | 0,165 | 56,0 | 383,44 |
| | 0,1467 | 0,0667 | 0,150 | 59,5 | 473,30 |
| | 0,1580 | 0,0721 | 0,138 | 63,0 | 578,08 |
| CLT280-H-J | 0,0041 | 0,0019 | 2,105 | 7,0 | 0,71 |
| Max height: | 0,0083 | 0,0037 | 1,448 | 10,5 | 2,02 |
| ISO10137 | 0,0134 | 0,0060 | 1,078 | 14,0 | 4,38 |
| 56 | 0,0194 | 0,0087 | 0,844 | 17,5 | 8,16 |
| ISO6897 | 0,0263 | 0,0118 | 0,684 | 21,0 | 13,75 |
| 49 | 0,0339 | 0,0152 | 0,568 | 24,5 | 21,63 |
| Deflection | 0,0423 | 0,0189 | 0,480 | 28,0 | 32,38 |
| 35 | 0,0514 | 0,0229 | 0,412 | 31,5 | 46,66 |
| | 0,0610 | 0,0273 | 0,358 | 35,0 | 65,13 |
| | 0,0713 | 0,0319 | 0,314 | 38,5 | 88,63 |
| | 0,0819 | 0,0367 | 0,278 | 42,0 | 118,09 |
| | 0,0929 | 0,0417 | 0,247 | 45,5 | 154,35 |
| | 0,1040 | 0,0468 | 0,222 | 49,0 | 198,46 |
| | 0,1153 | 0,0520 | 0,200 | 52,5 | 251,54 |

| | | | | | |
|---|---|---|---|---|---|
| | 0,1266 | 0,0573 | 0,182 | 56,0 | 314,75 |
| | 0,1379 | 0,0625 | 0,165 | 59,5 | 389,32 |
| | 0,1490 | 0,0678 | 0,151 | 63,0 | 476,48 |
| CLT320-H-J | 0,0038 | 0,0017 | 2,267 | 7,0 | 0,61 |
| Max height: | 0,0077 | 0,0035 | 1,558 | 10,5 | 1,74 |
| ISO10137 | 0,0124 | 0,0056 | 1,159 | 14,0 | 3,79 |
| 56 | 0,0180 | 0,0081 | 0,907 | 17,5 | 7,05 |
| ISO6897 | 0,0244 | 0,0109 | 0,735 | 21,0 | 11,89 |
| 49 | 0,0315 | 0,0141 | 0,610 | 24,5 | 18,71 |
| Deflection | 0,0393 | 0,0176 | 0,516 | 28,0 | 27,99 |
| 38,5 | 0,0479 | 0,0214 | 0,443 | 31,5 | 40,31 |
| | 0,0570 | 0,0255 | 0,385 | 35,0 | 56,23 |
| | 0,0666 | 0,0298 | 0,338 | 38,5 | 76,49 |
| | 0,0767 | 0,0344 | 0,299 | 42,0 | 101,87 |
| | 0,0872 | 0,0391 | 0,266 | 45,5 | 133,13 |
| | 0,0979 | 0,0440 | 0,239 | 49,0 | 171,16 |
| | 0,1088 | 0,0490 | 0,215 | 52,5 | 216,96 |
| | 0,1197 | 0,0540 | 0,195 | 56,0 | 271,54 |
| | 0,1307 | 0,0591 | 0,178 | 59,5 | 335,97 |
| | 0,1416 | 0,0642 | 0,163 | 63,0 | 411,37 |
| ST990-H-J | 0,0051 | 0,0023 | 1,789 | 7,0 | 1,00 |
| Max height: | 0,0127 | 0,0057 | 1,083 | 10,5 | 3,70 |
| ISO10137 | 0,0216 | 0,0096 | 0,817 | 14,0 | 7,87 |
| 38,5 | 0,0329 | 0,0147 | 0,619 | 17,5 | 15,85 |
| ISO6897 | 0,0465 | 0,0207 | 0,479 | 21,0 | 29,65 |
| 31,5 | 0,0597 | 0,0266 | 0,401 | 24,5 | 45,91 |
| Deflection | 0,0740 | 0,0330 | 0,337 | 28,0 | 69,96 |
| 24,5 | 0,0890 | 0,0397 | 0,285 | 31,5 | 104,05 |
| | 0,1030 | 0,0461 | 0,252 | 35,0 | 140,03 |
| | 0,1171 | 0,0525 | 0,223 | 38,5 | 187,49 |
| | 0,1311 | 0,0590 | 0,197 | 42,0 | 248,72 |
| | 0,1441 | 0,0650 | 0,180 | 45,5 | 310,52 |
| | 0,1568 | 0,0710 | 0,163 | 49,0 | 387,09 |
| | 0,1690 | 0,0768 | 0,149 | 52,5 | 480,64 |
| | 0,1807 | 0,0823 | 0,137 | 56,0 | 582,38 |
| | 0,1917 | 0,0876 | 0,126 | 59,5 | 703,62 |
| | 0,2023 | 0,0928 | 0,116 | 63,0 | 846,64 |
| ST500-H-J | 0,0077 | 0,0035 | 1,154 | 7,0 | 2,42 |
| Max height: | 0,0165 | 0,0073 | 0,769 | 10,5 | 7,29 |
| ISO10137 | 0,0261 | 0,0116 | 0,591 | 14,0 | 14,85 |
| 42 | 0,0377 | 0,0167 | 0,465 | 17,5 | 27,55 |
| ISO6897 | 0,0509 | 0,0226 | 0,373 | 21,0 | 47,47 |
| 35 | 0,0636 | 0,0283 | 0,318 | 24,5 | 71,35 |
| Deflection | 0,0771 | 0,0344 | 0,272 | 28,0 | 104,58 |

| | | | | | |
|---|---|---|---|---|---|
| 17,5 | 0,0912 | 0,0408 | 0,234 | 31,5 | 149,45 |
| | 0,1042 | 0,0468 | 0,209 | 35,0 | 197,88 |
| | 0,1173 | 0,0528 | 0,186 | 38,5 | 259,50 |
| | 0,1303 | 0,0589 | 0,167 | 42,0 | 336,64 |
| | 0,1422 | 0,0645 | 0,153 | 45,5 | 416,14 |
| | 0,1539 | 0,0700 | 0,140 | 49,0 | 512,24 |
| | 0,1652 | 0,0755 | 0,128 | 52,5 | 627,19 |
| | 0,1759 | 0,0806 | 0,119 | 56,0 | 752,22 |
| | 0,1861 | 0,0856 | 0,110 | 59,5 | 898,68 |
| | 0,1959 | 0,0904 | 0,102 | 63,0 | 1068,87 |
| DT990-H-J | 0,0028 | 0,0013 | 2,854 | 7,0 | 0,39 |
| Max height: | 0,0062 | 0,0028 | 1,878 | 10,5 | 1,21 |
| ISO10137 | 0,0103 | 0,0047 | 1,440 | 14,0 | 2,48 |
| 59,5 | 0,0154 | 0,0070 | 1,124 | 17,5 | 4,69 |
| ISO6897 | 0,0218 | 0,0098 | 0,894 | 21,0 | 8,24 |
| 52,5 | 0,0282 | 0,0127 | 0,758 | 24,5 | 12,50 |
| Deflection | 0,0354 | 0,0159 | 0,645 | 28,0 | 18,53 |
| 49 | 0,0434 | 0,0195 | 0,553 | 31,5 | 26,81 |
| | 0,0510 | 0,0229 | 0,491 | 35,0 | 35,71 |
| | 0,0591 | 0,0265 | 0,437 | 38,5 | 47,17 |
| | 0,0677 | 0,0303 | 0,390 | 42,0 | 61,68 |
| | 0,0756 | 0,0339 | 0,356 | 45,5 | 76,55 |
| | 0,0839 | 0,0376 | 0,326 | 49,0 | 94,69 |
| | 0,0923 | 0,0414 | 0,298 | 52,5 | 116,57 |
| | 0,1004 | 0,0451 | 0,275 | 56,0 | 140,40 |
| | 0,1087 | 0,0489 | 0,254 | 59,5 | 168,51 |
| | 0,1170 | 0,0527 | 0,235 | 63,0 | 201,38 |
| DT500-H-J | 0,0051 | 0,0023 | 1,636 | 7,0 | 1,20 |
| Max height: | 0,0101 | 0,0045 | 1,143 | 10,5 | 3,26 |
| ISO10137 | 0,0155 | 0,0070 | 0,887 | 14,0 | 6,46 |
| 63 | 0,0218 | 0,0097 | 0,713 | 17,5 | 11,36 |
| ISO6897 | 0,0289 | 0,0129 | 0,589 | 21,0 | 18,41 |
| 59,5 | 0,0359 | 0,0160 | 0,506 | 24,5 | 27,01 |
| Deflection | 0,0434 | 0,0193 | 0,440 | 28,0 | 38,27 |
| 35 | 0,0514 | 0,0229 | 0,386 | 31,5 | 52,70 |
| | 0,0589 | 0,0263 | 0,346 | 35,0 | 68,70 |
| | 0,0667 | 0,0298 | 0,312 | 38,5 | 88,23 |
| | 0,0748 | 0,0335 | 0,283 | 42,0 | 111,81 |
| | 0,0823 | 0,0369 | 0,260 | 45,5 | 136,78 |
| | 0,0899 | 0,0404 | 0,240 | 49,0 | 166,06 |
| | 0,0977 | 0,0440 | 0,222 | 52,5 | 200,15 |
| | 0,1051 | 0,0474 | 0,206 | 56,0 | 237,26 |
| | 0,1126 | 0,0509 | 0,192 | 59,5 | 279,75 |
| | 0,1201 | 0,0544 | 0,180 | 63,0 | 328,11 |

| | | | | | |
|---|---|---|---|---|---|
| ST990-J | 0,0088 | 0,0040 | 2,566 | 7,0 | 1,13 |
| Max height: | 0,0206 | 0,0093 | 1,619 | 10,5 | 3,99 |
| ISO10137 | 0,0348 | 0,0157 | 1,229 | 14,0 | 8,48 |
| 17,5 | 0,0537 | 0,0241 | 0,931 | 17,5 | 17,27 |
| ISO6897 | 0,0773 | 0,0346 | 0,715 | 21,0 | 32,90 |
| 17,5 | 0,1008 | 0,0450 | 0,596 | 24,5 | 51,63 |
| Deflection | 0,1271 | 0,0567 | 0,497 | 28,0 | 79,91 |
| 21 | 0,1556 | 0,0693 | 0,417 | 31,5 | 120,93 |
| | 0,1823 | 0,0812 | 0,367 | 35,0 | 164,71 |
| | 0,2098 | 0,0935 | 0,322 | 38,5 | 223,38 |
| | 0,2377 | 0,1060 | 0,284 | 42,0 | 300,38 |
| | 0,2635 | 0,1176 | 0,257 | 45,5 | 378,71 |
| | 0,2889 | 0,1292 | 0,233 | 49,0 | 476,92 |
| | 0,3140 | 0,1406 | 0,211 | 52,5 | 598,51 |
| | 0,3376 | 0,1514 | 0,193 | 56,0 | 732,02 |
| | 0,3604 | 0,1620 | 0,177 | 59,5 | 893,04 |
| | 0,3823 | 0,1722 | 0,162 | 63,0 | 1085,39 |
| ST500-J | 0,0125 | 0,0056 | 1,749 | 7,0 | 2,55 |
| Max height: | 0,0263 | 0,0118 | 1,182 | 10,5 | 7,59 |
| ISO10137 | 0,0421 | 0,0188 | 0,911 | 14,0 | 15,46 |
| 17,5 | 0,0617 | 0,0275 | 0,714 | 17,5 | 28,97 |
| ISO6897 | 0,0852 | 0,0380 | 0,570 | 21,0 | 50,73 |
| 17,5 | 0,1083 | 0,0482 | 0,483 | 24,5 | 77,08 |
| Deflection | 0,1338 | 0,0595 | 0,411 | 28,0 | 114,53 |
| 17,5 | 0,1612 | 0,0717 | 0,352 | 31,5 | 166,34 |
| | 0,1865 | 0,0831 | 0,312 | 35,0 | 222,56 |
| | 0,2126 | 0,0948 | 0,277 | 38,5 | 295,39 |
| | 0,2391 | 0,1068 | 0,247 | 42,0 | 388,30 |
| | 0,2633 | 0,1178 | 0,225 | 45,5 | 484,34 |
| | 0,2873 | 0,1287 | 0,205 | 49,0 | 602,07 |
| | 0,3110 | 0,1396 | 0,187 | 52,5 | 745,06 |
| | 0,3332 | 0,1499 | 0,172 | 56,0 | 901,87 |
| | 0,3548 | 0,1599 | 0,159 | 59,5 | 1088,10 |
| | 0,3756 | 0,1697 | 0,147 | 63,0 | 1307,62 |
| DT990-J | 0,0057 | 0,0026 | 3,686 | 7,0 | 0,50 |
| Max height: | 0,0108 | 0,0050 | 2,668 | 10,5 | 1,36 |
| ISO10137 | 0,0168 | 0,0077 | 2,111 | 14,0 | 2,69 |
| 28 | 0,0247 | 0,0113 | 1,671 | 17,5 | 5,05 |
| ISO6897 | 0,0348 | 0,0158 | 1,335 | 21,0 | 8,92 |
| 28 | 0,0452 | 0,0205 | 1,131 | 24,5 | 13,60 |
| Deflection | 0,0572 | 0,0259 | 0,961 | 28,0 | 20,36 |
| 45,5 | 0,0710 | 0,0321 | 0,820 | 31,5 | 29,83 |
| | 0,0842 | 0,0380 | 0,726 | 35,0 | 40,07 |
| | 0,0986 | 0,0444 | 0,644 | 38,5 | 53,46 |

| | | | | | |
|---|---|---|---|---|---|
| | 0,1140 | 0,0513 | 0,572 | 42,0 | 70,69 |
| | 0,1286 | 0,0578 | 0,521 | 45,5 | 88,43 |
| | 0,1439 | 0,0646 | 0,474 | 49,0 | 110,32 |
| | 0,1597 | 0,0716 | 0,432 | 52,5 | 137,07 |
| | 0,1753 | 0,0786 | 0,397 | 56,0 | 166,43 |
| | 0,1912 | 0,0857 | 0,365 | 59,5 | 201,47 |
| | 0,2074 | 0,0929 | 0,337 | 63,0 | 242,96 |
| DT500-J | 0,0085 | 0,0039 | 2,399 | 7,0 | 1,31 |
| Max height: | 0,0160 | 0,0073 | 1,732 | 10,5 | 3,41 |
| ISO10137 | 0,0243 | 0,0110 | 1,361 | 14,0 | 6,68 |
| 28 | 0,0342 | 0,0154 | 1,100 | 17,5 | 11,72 |
| ISO6897 | 0,0457 | 0,0206 | 0,909 | 21,0 | 19,09 |
| 24,5 | 0,0572 | 0,0257 | 0,780 | 24,5 | 28,11 |
| Deflection | 0,0700 | 0,0314 | 0,677 | 28,0 | 40,10 |
| 31,5 | 0,0841 | 0,0377 | 0,592 | 31,5 | 55,72 |
| | 0,0975 | 0,0437 | 0,530 | 35,0 | 73,05 |
| | 0,1118 | 0,0501 | 0,477 | 38,5 | 94,52 |
| | 0,1269 | 0,0568 | 0,430 | 42,0 | 120,82 |
| | 0,1410 | 0,0631 | 0,395 | 45,5 | 148,66 |
| | 0,1555 | 0,0696 | 0,363 | 49,0 | 181,68 |
| | 0,1706 | 0,0763 | 0,334 | 52,5 | 220,64 |
| | 0,1852 | 0,0829 | 0,310 | 56,0 | 263,27 |
| | 0,2001 | 0,0896 | 0,288 | 59,5 | 312,70 |
| | 0,2152 | 0,0965 | 0,268 | 63,0 | 369,68 |
| ST990C320-H-J | 0,0084 | 0,0039 | 5,429 | 7,0 | 0,03 |
| Max height: | 0,0081 | 0,0038 | 5,003 | 10,5 | 0,10 |
| ISO10137 | 0,0026 | 0,0012 | 4,378 | 14,0 | 0,24 |
| 63 | 0,0043 | 0,0020 | 3,214 | 17,5 | 0,53 |
| ISO6897 | 0,0066 | 0,0031 | 2,437 | 21,0 | 1,03 |
| 63 | 0,0095 | 0,0044 | 1,909 | 24,5 | 1,84 |
| Deflection | 0,0130 | 0,0060 | 1,531 | 28,0 | 3,08 |
| 63 | 0,0172 | 0,0079 | 1,253 | 31,5 | 4,90 |
| | 0,0220 | 0,0100 | 1,045 | 35,0 | 7,42 |
| | 0,0273 | 0,0124 | 0,884 | 38,5 | 10,84 |
| | 0,0333 | 0,0151 | 0,757 | 42,0 | 15,39 |
| | 0,0396 | 0,0179 | 0,657 | 45,5 | 21,19 |
| | 0,0465 | 0,0210 | 0,575 | 49,0 | 28,55 |
| | 0,0537 | 0,0242 | 0,508 | 52,5 | 37,70 |
| | 0,0612 | 0,0276 | 0,452 | 56,0 | 48,90 |
| | 0,0690 | 0,0310 | 0,404 | 59,5 | 62,45 |
| | 0,0770 | 0,0346 | 0,364 | 63,0 | 78,73 |
| ST990C320-J | 0,0860 | 0,0407 | 8,108 | 7,0 | 0,03 |
| Max height: | 0,0544 | 0,0259 | 7,804 | 10,5 | 0,09 |
| ISO10137 | 0,0049 | 0,0023 | 6,406 | 14,0 | 0,24 |

| | | | | | |
|---|---|---|---|---|---|
| 45,5 | 0,0069 | 0,0033 | 4,722 | 17,5 | 0,53 |
| ISO6897 | 0,0098 | 0,0046 | 3,586 | 21,0 | 1,04 |
| 45,5 | 0,0136 | 0,0064 | 2,809 | 24,5 | 1,86 |
| Deflection | 0,0184 | 0,0085 | 2,250 | 28,0 | 3,12 |
| 63 | 0,0241 | 0,0112 | 1,839 | 31,5 | 4,97 |
| | 0,0307 | 0,0142 | 1,531 | 35,0 | 7,55 |
| | 0,0383 | 0,0176 | 1,294 | 38,5 | 11,07 |
| | 0,0468 | 0,0214 | 1,106 | 42,0 | 15,76 |
| | 0,0561 | 0,0256 | 0,958 | 45,5 | 21,76 |
| | 0,0662 | 0,0301 | 0,837 | 49,0 | 29,42 |
| | 0,0769 | 0,0349 | 0,737 | 52,5 | 38,98 |
| | 0,0883 | 0,0400 | 0,654 | 56,0 | 50,73 |
| | 0,1002 | 0,0453 | 0,585 | 59,5 | 64,99 |
| | 0,1127 | 0,0509 | 0,526 | 63,0 | 82,21 |
| ST990CLT320-H-J | 0,0028 | 0,0013 | 2,896 | 7,0 | 0,05 |
| Max height: | 0,0062 | 0,0028 | 1,913 | 10,5 | 0,19 |
| ISO10137 | 0,0102 | 0,0046 | 1,442 | 14,0 | 0,50 |
| 59,5 | 0,0152 | 0,0069 | 1,121 | 17,5 | 1,05 |
| ISO6897 | 0,0210 | 0,0095 | 0,896 | 21,0 | 1,95 |
| 52,5 | 0,0273 | 0,0123 | 0,749 | 24,5 | 3,27 |
| Deflection | 0,0344 | 0,0154 | 0,633 | 28,0 | 5,19 |
| 63 | 0,0421 | 0,0189 | 0,540 | 31,5 | 7,83 |
| | 0,0501 | 0,0224 | 0,473 | 35,0 | 11,32 |
| | 0,0587 | 0,0263 | 0,415 | 38,5 | 15,86 |
| | 0,0678 | 0,0303 | 0,367 | 42,0 | 21,73 |
| | 0,0769 | 0,0345 | 0,330 | 45,5 | 28,93 |
| | 0,0864 | 0,0387 | 0,297 | 49,0 | 37,91 |
| | 0,0960 | 0,0431 | 0,268 | 52,5 | 48,84 |
| | 0,1058 | 0,0476 | 0,244 | 56,0 | 62,03 |
| | 0,1155 | 0,0520 | 0,223 | 59,5 | 77,71 |
| | 0,1253 | 0,0566 | 0,204 | 63,0 | 96,44 |
| ST990CLT320-J | 0,0044 | 0,0021 | 4,327 | 7,0 | 0,39 |
| Max height: | 0,0097 | 0,0044 | 2,817 | 10,5 | 1,27 |
| ISO10137 | 0,0164 | 0,0075 | 2,083 | 14,0 | 2,83 |
| 28 | 0,0252 | 0,0115 | 1,595 | 17,5 | 5,57 |
| ISO6897 | 0,0359 | 0,0163 | 1,260 | 21,0 | 9,95 |
| 28 | 0,0473 | 0,0214 | 1,047 | 24,5 | 15,70 |
| Deflection | 0,0600 | 0,0271 | 0,880 | 28,0 | 23,83 |
| 42 | 0,0739 | 0,0333 | 0,749 | 31,5 | 34,90 |
| | 0,0882 | 0,0397 | 0,655 | 35,0 | 48,04 |
| | 0,1033 | 0,0464 | 0,575 | 38,5 | 65,03 |
| | 0,1193 | 0,0535 | 0,508 | 42,0 | 86,65 |
| | 0,1353 | 0,0606 | 0,457 | 45,5 | 111,10 |
| | 0,1518 | 0,0680 | 0,412 | 49,0 | 141,26 |

| | | | | | |
|---|---|---|---|---|---|
| | 0,1689 | 0,0756 | 0,372 | 52,5 | 177,95 |
| | 0,1860 | 0,0833 | 0,339 | 56,0 | 220,16 |
| | 0,2033 | 0,0911 | 0,310 | 59,5 | 270,43 |
| | 0,2208 | 0,0989 | 0,283 | 63,0 | 329,87 |
| DT990C320-H-J | 0,0040 | 0,0019 | 5,499 | 7,0 | 0,03 |
| Max height: | 0,0057 | 0,0027 | 5,049 | 10,5 | 0,09 |
| ISO10137 | 0,0024 | 0,0011 | 4,524 | 14,0 | 0,23 |
| 63 | 0,0040 | 0,0019 | 3,332 | 17,5 | 0,49 |
| ISO6897 | 0,0061 | 0,0029 | 2,538 | 21,0 | 0,95 |
| 63 | 0,0088 | 0,0041 | 2,002 | 24,5 | 1,66 |
| Deflection | 0,0120 | 0,0055 | 1,616 | 28,0 | 2,74 |
| 63 | 0,0157 | 0,0072 | 1,331 | 31,5 | 4,30 |
| | 0,0199 | 0,0091 | 1,120 | 35,0 | 6,40 |
| | 0,0246 | 0,0112 | 0,955 | 38,5 | 9,20 |
| | 0,0297 | 0,0135 | 0,824 | 42,0 | 12,86 |
| | 0,0352 | 0,0159 | 0,722 | 45,5 | 17,38 |
| | 0,0409 | 0,0185 | 0,637 | 49,0 | 23,00 |
| | 0,0469 | 0,0212 | 0,567 | 52,5 | 29,88 |
| | 0,0532 | 0,0240 | 0,509 | 56,0 | 38,07 |
| | 0,0596 | 0,0269 | 0,460 | 59,5 | 47,81 |
| | 0,0662 | 0,0298 | 0,417 | 63,0 | 59,33 |
| DT990C320-J | 0,0379 | 0,0179 | 8,248 | 7,0 | 0,03 |
| Max height: | 0,0451 | 0,0215 | 7,891 | 10,5 | 0,09 |
| ISO10137 | 0,0040 | 0,0019 | 6,631 | 14,0 | 0,22 |
| 49 | 0,0059 | 0,0028 | 4,888 | 17,5 | 0,49 |
| ISO6897 | 0,0086 | 0,0040 | 3,718 | 21,0 | 0,95 |
| 49 | 0,0121 | 0,0057 | 2,927 | 24,5 | 1,68 |
| Deflection | 0,0165 | 0,0077 | 2,356 | 28,0 | 2,80 |
| 63 | 0,0217 | 0,0101 | 1,934 | 31,5 | 4,42 |
| | 0,0277 | 0,0128 | 1,621 | 35,0 | 6,62 |
| | 0,0345 | 0,0159 | 1,378 | 38,5 | 9,59 |
| | 0,0421 | 0,0193 | 1,184 | 42,0 | 13,52 |
| | 0,0502 | 0,0230 | 1,032 | 45,5 | 18,40 |
| | 0,0590 | 0,0269 | 0,908 | 49,0 | 24,56 |
| | 0,0684 | 0,0311 | 0,804 | 52,5 | 32,17 |
| | 0,0782 | 0,0355 | 0,719 | 56,0 | 41,34 |
| | 0,0885 | 0,0401 | 0,646 | 59,5 | 52,38 |
| | 0,0993 | 0,0449 | 0,583 | 63,0 | 65,61 |
| DT990CLT320-H-J | 0,0021 | 0,0010 | 3,645 | 7,0 | 0,24 |
| Max height: | 0,0045 | 0,0021 | 2,432 | 10,5 | 0,71 |
| ISO10137 | 0,0074 | 0,0034 | 1,843 | 14,0 | 1,49 |
| 63 | 0,0110 | 0,0050 | 1,441 | 17,5 | 2,79 |
| ISO6897 | 0,0154 | 0,0070 | 1,157 | 21,0 | 4,80 |
| 63 | 0,0200 | 0,0091 | 0,974 | 24,5 | 7,36 |

| | | | | | |
|---|---|---|---|---|---|
| Deflection | 0,0253 | 0,0114 | 0,828 | 28,0 | 10,92 |
| 52,5 | 0,0311 | 0,0140 | 0,711 | 31,5 | 15,72 |
| | 0,0369 | 0,0166 | 0,628 | 35,0 | 21,24 |
| | 0,0432 | 0,0194 | 0,556 | 38,5 | 28,28 |
| | 0,0499 | 0,0224 | 0,495 | 42,0 | 37,12 |
| | 0,0565 | 0,0254 | 0,449 | 45,5 | 46,79 |
| | 0,0634 | 0,0284 | 0,408 | 49,0 | 58,50 |
| | 0,0704 | 0,0316 | 0,372 | 52,5 | 72,51 |
| | 0,0775 | 0,0348 | 0,342 | 56,0 | 88,19 |
| | 0,0846 | 0,0380 | 0,315 | 59,5 | 106,54 |
| | 0,0918 | 0,0413 | 0,291 | 63,0 | 127,84 |
| DT990CLT320-J | 0,0038 | 0,0018 | 5,115 | 7,0 | 0,27 |
| Max height: | 0,0074 | 0,0034 | 3,515 | 10,5 | 0,79 |
| ISO10137 | 0,0120 | 0,0055 | 2,668 | 14,0 | 1,67 |
| 35 | 0,0178 | 0,0082 | 2,082 | 17,5 | 3,17 |
| ISO6897 | 0,0250 | 0,0115 | 1,661 | 21,0 | 5,55 |
| 31,5 | 0,0327 | 0,0149 | 1,393 | 24,5 | 8,61 |
| Deflection | 0,0416 | 0,0190 | 1,180 | 28,0 | 12,92 |
| 49 | 0,0517 | 0,0235 | 1,008 | 31,5 | 18,83 |
| | 0,0618 | 0,0280 | 0,887 | 35,0 | 25,60 |
| | 0,0729 | 0,0330 | 0,784 | 38,5 | 34,33 |
| | 0,0849 | 0,0384 | 0,695 | 42,0 | 45,45 |
| | 0,0967 | 0,0436 | 0,629 | 45,5 | 57,56 |
| | 0,1092 | 0,0492 | 0,570 | 49,0 | 72,42 |
| | 0,1223 | 0,0551 | 0,518 | 52,5 | 90,47 |
| | 0,1355 | 0,0609 | 0,474 | 56,0 | 110,81 |
| | 0,1492 | 0,0670 | 0,435 | 59,5 | 134,99 |
| | 0,1633 | 0,0733 | 0,400 | 63,0 | 163,57 |

**Table B.1:** Data from analysis

# C

# Grasshopper script

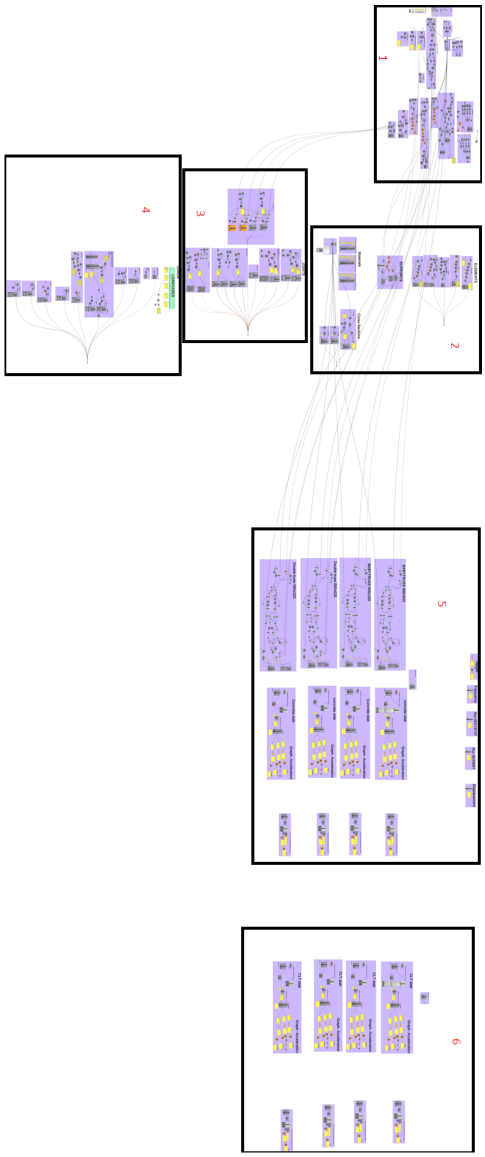

Figure C.1: Orientational image of script

**Figure C.2:** Part 1 of grasshopper script

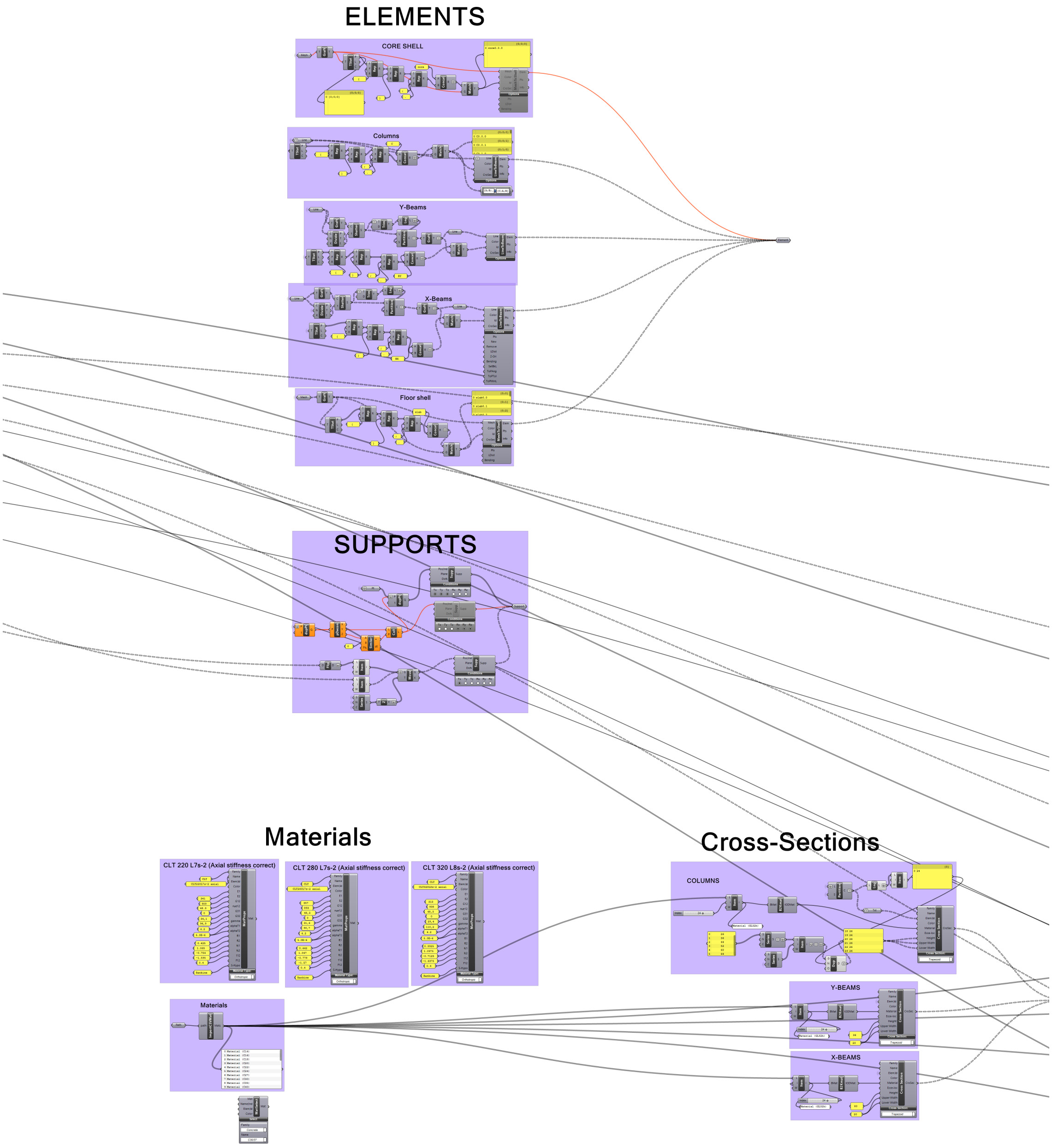


**Figure C.3:** Part 2 of grasshopper script

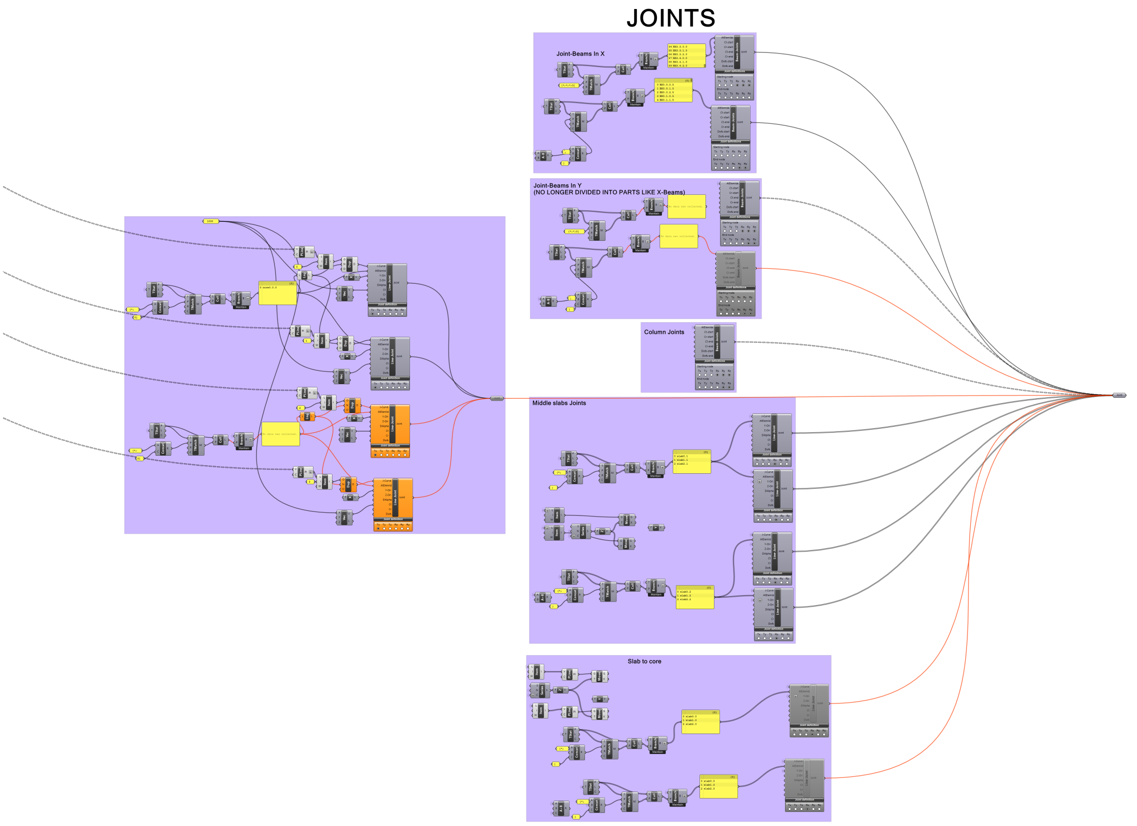


**Figure C.4:** Part 3 of grasshopper script

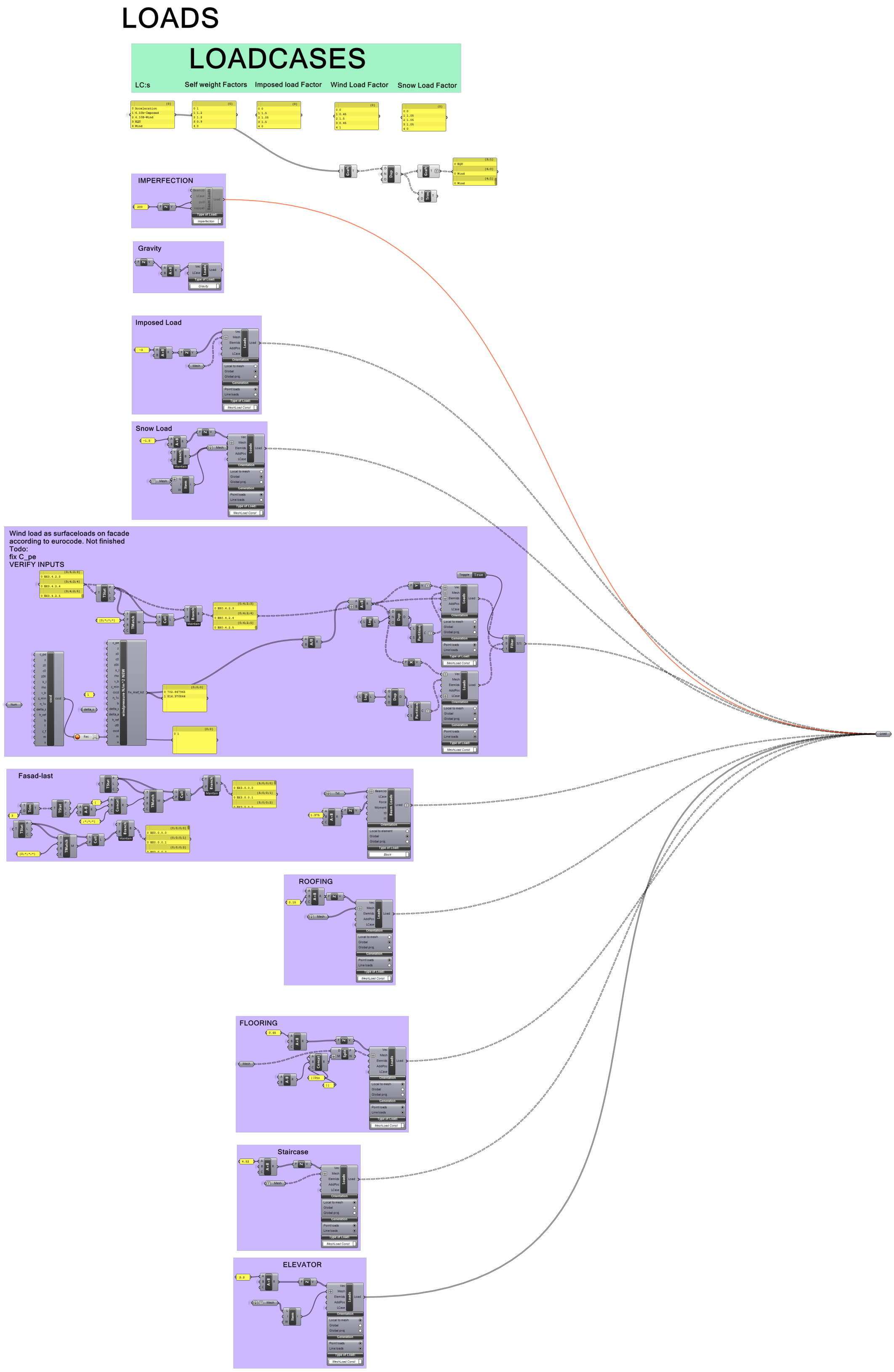


**Figure C.5:** Part 4 of grasshopper script

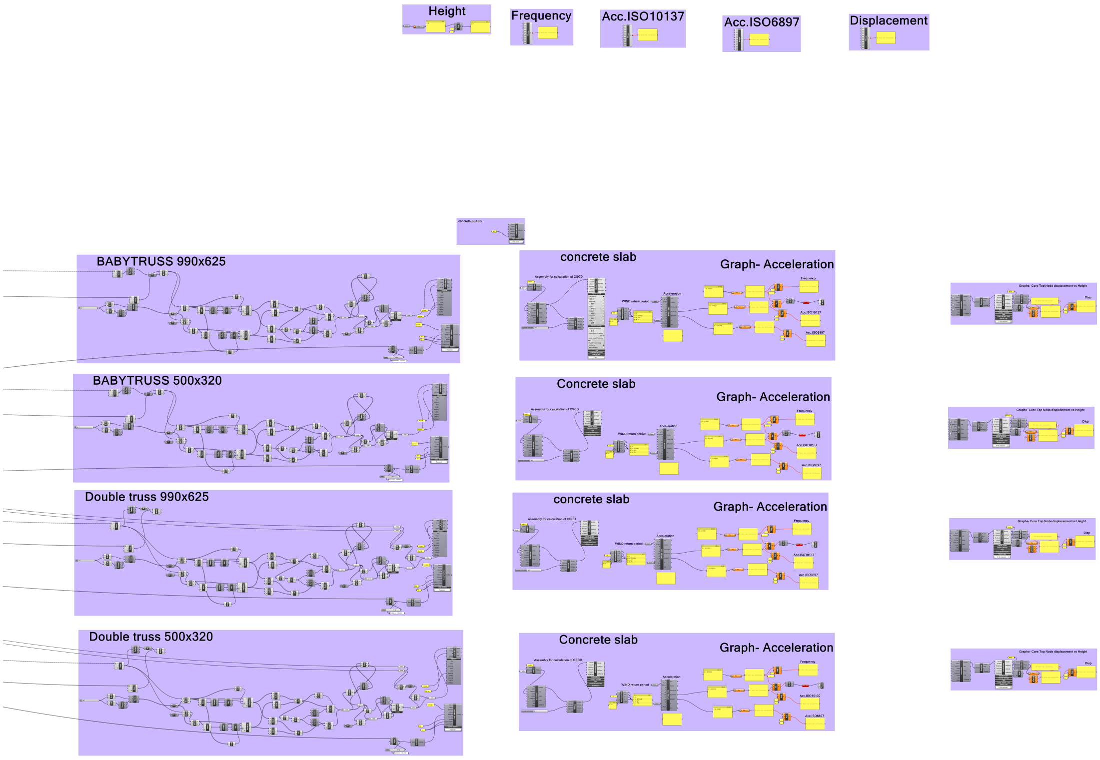


**Figure C.6:** Part 5 of grasshopper script

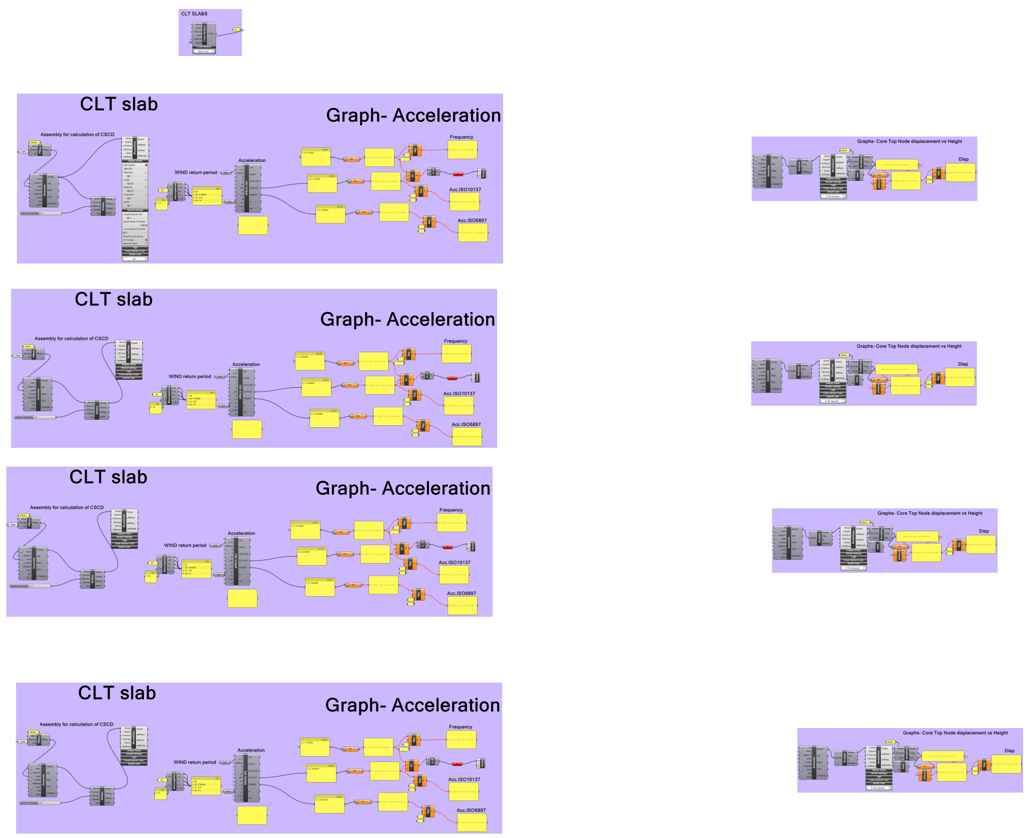


**Figure C.7:** Part 6 of grasshopper script

# D

# Coefficients

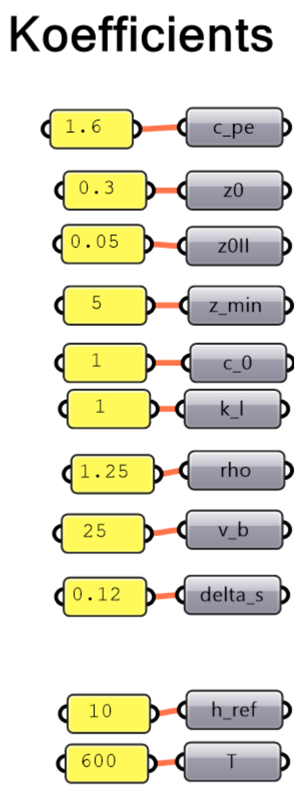


**Figure D.1:** Coefficients used in calulation of wind load and accelerations

**DEPARTMENT OF ARCHITECTURE AND CIVIL ENGINEERING**
**CHALMERS UNIVERSITY OF TECHNOLOGY**
Gothenburg, Sweden 2023
www.chalmers.se

CHALMERS
UNIVERSITY OF TECHNOLOGY